REPORT DOCUMENTATION PAGE

Form Approved

Public reporting burden for this collection of information is estimated to average 1 hour per response, including the time fo. gathering and maintaining the data needed, and completing and reviewing the collection of information. Send comments re collection of information, including suggestions for reducing this burden, to Washington Headquarters Services, Directorate Davis Highway, Suite 1204, Arlington, VA 22202-4302, and to the Office of Management and Budget, Paperwork Reduction Pr

AFRL-SR-BL-TR-02-0002

1. AGENCY USE ONLY (Leave blank)	2. REPORT DATE	3. REPORT TYPE AI
	November 2001	Final Report

4. TITLE AND SUBTITLE

Dielectric Relaxation Spectroscopy of Adhesively Bonded Joints

5. FUNDING NUMBERS

F49620-99-C-0057
65502F
STTR-TX

6. AUTHOR(S)

Rajesh K. Tiwari, Mohan Balan, Patricia Stumpff, Som R. Soni, Jovan Mijovic, Nobuhiro Miura, Hua Zhang, Yuzhi Duan

7. PERFORMING ORGANIZATION NAME(S) AND ADDRESS(ES)

AdTech Systems Research, Inc.
1342 N. Fairfield Road
Beavercreek OH 45432

Polytechnic University
The Herman F. Mark Polymer Research Institute
Six Metrotech Center
Brooklyn NY 11201

8. PERFORMING ORGANIZATION REPORT NUMBER

738 Final Report

9. SPONSORING/MONITORING AGENCY NAME(S) AND ADDRESS(ES)

Air Force Office of Scientific Research (AFOSR/NA)
801 Randolph
Arlington VA 22203

10. SPONSORING/MONITORING AGENCY REPORT NUMBER

AFOSR-TR-01-

11. SUPPLEMENTARY NOTES

12a. DISTRIBUTION/AVAILABILITY STATEMENT

Approved for public release; distribution unlimited.

AIR FORCE OFFICE OF SCIENTIFIC RESEARCH (AFOSR)
NOTICE OF TRANSMITTAL TO DTIC. THIS TECHNICAL REPORT HAS BEEN REVIEWED AND IS APPROVED FOR PUBLIC RELEASE
LAW AFR 190-12. DISTRIBUTION IS UNLIMITED.

12b. DISTRIBUTION CODE

13. ABSTRACT *(Maximum 200 words)*

Molecular aspects of chemical and physical changes in adhesively bonded joints caused by absorbed moisture were investigated. The focus was on the pre-damage stage that precedes the formation of voids and microcracks. Dielectric relaxation spectroscopy was used as a non-destructive tool to characterize the molecular level changes in the adhesive when exposed to hygrothermal environments. Three adhesive types, a commercial epoxy-amine formulation (FM73U), a model epoxy formulation consisting of diglycidyl ether of Bisphenol A (DGEBA) and methylene dianiline (MDA), and a bismaleimide formulation consisting of 4,4' bismaleimidodiphenyl methane (component A) and 0,0' diallyl bisphenol A (component B) were studied. Local dynamics were monitored by broad-band dielectric relaxation spectroscopy (DRS) and the changes in the chemical state of the matter were monitored by FTIR. The influence of moisture on the strength and durability of adhesively bonded joints were also investigated.

14. SUBJECT TERMS

15. NUMBER OF PAGES
127

16. PRICE CODE

17. SECURITY CLASSIFICATION OF REPORT	18. SECURITY CLASSIFICATION OF THIS PAGE	19. SECURITY CLASSIFICATION OF ABSTRACT	20. LIMITATION OF ABSTRACT
Unclass	Unclass	Unclass	Unclass

AFOSR-TR-01-

DIELECTRIC RELAXATION SPECTROSCOPY OF ADHESIVELY BONDED JOINTS

Rajesh K. Tiwari
Mohan Balan
Patricia Stumpff
Som R. Soni

AdTech Systems Research, Inc
1342 North Fairfield Road
Beavercreek, OH 45432

Jovan Mijovic
Nobuhiro Miura
Hua Zhang
Yuzhi Duan

Polytechnic University
Department of Chemical Engineering & Chemistry
and
The Herman F. Mark Polymer Research Institute
Six MetroTech Center
Brooklyn, NY 11201

NOVEMBER 2001

FINAL REPORT FOR PERIOD 10 AUGUST 1999 – 9 AUGUST 2001

Approved for public release; distribution unlimited

AIR FORCE OFFICE OF SCIENTIFIC RESEARCH
801 RANDOLPH
ARLINGTON VA 22203

20020118 101

NOTICE

USING GOVERNMENT DRAWINGS, SPECIFICATIONS, OR OTHER DATA INCLUDED IN THIS DOCUMENT FOR ANY PURPOSE OTHER THAN GOVERNMENT PROCUREMENT DOES NOT IN ANY WAY OBLIGATE THE US GOVERNMENT. THE FACT THAT THE GOVERNMENT FORMULATED OR SUPPLIED THE DRAWINGS, SPECIFICATIONS OR OTHER DATA DOES NOT LICENSE THE HOLDER OR ANY OTHER PERSON OR CORPORATION; OR CONVEY ANY RIGHTS OR PERMISSION TO MANUFACTURE, USE ,OR SELL ANY PATENTED INVENTION THAT MAY RELATE TO THEM.

GOVERNMENT PURPOSE LICENSE RIGHTS LEGEND (SBIR PROGRAM)

Contract Number: F49620-99-C-0057
Contractor: AdTech Systems Research, Inc.

For a period of two (2) years after the delivery and acceptance of the last deliverable item under the above contract, all technical data contained in this report marked as Government Purpose License Rights data shall be subject to the restrictions contained in the definition of "Limited Rights in DFARS clause 252.227-7013 (October 1988). After the two-year period, the data shall be subject to the restrictions contained in the definition of Government Purpose License Rights" in DFARS clause 252.227.7013 (October 1988). The Government assumes no liability for unauthorized use or disclosure by others. This legend, together with the indications of the portions of the data which are subject to such limitations, shall be included on any reproduction hereof which contains any portions subject to such limitations and shall be honored only as long as the data continues to meet the definition on Government purpose license rights.

This technical report has been reviewed and is accepted under the provisions of the Small Business Innovative Research Program.

This technical report is published in the interest of scientific and technical information exchange and does not constitute approval or disapproval of its ideas or findings.

Do not return copies of this report unless contractual obligations or notice on a specific document requires its return.

TABLE OF CONTENTS

Section		Page
1.0		1
	1.1 Introduction	3
	1.2 Research Objectives	4
	1.3 Overview of the Study	5
	References	5
2.0	DIELECTRIC RELAXATION SPECTROSCOPY OF FM-73U AND MODEL EPOXY	7
	2.1 Introduction	7
	2.2 Theoretical Background	9
	2.3 Experimental Materials	10
	2.4 Techniques	11
	2.5 Results and Discussion	12
	2.6 Work in Progress	22
	2.7 Conclusions	23
	References and Notes	24
3.0	DIELECTRIC RELAXATION SPECTROSCOPY OF BISMALEIMIDE (BMI)	41
	3.1 Introduction	41
	3.2 Theoretical Background	44
	3.3 Experimental Materials	45
	3.4 Techniques	46
	3.5 Results and Discussion	47
	3.6 Conclusions	60
	References and Notes	62
4.0	THE STRENGTH AND DURABILITY OF ADHESIVELY BONDED JOINTS AND ITS CORRELATION WITH DIELECTRIC RELAXATION DATA	80
	4.1 Introduction	80
	4.2 Experimental	80
	4.2.1 Test Equipment, Materials and Supplies	81
	4.2.2 Surface Pretreatment	82
	4.2.3 Adhesive Bonding	83
	4.2.4 Doble Notch Shear (DNS) Tests	84
	4.2.5 Wedge Test	85
	4.3 Results and Discussion	85
	4.3.1 Adherend Surface Characterization	85
	4.3.2 DNS Test Results for FM73U/aluminum Joints	86
	4.3.3 Wedge Test Results for FM73U/aluminum Joints	89
	4.3.4 Wedge Test Results for Model Epoxy/aluminum Joints	90
	4.3.5 DNS Test Results for Model Epoxy/aluminum Joints	91
	4.3.6 Mechanical strength – Dielectric Relaxation Data Correlation	91

TABLE OF CONTENTS (Cont'd)

Section		Page
	4.4 Conclusions	93
	References	94
5.0	FINITE ELEMENT ANALYSIS OF DOUBLE NOTCH SHEAR TEST SPECIMENS	106
	Summary	114

List of Figures

Figure		Page
2.1.	Dielectric permittivity and loss in the frequency domain for uncured DGEBA/MDA mixture with temperature as a parameter. Solid lines are fits to Havriliak-Negami equation.	27
2.2.	Dielectric loss in the frequency domain for fully-cured DGEBA/MDA with temperature as a parameter. Solid lines are fits to Havriliak-Negami equation.	28
2.3.	Dielectric loss in the frequency domain for fully-cured DGEBA/MDA with temperature as a parameter after 3-day exposure to environment. Solid lines are fits to Havriliak-Negami equation.	28
2.4.	Dielectric loss in the frequency domain for fully-cured DGEBA/MDA with temperature as a parameter after 5-day exposure to environment. Solid lines are fits to Havriliak-Negami equation.	29
2.5.	Dielectric loss in the frequency domain after 5-day exposure to environment, measured at -30°C. β and γ processes were fit to the Cole-Cole equation.	29
2.6.	Dielectric loss in the frequency for the fully-cured DGEBA/MDA with exposure time as a parameter, measured at -30°C. Solid lines are fits to Havriliak-Negami equation.	30
2.7.	Frequency of dielectric loss maximum f_m as a function of reciprocal temperature for dry, and moist DGEBA/MDA.	30
2.8.	Dielectric loss in the frequency domain for fully cured FM73U with temperature as a parameter. Solid lines are fits to Havriliak-Negami equation.	31
2.9.	Dielectric loss in the frequency domain for cured FM73U with exposure time as a parameter. Solid lines are fits to Havriliak-Negami equation.	31
2.10.	Dielectric loss in the frequency domain for FM73U after 10-day exposure, with temperature as a parameter. Solid lines are fits to Havriliak-Negami equation.	32
2.11.	Dielectric loss in the frequency domain for FM73U with exposure time as a parameter, measured at 60°C. Solid lines are fits to Havriliak-Negami equation.	32
2.12.	Dielectric loss in the frequency domain for FM73U with exposure time as a parameter, measured at -70°C. Solid lines are fits to Havriliak-Negami equation.	33

List of Figures (Cont'd)

Figure		Page
2.13.	Frequency of dielectric loss maximum f_m as a function of reciprocal temperature for dry, and moist FM73U.	33
2.14.	Near-IR spectra of DGEBA/MDA: (A)dry and (B) after 1-day exposure.	34
2.15.	Near-IR spectra for DGEBA/MDA at different exposure times: dry, 2 hours, 1 day, 13 days.	34
2.16.	Deconvolution of the 5400-4800cm^{-1} range after 13-day exposure. Two separate processes were described by Gaussian function.	35
2.17.	Absorbance area as a function of water content for absorbances of 5230cm^{-1}, 5137cm^{-1}, and their sum.	35
2.18.	Mid-IR spectra for DGEBA/MDA at different exposure times: dry, 10 minutes, 1 hour, 1 day, and 8 days.	36
2.19.	Mid-IR difference spectra for DGEBA/MDA at different exposure times: 10 minutes, 1 hour, and 1 day.	36
2.20.	Deconvolution of difference spectra in the range of 3700-3100cm^{-1} after 1-day exposure. Each separate peak was described by a Gaussian function.	37
2.21.	Absorbance area of each separated peak as a function of exposure time.	37
2.22.	Normalized absorbance area of each peak as a function of exposure time.	38
2.23.	Dielectric permittivity and loss in the frequency domain for cured BMI with temperature as a parameter after 1-day exposure to environment. Solid lines are fits to Cole-Cole equation.	39
2.24.	Composite plot of frequency of dielectric loss maximum f_m as a function of reciprocal temperature for BMI, DGEBA/MDA and FM73U at various exposure times.	40
3.1.	Chemical composition of the BMI formulation.	66
3.2.	Photograph of our setup for dielectric measurements. On the right is Novocontrol's Alpha analyzer, and a 4291 RF impedance analyzer on top of it. On the left is the cryostat with the mobile unit behind it and the two cells in their uppermost (high frequency - left and low frequency – right).	66

List of Figures (Cont'd)

Figure		Page
3.3.	Dielectric permittivity (a) and loss (b) in the frequency domain for uncured BMI with temperature as a parameter. Solid lines are fits to the Havriliak-Negami equation.	67
3.4.	Log frequency at maximum loss as a function of reciprocal temperature for uncured BMI. Solid line is a VFT fit.	67
3.5.	Dielectric permittivity and loss in the frequency domain for cured BMI with temperature as a parameter. Solid lines are fits to the Havriliak-Negami equation.	68
3.6.	Dielectric loss in the frequency domain measured at 50°C for 0, 3 and 5-day exposure to 60°C/98% RH.	68
3.7.	Dielectric loss in the frequency domain for cured BMI exposed to 60°C/98% RH with exposure time as a parameter, measured at (a) -20°C, (b) -60°C and (c) -100°C.	69
3.8.	Dielectric loss in the frequency domain for cured BMI exposure to 80°C/98% RH with exposure time as a parameter, measured at (a) 20°C, (b) –20°C and (c) -60°C.	70
3.9.	Dielectric loss in the frequency domain for cured BMI after (a) 1day, (b) 3days and (c) 5days exposure at 80°C/98% RH, with measuring temperature as a parameter.	71
3.10.	Log frequency at maximum loss as a function of reciprocal temperature for different exposure times in dry and moist BMI.	72
3.11.	Dielectric relaxation strength of cured BMI after exposure to 60 and 80°C environments as a function of exposure time.	72
3.12.	Chemical structure of a fragment of cured BMI network. Note: Different network sites that could participate in hydrogen bonding with absorbed water (shown in bold).	73
3.13.	NIR spectrum of cured BMI.	73

List of Figures (Cont'd)

Figure		Page
3.14.	a - NIR spectra of BMI at different exposure times: dry, 2hrs, 1day, 4 days and 23 days; b – difference spectra.	74
3.15.	Deconvoluted difference spectra in the 5000-5400 cm^{-1} range after a 4-day exposure to 60°C /98%RH.	75
3.16.	Absorbance area as a function of water content.	75
3.17.	Deconvoluted NIR spectrum of cured BMI after exposure to 80°C for 5h.	76
3.18.	Ratio of non hydrogen-bonded (S_0) to total (S_t) absorbed water as a function of water content, calculated from the NIR data.	76
3.19.	Ratio of non hydrogen-bonded (S_0) to total (S_t) absorbed water as a function of water content, calculated from the DRS data; filled symbols (Eq. 6); open symbols (Eq. 7).	77
3.20.	MIR spectrum of cured BMI.	77
3.21.	Deconvoluted MIR spectrum of cured BMI in the 3700-2800cm^{-1} region.	78
3.22.	MIR spectra of cured BMI after exposure to different periods of time.	78
3.23.	Difference spectra of cured BMI in the 3700-3000cm^{-1} range after exposure to 60°C/98 %RH for different time.	79
3.24.	Deconvoluted MIR spectrum of cured BMI in the 3700-2800cm^{-1} region, following exposure to 60°C/98 %RH environment for 30min.	79
4.1.	AES depth-profile of a PAA treated non-bonded aluminum surface	95
4.2.	SEM photomicrograph of a PAA treated aluminum surface	96
4.3.	Load versus stroke trace for bonded (no-exposure) DNS specimen	96
4.4.	Load versus stroke data for DNS specimens exposed to 95% relative humidity at 50°C for various times	97
4.5.	Load versus stroke data for DNS specimens exposed to 95% relative humidity at 60°C for various times	97

List of Figures (Cont'd)

Figure		Page
4.6.	Load versus stroke data for DNS specimens exposed to 95% relative humidity at 80°C for various times	98
4.7.	Photographs of failure surfaces of DNS specimens exposed to 95% relative humidity at 50°C for (a) 1 day, (b) 3 days, (c) 7 days and (d) 14 days.	99
4.8.	Wedge test crack length vs. Exposure time for FM73U/aluminum bonded specimens exposed to 95% relative humidity at 40°C, 50°C, 60°C and 80°C	99
4.9.	Wedge test crack length vs. Exposure time for FM73U/aluminum bonded specimens exposed to boiling water.	100
4.10.	Wedge test crack length vs. Exposure time for model epoxy/aluminum bonded specimens exposed to (a)<15% relative humidity at 24°C in desiccator, (b) 95% relative humidity at 60°C and (c) 95% relative humidity at 80°C	101
4.11.	Load versus stroke data for model epoxy/aluminum DNS specimens exposed to 95% relative humidity at 60°C for various times	102
4.12.	Dielectric loss maximum as a function of exposure time (t) for cured model epoxy after exposure to 60°C at 95% relative humidity. Dielectric loss maximum was measured at 10°C (X) and 50°C (o). Straight lines are the least-squares fits from the regression analyses	103
4.13.	Relaxation strength as a function of exposure time (t) for cured model epoxy after exposure to 60°C at 95% relative humidity. Relaxation strength was measured at 10°C (X) and 50°C (o). Straight lines are the least-squares Fitz from the regression analyses	103
4.14.	Shear strength as a function of dielectric relaxation strength, measured at 10°C (X) and 50°C (o), for model epoxy/aluminum bonded joints exposed to 60°C/95% relative humidity for various times. Straight lines are the least-squares fits from the regression analyses	104
4.15.	Shear strength as a function of dielectric loss max., measured at 10°C (X) and 50°C (o), for model epoxy/aluminum bonded joints exposed to 60°C/95% relative humidity for various times. Straight lines are the least-squares fits from the regression analyses	104
4.16.	Dielectric loss maximum as a function of exposure time (t) for cured FM-73U adhesive after exposure to 60°C at 95% relative humidity. Dielectric loss maximum was measured at 50°C (X). Straight line is the least-squares fits from the regression analysis	105

List of Figures (Cont'd)

Figure		Page
4.17.	Shear strength as a function of dielectric loss max., measured at 50°C (X), for FM-73U/aluminum bonded joints exposed to 60°C/95% relative humidity for various times. Straight line is the least-squares fits from the regression analysis	105
5.1.	Geometry of DNS specimen.	109
5.2.	Boundary Conditions for a DNS specimen.	110
5.3.	Three-dimensional contour plot of shear stress distribution in the overlap regions.	110
5.4.	The influence of bond line thickness on the stress distribution along the bonded joint overlap.	111
5.5.	A schematic of DNS test geometry in the overlap region with: (a) square edge adhesive layer and (b) Continuous adhesive layer.	111
5.6.	Stress distribution profile in the bond overlap region for a square edge adhesive layer and continuous adhesive layer in DNS specimens.	112
5.7.	Two-dimensional contour plot of maximum principal stress distribution in the overlap region of a DNS specimen.	112
5.8.	The maximum principal stress distribution is plotted as a function of bond overlap for the top, middle and bottom adhesive layers.	113
5.9	The photographs of failure surfaces of unexposed FM-73U/aluminum DNS specimens	113

List of Tables

Table		Page
4.1	XPS analysis results of a PAA treated non-bonded aluminum surface.	95
4.2	Shear strengths (MPa) as a function of exposure time in various temperature/humidity environments for FM-73U/Aluminum DNS bonded joints. Standard deviations are given at 95% confidence limit.	98
4.3	Shear strengths (MPa) for model epoxy/aluminum DNS bonded joints exposed to 95% relative humidity at 60°C for various times. Standard deviations are given at 95% confidence limit.	102

1.0 INTRODUCTION

The continuing under-utilization of adhesive joints in the military and commercial aerospace structures is a well-recognized fact. Although adhesive joints offer distinct advantages over riveted joints in terms of weight savings, structural integrity and design flexibility, there is a general lack of confidence in their use. This is primarily caused by insufficient understanding of the science behind the environmental effects on adhesive joints, including bondline interfaces. These, in turn, create expensive repercussion on the aerospace industry while placing undue limits on the entire adhesives technology base. To remedy this, a strong initiative has immerged (led by the AFOSR) aimed at the development of a new generation of adhesives, environmentally-friendly surface preparation methods and novel inspection techniques capable of detecting subtle, "pre-damage" changes in the chemical and physical properties of adhesives, i.e., the changes that precede the formation of cracks that lead to the degradation of joint. In fact, the development of a methodology for non-destructive monitoring of the effect of environmental factors on the adhesively bonded joints in the pre-damage stage has been identified as critical to the successful inception of a new adhesives technology base.

The principal prerequisite for a successful development and implementation of a non destructive inspection (NDI) technique capable of detecting the pre-damage changes in bonded joints that translate to degradation in joint integrity, is an understanding of the underlying science.

The chemo-physical properties of adhesive joints change with time in service and the type and severity of the aggressive environment. The term "aggressive" is used here to stress that every service environment will have an adverse affect (though on a different time-scale) on the properties of the bondline. For example, the degradation of a bondline exposed to an aqueous

environment begins from the moment water molecules enter the adhesive. Current inspection methods are suitable for the detection of delamination and loss of adhesion, which occurs when water eventually diffuses through the adhesive and reaches the adhesive-adherend interface/interpahse where corrosion initiates. The focus of this study, however, is on the chemical and physical changes in the adhesive on a molecular level in the early, pre-damage stage that precedes microcracking and delamination, because that phase holds key to the understanding of the initiation and propagation of failure. The molecular picture of these events is far from complete and numerous questions remain unresolved. In what form (free, cluster, complexes etc.) does moisture exist in the adhesive? How does moisture interact with the host matrix and what effect does it have on the local dynamics and various properties? What is the nature of other migrating charges, extrinsic (e.g., ionic impurities) and/or intrinsic (e.g., hydrogen bond paths) in the adhesive and how these interact with moisture? What chemical changes (e.g., reactions) occur in the adhesive and do they include polymeric chains, moisture, other migrating charges, complexes etc.? What are the kinetics of all those events? What are the effects of temperature, pressure and relative humidity of the environment?

Let us now revert our attention to the major theme of the work presented here– elucidation of the fundamental science that describes the effect of environment on the microstructure and chemo-physical properties of adhesively bonded joints in the pre-damage stage. An essential condition that must be satisfied in a study of this kind is the ability to detect physical and chemical changes on a molecular level. The time scales of molecular dynamics that characterize the physics of adhesive joints range from picoseconds for segmental motions in the bulk to minutes or hours for reactions at interfaces, but it is the rapid (high-frequency) actions that are crucial here. Another important consideration is that in-situ real-time non-destructive measurements be used to

determine the on-set of failure (in addition to the various destructive and post-failure analyses that provide only an indirect insight into the temporal evolution of the chemo-physical changes in adhesive joints). The dielectric relaxation spectroscopy (DRS) and Fourier Transform Infrared (FTIR) spectroscopy are well-established non-destructive experimental techniques, and were extensively utilized in the present work for probing physical and chemical changes in adhesives on a molecular scale.

1.1 Background Information

Numerous authors [1-6] have studied the effect of environmental exposure on adhesive joints. The vast majority of those reports are based on (destructive) mechanical tests that are often followed by a microscopic investigation of fracture surfaces aimed at elucidating the locus of failure. Such studies, however, offer little direct information about the evolution of chemical and physical changes in adhesives during exposure to an aggressive environment. The reported dielectric measurements of adhesively joints exposed to aggressive environments were performed, as a rule, at lower frequencies and were directed towards an understanding of the effect of charge migration on resistivity and/or the mechanism and kinetics of chemical reactions at the polymer-metal interface that cause corrosion [7-11].

The action of the aggressive environment causes chemical and physical changes in the adhesive on a molecular level. The physical changes encompass molecular motions, mobility, relaxations, dynamics, etc. Chemical changes relate to the chemical state of the matter, chemical interactions that include hydrogen-bonded complexes, etc. The effect of absorbed moisture on molecular mobility and relaxations in the glassy state (physical aspect) is instantaneous but it can be detected only with an appropriate technique, such as (high frequency) DRS. Consider, for example, that

water at 20°C has a dielectric loss peak at about 20 GHz, which corresponds to the relaxation time of 9 picoseconds (1 ps = 10^{-12}s), and although the bulk of the adsorbed moisture in the adhesive is more likely to form hydrogen-bonded complex with the matrix, such relaxation process are still very fast and have been shown (see phase I results) to take place at frequencies above 1 MHz. A comprehensive dielectric study of the dynamics of such interactions, however, has not been reported hitherto in the literature. A rare example of the use of high-frequency dielectric measurements to study moisture absorption in adhesive joints is the work of Pethrick and coworkers [12-14], though their efforts have not focused on the underlying molecular mechanism. Instead, the main thrust of their work was aimed at the development of a field-operable non-destructive inspection (NDI) tool based on DRS. It is clear, however, that the success of their efforts hinges upon a through understanding of the relevant science, and hence our approaches are complementary. It is also worth noting that an excellent series of studies of water dynamics in biopolymers (DNA, proteins) by time domain reflectometry was reported by Mashimo and coworkers [15-17].

1.2 Research Objectives

The Principal objective of the present work is to perform scientific investigation of the correlation of high frequency dielectric measurements and chemical and physical changes in the adhesively bonded joints prior to damage initiation. Specifically, the technical objectives are:

a) to determine whether or not Dielectric Relaxation Spectroscopy (DRS), in conjunction with Fourier Transform Infrared Spectroscopy, could be used as a viable NDE technique to evaluate the pre-damage state of adhesively bonded joints exposed to an aggressive hygrothermal environment

Cont'd)

	Page
xposed to 95% relative	98
mens exposed to 95% relative 7 days and (d) 14 days.	99
r FM73U/aluminum bonded at 40°C, 50°C, 60°C and 80°C	99
: FM73U/aluminum bonded	100
· model epoxy/aluminum e humidity at 24°C in desiccator, relative humidity at 80°C	101
inum DNS specimens various times	102
sure time (t) for cured model umidity. Dielectric loss (o). Straight lines are the	103
ime (t) for cured model epoxy y. Relaxation strength was nes are the least-squares Fitz	103
ition strength, measured at num bonded joints exposed s. Straight lines are the	104
ax., measured at 10°C (X) and oints exposed to 60°C/95% nes are the least-squares fits from	104
sure time (t) for cured FM-73U humidity. Dielectric loss line is the least-squares	105

List of Figures (Cont'd)

Figure		Page
4.17.	Shear strength as a function of dielectric loss max., measured at 50°C (X), for FM-73U/aluminum bonded joints exposed to 60°C/95% relative humidity for various times. Straight line is the least-squares fits from the regression analysis	105
5.1.	Geometry of DNS specimen.	109
5.2.	Boundary Conditions for a DNS specimen.	110
5.3.	Three-dimensional contour plot of shear stress distribution in the overlap regions.	110
5.4.	The influence of bond line thickness on the stress distribution along the bonded joint overlap.	111
5.5.	A schematic of DNS test geometry in the overlap region with: (a) square edge adhesive layer and (b) Continuous adhesive layer.	111
5.6.	Stress distribution profile in the bond overlap region for a square edge adhesive layer and continuous adhesive layer in DNS specimens.	112
5.7.	Two-dimensional contour plot of maximum principal stress distribution in the overlap region of a DNS specimen.	112
5.8.	The maximum principal stress distribution is plotted as a function of bond overlap for the top, middle and bottom adhesive layers.	113
5.9	The photographs of failure surfaces of unexposed FM-73U/aluminum DNS specimens	113

List of Tables

Table		Page
4.1	XPS analysis results of a PAA treated non-bonded aluminum surface.	95
4.2	Shear strengths (MPa) as a function of exposure time in various temperature/humidity environments for FM-73U/Aluminum DNS bonded joints. Standard deviations are given at 95% confidence limit.	98
4.3	Shear strengths (MPa) for model epoxy/aluminum DNS bonded joints exposed to 95% relative humidity at 60°C for various times. Standard deviations are given at 95% confidence limit.	102

1.0 INTRODUCTION

The continuing under-utilization of adhesive joints in the military and commercial aerospace structures is a well-recognized fact. Although adhesive joints offer distinct advantages over riveted joints in terms of weight savings, structural integrity and design flexibility, there is a general lack of confidence in their use. This is primarily caused by insufficient understanding of the science behind the environmental effects on adhesive joints, including bondline interfaces. These, in turn, create expensive repercussion on the aerospace industry while placing undue limits on the entire adhesives technology base. To remedy this, a strong initiative has immerged (led by the AFOSR) aimed at the development of a new generation of adhesives, environmentally-friendly surface preparation methods and novel inspection techniques capable of detecting subtle, "pre-damage" changes in the chemical and physical properties of adhesives, i.e., the changes that precede the formation of cracks that lead to the degradation of joint. In fact, the development of a methodology for non-destructive monitoring of the effect of environmental factors on the adhesively bonded joints in the pre-damage stage has been identified as critical to the successful inception of a new adhesives technology base.

The principal prerequisite for a successful development and implementation of a non destructive inspection (NDI) technique capable of detecting the pre-damage changes in bonded joints that translate to degradation in joint integrity, is an understanding of the underlying science.

The chemo-physical properties of adhesive joints change with time in service and the type and severity of the aggressive environment. The term "aggressive" is used here to stress that every service environment will have an adverse affect (though on a different time-scale) on the properties of the bondline. For example, the degradation of a bondline exposed to an aqueous

environment begins from the moment water molecules enter the adhesive. Current inspection methods are suitable for the detection of delamination and loss of adhesion, which occurs when water eventually diffuses through the adhesive and reaches the adhesive-adherend interface/interpahse where corrosion initiates. The focus of this study, however, is on the chemical and physical changes in the adhesive on a molecular level in the early, pre-damage stage that precedes microcracking and delamination, because that phase holds key to the understanding of the initiation and propagation of failure. The molecular picture of these events is far from complete and numerous questions remain unresolved. In what form (free, cluster, complexes etc.) does moisture exist in the adhesive? How does moisture interact with the host matrix and what effect does it have on the local dynamics and various properties? What is the nature of other migrating charges, extrinsic (e.g., ionic impurities) and/or intrinsic (e.g., hydrogen bond paths) in the adhesive and how these interact with moisture? What chemical changes (e.g., reactions) occur in the adhesive and do they include polymeric chains, moisture, other migrating charges, complexes etc.? What are the kinetics of all those events? What are the effects of temperature, pressure and relative humidity of the environment?

Let us now revert our attention to the major theme of the work presented here– elucidation of the fundamental science that describes the effect of environment on the microstructure and chemo-physical properties of adhesively bonded joints in the pre-damage stage. An essential condition that must be satisfied in a study of this kind is the ability to detect physical and chemical changes on a molecular level. The time scales of molecular dynamics that characterize the physics of adhesive joints range from picoseconds for segmental motions in the bulk to minutes or hours for reactions at interfaces, but it is the rapid (high-frequency) actions that are crucial here. Another important consideration is that in-situ real-time non-destructive measurements be used to

determine the on-set of failure (in addition to the various destructive and post-failure analyses that provide only an indirect insight into the temporal evolution of the chemo-physical changes in adhesive joints). The dielectric relaxation spectroscopy (DRS) and Fourier Transform Infrared (FTIR) spectroscopy are well-established non-destructive experimental techniques, and were extensively utilized in the present work for probing physical and chemical changes in adhesives on a molecular scale.

1.1 Background Information

Numerous authors [1-6] have studied the effect of environmental exposure on adhesive joints. The vast majority of those reports are based on (destructive) mechanical tests that are often followed by a microscopic investigation of fracture surfaces aimed at elucidating the locus of failure. Such studies, however, offer little direct information about the evolution of chemical and physical changes in adhesives during exposure to an aggressive environment. The reported dielectric measurements of adhesively joints exposed to aggressive environments were performed, as a rule, at lower frequencies and were directed towards an understanding of the effect of charge migration on resistivity and/or the mechanism and kinetics of chemical reactions at the polymer-metal interface that cause corrosion [7-11].

The action of the aggressive environment causes chemical and physical changes in the adhesive on a molecular level. The physical changes encompass molecular motions, mobility, relaxations, dynamics, etc. Chemical changes relate to the chemical state of the matter, chemical interactions that include hydrogen-bonded complexes, etc. The effect of absorbed moisture on molecular mobility and relaxations in the glassy state (physical aspect) is instantaneous but it can be detected only with an appropriate technique, such as (high frequency) DRS. Consider, for example, that

water at 20°C has a dielectric loss peak at about 20 GHz, which corresponds to the relaxation time of 9 picoseconds (1 ps = 10^{-12}s), and although the bulk of the adsorbed moisture in the adhesive is more likely to form hydrogen-bonded complex with the matrix, such relaxation process are still very fast and have been shown (see phase I results) to take place at frequencies above 1 MHz. A comprehensive dielectric study of the dynamics of such interactions, however, has not been reported hitherto in the literature. A rare example of the use of high-frequency dielectric measurements to study moisture absorption in adhesive joints is the work of Pethrick and coworkers [12-14], though their efforts have not focused on the underlying molecular mechanism. Instead, the main thrust of their work was aimed at the development of a field-operable non-destructive inspection (NDI) tool based on DRS. It is clear, however, that the success of their efforts hinges upon a through understanding of the relevant science, and hence our approaches are complementary. It is also worth noting that an excellent series of studies of water dynamics in biopolymers (DNA, proteins) by time domain reflectometry was reported by Mashimo and coworkers [15-17].

1.2 Research Objectives

The Principal objective of the present work is to perform scientific investigation of the correlation of high frequency dielectric measurements and chemical and physical changes in the adhesively bonded joints prior to damage initiation. Specifically, the technical objectives are:

a) to determine whether or not Dielectric Relaxation Spectroscopy (DRS), in conjunction with Fourier Transform Infrared Spectroscopy, could be used as a viable NDE technique to evaluate the pre-damage state of adhesively bonded joints exposed to an aggressive hygrothermal environment

b) Developing fundamental correlations between the measured dielectric and infrared response, and the chemical and physical changes in the pre-damage stage (i.e., before cracks and voids lead to degradation) in a series of adhesive joints with different chemical structures, exposed to aggressive environments,

c) Performing mechanical testing of double-notch shear bonded joints exposed to aggressive environmental conditions. Experimentally determine the effects of severe environment on bonded joint strength and failure modes, and

d) To correlate the measured dielectric and infrared response and the mechanical strength degradation of various adhesive-substrate systems.

1.3 Overview of the Study

This study is divided into six sections. Section 1 includes a general introduction and the objectives for the present research. Section 2 deals with the dielecetric relaxation spectroscopy and FTIR characterization of aluminum/model epoxy and aluminum/FM-73U adhesively bonded joints. Section 3 deals with the dielecetric relaxation spectroscopy and FTIR characterization of aluminum/bismaleimide bonded joints. Section 4 deals with the influence of environments on the strength and durability of adhesively bonded joints. The correlation between mechanical test results with dielectric relaxation data is also discussed in Section 4. The finite element analysis of adhesively bonded joints is discussed in section 5. The important findings of the present work are summarized in section 6.

References

1. Carfagna, C.; Apicella, A., J. Appl. Polym. Sci. 1983, 28, 2881.
2. Tiwari, R.K.; Dillard, J.G., J. Adhesion 2000, 73, 233.

3. Moy, P.; Karasz F.E., Polym. Eng. Sci. 1980, 20, 315.

4. Jelinski, L.W.; Dumais, J.J.; Stark, R.E.; Ellis, T.E.; Karasz, F.E. Macromolecules 1983, 16, 1019.

5. Kennan J.D.; Seferis, J.C.; Quinlivian, J.T. J. Appl. Polym. Sci. 1979, 24, 2375.

6. Mikols, W.J.; Sefiris, J.C.; Apicella, A.; Nicolais, L. Polym. Comp. 1982, 3, 118.

7. Kinloch, A.J. Adhesion and Adhesives, Chapman and Hall, NY, 1987, pp. 350-395.

8. Mansfeld, F. Corrosion 1996, 52, 417.

9. De Neve, B.; Shanahan, M.E.R. J. Adhesion 1995, 49, 165.

10. Nairn, B.J.; Dickstein, P.A.; Plausinis, D.J.; Spelt, J.K. J. Adhesion 1995, 48, 121.

11. Narducci, D; Cuomo, J.J.; Pappas, D.L.; Sachdev, K. in metallized Plastics 3: Fundamental and Applied Aspects, Mittal, K.L. Ed. Plenum Press, NY 1992, pp. 365-383.

12. Hayward, D.; Affrossman, S; Pethrick, R.A.; Wilford, P. Nondestr. Test Eval. 1991, 6, 45.

13. Li, Z-C; Hayward, D.; Gilmore, R.; Pethrick, R.A. J. Mater. Sci. 1997, 32, 879.

14. Pethrick, R.A. MRS Fall Meeting, Boston, MA, Dec. 1997.

15. Mashimo, S.; Miura, N.; Umchara, T. J. Chem. Phys. 1992, 97, 6759.

16. Miura, N.; Hayashi, Y.; Shinyashiki, N.; Mashimo, S. Biopolymers 1995, 36, 9.

17. Mashimo, S.; Miura, N. in Microwave Aquametry, IEEE Press, NY, 1996, pp. 93-99.

:TRIC RELAXATION SPECTROSCOPY OF FM-73U AND MODEL

›ects of chemical and physical changes in adhesive joints caused by absorbed investigated. The focus was on the pre-damage stage that precedes the formation microcracks. A model and a commercial epoxy-amine formulation were studied. cs were monitored by broad-band dielectric relaxation spectroscopy (DRS). One absorbed water does not form hydrogen bonds with the network and gives rise to a ı process (termed γ) with activation energy of 28 kJ/mol. The local β dynamics are by the interactions between water and various sites on the network that include the , the hydroxyl group and the tertiary amine nitrogen. One particularly significant ıt the average relaxation time for the β process above 20^0C is of the order of or less, and hence its detection hinges on the ability to perform high precision DRS s above 1 MHz. This is an important consideration in the ongoing efforts aimed at ›ntation of DRS as non-destructive inspection (NDI) tool for adhesive joints. of cyanate ester resins and bismaleimide resins are in progress.

uction

ıl and physical changes in adhesive joints in service occur at a rate that depends on 1 severity of the aggressive environment (we use term "aggressive" to stress that ›nment will have some effect on the bondline, though on a different time scale). ıanges relate to the chemical state of the matter, as defined by the composition and teractions (e.g., complex formation, hydrogen bonding), while *physical* changes the variations in molecular motions and mobility, relaxation dynamics, etc. The the studies reported hitherto, however, have been concerned with the effect of

moisture on *macroscopic* (bulk) properties and the detection of delamination and loss of adhesion that occur when water eventually diffuses through the adhesive and reaches the adhesive/adherend interface/interphase[1-11]. Our interest focuses on the *molecular events* in glassy adhesives in the pre-damage stage, where numerous fundamental questions remain unanswered. In what form (single molecules, dimers, trimers, complexes) the absorbed water resides in the adhesive? How does water interact with the host matrix and what effect that has on the local dynamics? What are the effects of the temperature, pressure and relative humidity of the environment? It is expected that the knowledge gained in this program will usher the way for the development of methodology that can predict the course of subsequent degradation and thus anticipate failure.

There is paucity of information about the effect of absorbed moisture on the local dynamics in glassy adhesives. Difficulties arise because the time scale of molecular motions that characterize local dynamics in these materials can be as fast as few picoseconds, and an experimental technique operable at high frequency (where fast processes are observed) and adaptable to adhesive configuration is needed. Broad-band dielectric relaxation spectroscopy (DRS) is one method that meets those requirements. The interpretation of DRS data on a molecular level can be greatly aided by the use of a complementary technique capable of providing information in real time about the chemical state of the matter. Of such techniques, Fourier Transform Infrared Spectroscopy (FTIR) represents the most attractive choice because of: 1) the unmatched wealth of the information about the chemical state of the matter contained in the infrared portion of the electromagnetic spectrum, 2) the adaptability of near-IR (NIR) to remote (fiber-optic) in-situ real time application, and 3) the possibility of using NIR for NDI. The combined use of DRS and

NIR spectroscopy is designed to afford a simultaneous examination of *physical* (DRS) and *chemical* (FTIR) changes at a molecular level in adhesive joints exposed to an aggressive environment.

2.2 Theoretical Background

In an isotropic amorphous system, with negligible internal field factors, dielectric permittivity is related to the dipole moment correlation function by a Fourier transformation:[12]

$$\frac{\varepsilon^*(\omega)-\varepsilon_\infty}{\varepsilon_0-\varepsilon_\infty}=1-i\omega\int_0^\infty\left[\exp(-i\omega t)\right]\Phi(t)dt \qquad (1)$$

where ε_0 is the limiting low-frequency value of the dielectric permittivity, ε_∞ is the limiting high-frequency dielectric permittivity, ω is angular frequency, and $\Phi(t)$ is the relaxation kernel that can be obtained from the dipole correlation function:[12]

$$\Phi(t)=\frac{\sum_i^N\sum_j^N\langle\mu_i(0)\mu_j(t)\rangle}{\sum_i^N\sum_j^N\langle\mu_i(0)\mu_j(0)\rangle} \qquad (2)$$

where μ_i (0) and μ_i (t) denote the elementary dipole moment of a molecule i at time t=0 and t, respectively. The correlation function expressed in this form takes into account both equilibrium and dynamic angular correlations between molecules. The relaxation kernel, $\Phi(t)$, (eqs 1 and 2) is often quantified via a stretched exponential function of the Kohlrausch-Williams-Watts [14] (KWW) type:

$$\Phi(t)=Ce^{-(t/\tau)^\beta} \qquad (3)$$

where C is a constant, τ is the relaxation time and β is the stretching exponent ranging form 0 to 1. The KWW function is commonly used to describe the (skewed) α process in the isotropic

state. The relaxation kernel can be also evaluated from the experimental data. To do that it is sufficient to use only one portion of the permittivity, real or imaginary, in eq 1, since they are related by the Kramers-Kronig transform. For example, by taking the imaginary part of the Fourier transform of eq 1 we obtain:

$$\Phi(t) = \frac{2}{\pi}\int_0^\infty \frac{\varepsilon''(\omega)}{\varepsilon_0 - \varepsilon_\infty}\frac{\cos(\omega t)}{\omega}d\omega \qquad (4)$$

In our earlier studies, however, instead of transforming the frequency domain dielectric data into the time domain using a discrete Fourier transform, where spectral features may be truncated, we would transform the relaxation kernel $\Phi(t)$ into the frequency domain, using the technique described by Dishon et al.[15] and then fit the experimental data to the transformed kernel with appropriate parameters. Alternatively, ε^* may be modeled by a number of empirical functions in the frequency domain; a particularly popular and robust form is the Havriliak-Negami[16] (HN) function given as:

$$\varepsilon^*(\omega) = \varepsilon_\infty + \frac{\varepsilon_0 - \varepsilon_\infty}{\left[1 + (i\omega\tau_{HN})^a\right]^b} + i\frac{\sigma}{\omega\varepsilon_v} \qquad (5)$$

where a and b are the dispersion shape parameters, σ is the conductivity, ε_v is the vacuum permittivity, and the other parameters are defined in eq 1. The HN equation is a generalization of the Cole-Cole (CC) equation, to which it reduces for b=1, and a generalization of the Cole-Davidson (CD) equation, to which it reduces for a=1. HN and CC functional forms were employed in this study to describe local dynamics.

2.3 Experimental Materials

Two multifunctional epoxy-amine formulations were investigated: a model system and a commercial system. The model system consisted of diglycidyl ether of Bisphenol A or DGEBA

(Aldrich Chem. Co.) and methylene dianiline or MDA (Aldrich Chem. Co.). The stoichiometric amounts of epoxy groups and amine hydrogen were used and the components were mixed until a clear mixture was obtained. The cure schedule consisted in heating the sample from 20 to 180^{0}C at 5^{0}C/min and maintaining it at 180^{0}C for 30 min. The DSC Tg_∞ was 170^{0}C. The commercial sample investigated was an unsupported epoxy-amine adhesive film (FM73) supplied by Cytec fiberite. The cure schedule consisted in heating from 20 to 110^{0}C at 5^{0}C/min and maintaining it at 110^{0}C for 60 min. The DSC Tg_∞ was 93^{0}C. Samples were cured between aluminum adherends. The adherend surface was cleaned with a solvent (acetone) prior to the application of the resin. The bondline thickness was 50μm. All samples used in this study were fully cured (DSC and FTIR controls were run) and were subjected to an identical thermal history (by heating above the Tg_∞) prior to the exposure to environment in order to minimize the effect of structural relaxation between different samples. Then, samples were placed in a controlled environment at 60^{0}C and 98% relative humidity (maintained with a saturated $NaHSO_4$ solution) and tested at desired time intervals.

2.4 Techniques

The principal experimental technique we have used is broad-band dielectric relaxation spectroscopy (DRS). A detailed description of our experimental facility for dielectric measurements is given elsewhere; [17, 18] however, briefly, we have used Solartron 1260 Impedance Gain Phase Analyzer (10 μHz – 32 MHz) with broad-band dielectric converter (Novocontrol GmBh), Hewlett-Packard (HP) 4284 A Precision LCR Meter (20 Hz - 1 MHz), Hewlett-Packard 4291 A RF Impedance Analyzer (1 MHz - 1.8 GHz) and Hewlett-Packard 8752A Network Analyzer (300 kHz – 1.3 GHz). All instruments are interfaced to computers via

IEEE 488.2 and are equipped with heating/cooling capabilities, including Novocontrol's Novocool System. A variety of sample cells were employed, including parallel plates, high precision extension airlines, cells for the simultaneous dielectric/remote fiber optic FTIR tests, etc. Supporting evidence was obtained from Fourier transform infrared (FTIR) spectroscopy, using Nicolet Instrument's Magna 750 Spectrometer as described elsewhere,[19] and differential scanning calorimetry (DSC), using Perkin-Elmer model 7 DSC at a heating rate of 10°C/min.

2.5 Results and Discussion

We begin by presenting the results for our model system, composed of the stoichiometric amounts of DGEBA and MDA. This system is miscible and has a calorimetric Tg of -12^0C prior to the onset of curing reactions. Dielectric permittivity and loss in the frequency domain (note 11 decades of frequency) with temperature as a parameter *before* the onset of cure are shown in Figure 2.1. The solid lines are fits to the HN functional form (eq 5). Since dielectric permittivity and loss are related by the Kramers-Kronig transforms, the remaining figures in the paper contain only the dielectric loss data. The segmental α process and the local β process are clearly observed, in agreement with earlier results for similar systems.[20-22] We reiterate that the uncured system is shown as reference only and all subsequent results pertain to fully cured networks. A fully cured DGEBA-MDA network (prepared according to the schedule described in the experimental section) had a calorimetric Tg_∞ of 170^0C. Dielectric loss in the frequency domain of a fully cured sample is shown in Figure 2.2. In the temperature range of Figure 2.2 the network is well below its calorimetric Tg_∞ and we observe only the secondary β relaxation. Because of its localized nature, the β process is precisely what we are interested in (we shall not be concerned with the dynamics of the (slow) segmental α process in cured glassy networks). In

general, the origin of these β relaxations remains elusive, but appeals have been made in the literature to explanations ranging from far-IR phonon excitations,[23] cage-rattling motions,[24] a universal glassy state phenomenon,[25] and various types of local/side-chain motions.[26] In cured epoxy networks, however, it is generally agreed that the origin of the β process lies in the local motions associated with hydroxyl groups.[27] This interpretation seems to be amply supported by the results of our study, as will be shown later. With decreasing temperature the β process in Figure 2.2 slows down, broadens and decreases in intensity. Also, the β process is Arrhenius but thermodielectrically complex.

Once the dynamics of the fully cured dry network were established, we proceeded with a systematic study of the effect of absorbed moisture on the local dynamics. We preface the presentation and discussion of these results with two important comments. First, we stress that we shall not be principally concerned here with the kinetics of moisture absorption. And second, we acknowledge numerous efforts to quantitatively monitor moisture absorption by tracking dielectric permittivity at an arbitrary frequency, [8, 28-31] but hasten to add that the dielectric response of a changing structure is a function of both exposure time *and* frequency. Therefore, if one is interested in *dynamics*, the only fundamentally correct way to track it is by recording the relaxation spectrum over a wide frequency range. Because of the local nature of β relaxations, it was anticipated that the dynamics of this process would be particularly sensitive to the absorbed moisture from the very beginning of exposure to environment. In that case the β process could serve as a molecular indicator of the local dynamics that are governed by the interactions between the thermoset network and the absorbed moisture. Figure 2.3 shows dielectric loss in the frequency domain measured at various temperatures, following a 3-day exposure to

60^0C/90%RH. There is practically no change in the average relaxation time (defined as $\tau=1/2\pi f_{max}$) for the β process after 3 days, in comparison with a dry sample (contrast Figures 2.2 and 2.3). But we do observe an increase in intensity and a clear sign of the emergence of another relaxation, first manifested as a shoulder on the high frequency side. This new process, which we term γ, becomes more pronounced after a 5-day exposure, as seen in Figure 2.4. A deconvolution of two relaxations was performed and an example is shown in Figure 2.5; the presence of two processes is beyond doubt and the deconvolution is physically meaningful. Both processes are symmetric and the solid lines in Figure 2.5 are fits to the Cole-Cole (CC) equation. An alternative way of displaying the effect of absorbed moisture on the local dynamics is by plotting the dielectric loss in the frequency domain at a constant measuring temperature and with exposure time as a parameter. One such example is presented in Figure 2.6 (measured at -30^0C), which clearly shows the gradual development of β and γ relaxations with increasing exposure time.

The frequency of maximum loss for different relaxation processes is plotted as a function of reciprocal temperature in Figure 2.7. Both β and γ processes are Arrhenius, with activation energy of 53-57 kJ/mol and 28 kJ/mol, respectively. The β process in the dry sample appears to be a bit faster and to have a slightly lower activation energy than in the moist samples. The activation energy for the γ process is of the order of magnitude generally observed for the local (Johari-Goldstein[25]) processes in many polymers. The dielectric strength of β and γ processes was found to increase with exposure time and with measuring temperature.

An important question is what are DRS data telling us about the molecular origin of β and γ relaxations? First, it is evident that the dynamics of the β process change with absorbed moisture. The initial relaxations associated with hydroxyl groups are slowed down (by about ½ decade with respect to the dry sample) through the interactions between the network and a portion of the absorbed water molecules. The precise nature of these interactions will be discussed further with the results of FTIR measurements. The faster γ process is due to the other portion of the absorbed water molecules (that are not engaged in water-network interactions) although it is also not immediately clear from DRS data in what form (isolated single molecules, dimers, trimers) water resides within the adhesive. In comparison with liquid water, which at 20^0 C has a dielectric loss peak at about 20 GHz (corresponding to an average relaxation time of about 9 picoseconds),[32] the relaxation time of the γ process is longer by more than a decade on the frequency scale. Whether the reason for this is physical (e.g. steric hindrance due to neighboring benzene rings) or chemical (e.g. some weak interactions with network groups), is not apparent from the DRS data. The average relaxation time of the γ process at 20 ^{0}C is of the order of 1,000 ps. Interestingly, this is in agreement with the value of 700 ps reported by Jelinski et al. in their study of water in DGEBA/m-MDA networks by solid state NMR spectroscopy.[33] That time (700 ps) was described as the average residence time of a water molecule at one site before it hops to another site. These authors also argue that "free" water (defined as isotropically mobile with the same relaxation time as liquid water) is not present. Strictly speaking this is true, though our FTIR evidence (offered below) suggests that non hydrogen-bonded water exist as isolated molecules whose dynamics are slightly slowed down by steric hindrance. More about the size and form of the interactions that underlie the γ process will be said in conjunction with the results of FTIR measurements and molecular simulation studies.

The fully cured FM73 commercial adhesive (prepared according to the schedule described in experimental section) had a calorimetric Tg_{∞} of 93^0C. Dielectric loss in the frequency domain with temperature as a parameter for this sample is shown in Figure 2.8. With decreasing temperature the β process slows down and broadens, displaying a response similar to that of the model system. The loss spectrum for the β process in the dry sample is also symmetric and the solid lines in Figure 2.8 represent fits to the CC equation. In Figure 2.9 we show the loss data measured at 25^0C after 2, 4 and 8 hours of exposure to environment. The average relaxation time (see the location of f_{max}) increases slightly within the first two hours and then levels off, while the loss intensity continues to increase. The shape of the spectrum, however, remains symmetric and the solid lines in Figure 2.9 are CC fits. But after a 10-day exposure there was one noticeable difference; the spectra were asymmetric and were described by the HN functional form (see Figure 2.10). The asymmetric shape of the spectrum is not typical of the β process and we interpret it as a consequence of the overlap of β and γ relaxations. And although we did not observe a separate γ process, its presence is strongly supported by a broad high frequency tail that is particularly evident in the low temperature spectra. The fact that we do not see a separate γ process, as in the model system, is not necessarily surprising considering a difference in the chemical composition between these two formulations. We made no attempts at deconvolution of spectra in Figure 2.10 (because the result would have little physical justification) and have continued to treat this relaxation as one (β) process (while aware of possible drawbacks). An alternative view of the effect of absorbed moisture on the β dynamics is depicted in Figure 2.11, which shows dielectric loss in the frequency domain with exposure time as a parameter, measured at 60^0C. Solid lines in this figure are HN fits. Several important observations are made in this figure. First, note that the average relaxation time ($\tau=1/2\pi f_{max}$) for *the β process at*

temperatures above ca. 25^{0}C is of the order of nanoseconds or less and hence its detection hinges on the ability to conduct *high precision dielectric measurements in the frequency range above 1 MHz.* This is an important consideration in the ongoing efforts aimed at the implementation of DRS as a NDI tool for adhesive joints. Further, it is interesting to note that while the loss peak intensity increases with exposure time, the average relaxation time measured at 60^{0}C remains largely unaffected by the absorbed moisture. But as the measuring temperature is decreased, we observe a progressive divergence in the average relaxation time for dry and moist samples, as evidenced by data in Figure 2.12 measured at -70^{0}C. This divergence is best seen in the composite plot of frequency of maximum loss as a function of reciprocal temperature, shown in Figure 2.13. Note that both processes are Arrhenius, with activation energy of 41 kJ/mol and 60 kJ/mol for dry and moist samples, respectively. Finally, we note that the β dynamics were reversible upon moisture desorption.

Next we present and discuss the results of near-IR (NIR) and mid-IR (MIR) analysis of the model (DGEBA/MDA) system. The NIR spectra of dry and moist (fully cured) DGEBA/MDA networks are contrasted in Figure 2.14. All major peaks of relevance in epoxy/amine systems are present: epoxy absorption at 4530 and 6080 cm^{-1}, amine absorption at 5056 and 6670 cm^{-1}, and hydroxyl absorption at 4800-4900 cm^{-1} and 7000 cm^{-1}. A comprehensive identification of the NIR spectra of epoxy networks before, during and after cure is given elsewhere;[34] here we focus attention on the peak at 5210 cm^{-1}, which is associated with the absorbed moisture. The observed spectral difference in Figure 2.14 establishes this peak as the indicator of absorbed moisture. Figure 2.15 shows a sequence of NIR spectra taken at selected time intervals during environmental exposure. An increase in the absorption intensity is evident. Careful inspection of

Figure 2.15 also reveals a consistent increase in the absorption intensity at the lower wavenumber side of the 5210 cm^{-1} peak, suggesting a gradual development of another absorption mechanism. This is an interesting finding. A deconvolution of the broad absorption was carried out and two absorption peaks were clearly detected, as seen in Figure 2.16. These two peaks were centered at 5230 and 5137 cm^{-1}, respectively, and were both Gaussian. The absorption intensity of each peak is a linear function of absorbed moisture, as shown in Figure 2.17. But because the absorption in this range is associated with a combination of bending (1600-1650 cm^{-1}) and stretching (3100-3800 cm^{-1}) vibrations, we made no further attempts at identifying these peaks with specific interactions. In an excellent recent study of water absorption in a tetrafunctional epoxy/amine (TGDDM/DDS) network by NIR, Musto et al.[35, 36] were able to deconvolute the broad absorption at around 7000 cm^{-1} into three distinct components centered at 7075, 6820 and 6535 cm^{-1}, respectively. These peaks were associated with isolated single water molecules (7075), water molecules hydrogen-bonded to one site (6820) and water molecules hydrogen-bonded to two sites (6535). An important finding in their study was that each water molecule interacts with two proton acceptors. We were hesitant to deconvolute the absorption peak around 7000 cm^{-1} in our networks because of insufficiently high resolution.

The MIR spectra of a sample exposed to moisture for times ranging from 10 minutes to 8 days are shown in Figure 2.18. Of major interest here is the range between about 3100 and 3800 cm^{-1}, where vibrational modes due to various forms of hydrogen bonding are located. Normalization of spectra with respect to absorption due to phenyl group (at 3035 cm^{-1}) and alkyl groups (at 2963, 2930 and 2872 cm^{-1}) enables one to track the change in the absorption intensity in the range between 3100 and 3800 cm^{-1} as a function of exposure time. This is clearly seen in Figure 2.18.

A further insight into the progressive effect of absorbed moisture is obtained by subtracting the spectrum of a dry sample from that of each moist sample. The resulting spectra are shown in Figure 2.19 and two distinct regions are observed: a sharp absorption around 3600 cm^{-1} and a broad and asymmetric absorption between about 3600 and 3100 cm^{-1}. The intensity of both absorptions increases with increasing exposure time. The question is what is the origin of these absorption peaks? First, we consider the narrow absorption at high wavenumber that was fit to a Gaussian function with a peak at 3626 cm^{-1} (Figure 2.20). This absorption has been observed in a number of systems with low water concentration, ranging from polymer networks[35, 36] to mixtures of water and a non-polar solvent (e.g., CCl_4),[37-39] and has been associated with non-hydrogen bonded water. In our epoxy-amine network, this absorption is assigned to water molecules located in the pockets surrounded by hydrophobic moieties, such as benzene rings, where the likelihood of hydrogen bonding is low. Based on the MIR data, the non hydrogen-bonded water accounts for about 13% of the total absorbed water. The ability to measure precisely the concentration of a dipole group raises interesting possibilities as regards the correlation between vibrational and dielectric spectroscopy. Recall that non hydrogen-bonded water, that gives rise to a MIR absorption peak centered at 3626 cm^{-1}, is also at the origin of the dynamic γ process. This, in effect, provides a link between chemical (measured by FTIR) and physical (measured by DRS) phenomena that accompany water absorption into the network. For example, a correlation could be sought between the concentration of dipoles extracted from FTIR spectra and the dielectric strength of a relaxation process (e.g. β or γ) via the Kirkwood-Frohlich equation.

We next proceeded with attempts to deconvolute the broad absorption range between 3600 and 3100 cm^{-1}. The best results were obtained using three Gaussian functions, as shown in Figure 2.20, with peaks at 3523, 3380 and 3210 cm^{-1}. The intensity of each absorption (as defined by the area under the absorption peak) increases with increasing exposure time, as seen in Figure 2.21. But when each absorption intensity is normalized with respect to the total intensity, we observe an increase in the absorption at 3210 cm^{-1}, a decrease at 3380 cm^{-1}, and little change at 3523 and 3626 cm^{-1} (see Figure 2.22). The presence of several absorption peaks tells us two things: 1) the absorption mechanism is more complex than originally thought, and 2) the concept of two types of absorbed moisture, often lumped under "loosely" and "strongly" bound, is an oversimplification of the actual situation. But what can we say about the molecular origin of absorption at 3523, 3380 and 3210 cm^{-1}? For one, the hydrogen-bonded water accounts for approximately 87% of the total water absorbed in the network. We note that this number is considerably higher than the values between 60 and 40 % reported by other investigators.[29, 36] Further, it is known that the intensity of hydrogen bonding increases with decreasing wavenumber, i.e., from 3523 to 3210 cm^{-1} in our case. We have also observed an increase in the intensity of absorption peaks at 3380 and 3210 cm^{-1} during environmental exposure, as evidenced by a shift to lower frequency by about 40 and 50 cm^{-1}, respectively. But the identification of each absorption peak with a specific type of hydrogen bond is not straightforward. In a DGEBA/MDA network, absorbed water can form a hydrogen bond with a number of sites on the network, including the ether oxygen, the hydroxyl group and the tertiary amine nitrogen. Moreover, the same water molecule can participate in one or two hydrogen bonds (with two proton acceptors) when a favorable steric configuration is encountered. Naturally, if the absorbed water forms dimers or trimers, there will also be a possibility of

hydrogen bonding between the adjacent water molecules. The last scenario brings up an interesting question: how large are the absorbed water entities? In an attempt to answer this important question we performed a dynamics simulation study with the aid of a commercial software package Cerius[2]. A stoichiometric DGEBA/MDA composed of twenty-six molecules of DGEBA and thirteen molecules of MDA was constructed. Nine molecules of water were introduced into the network, bringing the water content to about 1.6% by weight (a reasonable value considering that the maximum water content at the conditions of this study was ca. 3% by weight). The molecules were annealed until the total energy reached a minimum value and the simulation was conducted at 300^0K. The positions of atoms were calculated at 0.001 picosecond intervals and this was repeated 1,000 times in the course of simulation. Although our simulation was limited to a relatively small network, important observations were made. First, fluctuations involving network atoms and water molecules were detected. But most importantly, the absorbed water molecules were always separate and no dimers or trimers were observed. Apparently, the available space in the fully cured networks is too small to accommodate larger structures. Simulation has also revealed that a water molecule participates in hydrogen bonding to only one site on the network, in contrast with the experimental results reported elsewhere. It is clear that a simulation study on a larger network would be useful in this context.

A final comment regards our current efforts aimed at the development of fundamental quantitative correlation between FTIR and DRS data. Specifically, we are seeking to correlate a dielectric material parameter (such as the average relaxation time, dielectric strength or a shape parameter of the dielectric spectrum) with a fundamental parameter deduced from the FTIR spectra (e.g., absorption strength, group concentration). This is the subject of our current work.

2.6 Work in Progress

We are currently investigating Ciba Geigy's Matrimid 5292 (this work is discussed in detail in section 3 of this report). This is a two-component bismaleimide (BMI) composed of bismaleimido diphenylmethane and diallyl bisphenol A. DSC runs were performed on the as-mixed and cured mixtures. The initial mixture had a Tg of 10^0C. The cured resin, on the other hand, is highly cross-linked, making it difficult to detect a Tg with great accuracy. We are working on that. DRS of dry samples shows a β relaxation above 50^0C but not at lower temperature. After a 24-hour exposure to environment, however, we observe a faster process (termed γ) at low temperature, as clearly seen in Figure 2.23. The solid lines are fits to the CC equation. The calculated value of activation energy was 40 kJ/mol. This value is closer to that for the β process (than the γ process) in DGEBA/MDA networks. A composite plot of frequency at dielectric loss maximum as a function of reciprocal temperature for BMI, DGEBA/MDA and FM73U is shown in Figure 2.24. It is clear that the γ process in BMI is related to absorbed water and a systematic study is underway. Initial NIR measurements show an increase in absorbance at 5200 cm^{-1}. Initial MIR result shows an effect of moisture on the 3100 – 3800 cm^{-1} absorption range and further analysis is in progress.

Finally, we have also initiated a study of a cyanate ester resin (Ciba Geigy's XU366). DRS spectra of a dry sample show a broad dielectric loss of low intensity ($\varepsilon''<0.02$). However, the loss intensity increases during exposure to moist environment and we anticipate that we will be able to relate the observed change in the dielectric loss to the absorbed moisture.

2.7 Conclusions

The results presented here provide new insight into the local molecular dynamics and interactions of epoxy/amine networks with water. A smaller portion of the absorbed water does not form hydrogen bonds with the network. The probable cause for that is steric hindrance imparted by the surrounding network. Molecular dynamics simulation indicates that water is absorbed in the form of isolated single molecules; no evidence of dimers or trimers was found. These water molecules also contribute to a dynamic γ process with activation energy of about 28 kJ/mol. The average relaxation time of the γ process at 20^0C is more than an order of magnitude longer than that of liquid water because of the steric factors.

A larger part of absorbed water interacts with various sites on the network that include the ether oxygen, the hydroxyl group and the tertiary amine nitrogen. Deconvolution of absorption peaks in NIR and MIR spectra was performed successfully, but the identification of each absorption with a specific type of water-network interaction is not straightforward and more should be learned before such assignments are made. The water-network interactions also have an effect on the local β dynamics. In the dry sample, the β process is associated with the localized motions of hydroxyl groups. The initial β relaxation is slowed down by almost a decade through the interactions of the absorbed water with the network, while the relaxation spectrum broadens with decreasing temperature. One particularly important finding is that the average relaxation time for the β process at temperatures above 25^0C is of the order of nanoseconds or less and hence its detection hinges on the ability to perform high precision dielectric measurements in the frequency range above 1 MHz. This is an important consideration in the ongoing efforts aimed at the implementation of DRS as non-destructive inspection tool for adhesive joints.

References and Notes

1. Gledhill, R. A. and Kinloch, A. J. *J. Adhesion* **6**, 315 (1974).
2. Browning, C. E., *Polym. Eng. Sci.* **18**, 16 (1978).
3. Keenan, J. D., Seferis, J. C. and Quinlivan, J. T., *J. Appl. Polym. Sci.* **24**, 2375-2387 (1979).
4. Rowland, S. P., Ed., *Water in Polymers* (ACS Symposium Series 127, American Chemical Society, Washington, DC, 1980).
5. Sedlacek, B. and Kahovec, J. Eds., *Crosslinked Epoxies* (Walter de Gruyter, Berlin, 1987).
6. Kaelble, D. H., Moacanin J. and Gupta, A., in *Epoxy Resins Chemistry and Technology* (Marcel Dekker, New York, 1988), May, C. A., Ed., Chap. 6, 603.
7. Apicella, A., in *International Encyclopedia of Composites* (VCH Publishers, New York, 1990), Lee, S. M. Ed., Vol. 2.
8. Nairn, B. J., Dickstein, P. A., Plausinis D. J. and Spelt, J. K., *J. Adhesion* **48**, 121-136 (1995).
9. de Neve, B. and Shanahan, M. E. R., *J. Adhesion* **49**, 165-176 (1995).
10. Maggana, C. and Pissis P., *J. Polym. Sci. Part B: Polym. Phys.* **37**, 1165-1182 (1999).
11. Soles, C. L., Chang, F. T., Gidley, D. W. and Yee, A. F., *J. Polym. Sci. Part B: Polym. Phys.* **38**, 776-791 (2000).
12. Willams, G., Dielectric Properties, in *Comprehensive Polymer Science* (Pergamon, Oxford, 1989), Eds., Allen G., Bevington J. C., Vol. 2, Chap. 7, 601-632.
13. Williams, G., Molecular Aspects of Multiple Dielectric Relaxation Processes in Solid Polymers, in *Advances in Polymer Science* (Springer-Verlag, Berlin, 1979), Eds., Cantow, H.-J. et al., Vol. 33, 59-92.
14. Williams, G., Watts, D. C., *Trans. Faraday Soc.* **66**, 80 (1970).
15. Dishon, M., Weiss, G. H., Bendler, J. T., *J. Res. Natl. Bur. Stand.* **90**, 27 (1985).

16. Havriliak, S. Jr. and Negami, S., *Polymer* **8**, 161 (1967).

17. Fitz, B., Andjelic, S. and Mijovic, J., *Macromolecules* **30**, 5227-5238 (1997).

18. Andjelic, S., Fitz, B. and Mijovic, J., *Macromolecules* **30**, 5239-5248 (1997).

19. Mijovic, J. and Andjelic, S., *Macromolecules* **29**, 239-246 (1996)

20. Casalini, R., Corezzi, S., Fioretto, D, Livi, A. and Rolla, P. A., *Chem. Phys. Lett.* **258**, 470 (1996).

21. Corezzi, S., Capaccioli, S., Gallone, G., Livi, A. and Rolla, P. A., *J. Phys.: Condens. Matter* **9**, 6199 (1997).

22. Fitz, B. D., Mijovic, J., *Macromolecules* **32**, 4134-4140 (1999).

23. Angell, C. A., Boehm, L., Oguni, M. and Smith, D. L., *J. Mol. Liq.* **56**, 275 (1993).

24. Lewis, L. J. and Wahnstrom, G., *Phys. Rev. E* **50**, 3865 (1994).

25. Johari, G. P. and Goldstein, M., *J. Chem. Phys.* **53**, 2372 (1970).

26. Meier, G., Fujara, F. and Petry, W., *Macromolecules* **22**, 4421 (1989).

27. Andjelic, S. and Mijovic, J., *Macromolecules* **31**, 8463-8473 (1997).

28. Li, Z-C., Hayward, D., Gilmore, R. and Pethrick, R. A., *J. Mater. Sci.* **32**, 879-886 (1997).

29. Grave, C., McEwan, I. and Pethrick, R. A., *J. Appl. Polym. Sci.* **69**, 2369-2376 (1998).

30. Affrossman, S., Banks, W. M., Hayward, D. and Pethrick, R. A., *Proc. Inst. Mech. Eng.* **214**, Part C, 87-102 (2000).

31. Day, D. R.; Shepard, D. D.; Craven, K. J. *Polym. Eng. Sci.* **32**, 524 (1992).

32. Barthel, J., Bachuber, K., Buchner, R., Hetzenauer, H., *Chem. Phys. Lett.* **195**, 369-373 (1990).

33. Jelinski, L. W., Dumais, J. J., Cholli, A. L., Ellis, T. S. and Karasz, F. E., *Macromolecules* **18**, 1091-1095 (1985)

34. Mijovic, J., Andjelic, S., *Macromolecules* **28**, 2787-2796 (1995).

35. Musto, P., Mascia, L., Ragosta, G., Scarinzi, G., Villano, P., *Polymer* **41**, 565-574 (2000).

36. Musto, P., Ragosta, G. and Mascia, L., *Chem. Mater.* **12**, 1331-1341 (2000).

37. Harris, D. C., Bertolucci, M. D., *Symmetry and Spectroscopy* (Dover Publications, New York, 1989), Chap. 3, 93-224.

38. Luck, W. A. P., Infrared Studies of Hydrogen Bonding in Pure Liquids and Solution, in *Water, A Comprehensive Treaties* (Plenum Press, New York, 1973), F. Franks Ed., Vol. 2, Chap. 4.

39. Gragson, D. E. and Richmond, G. L., *J. Phys. Chem. B* **102**, 569-576 (1998).

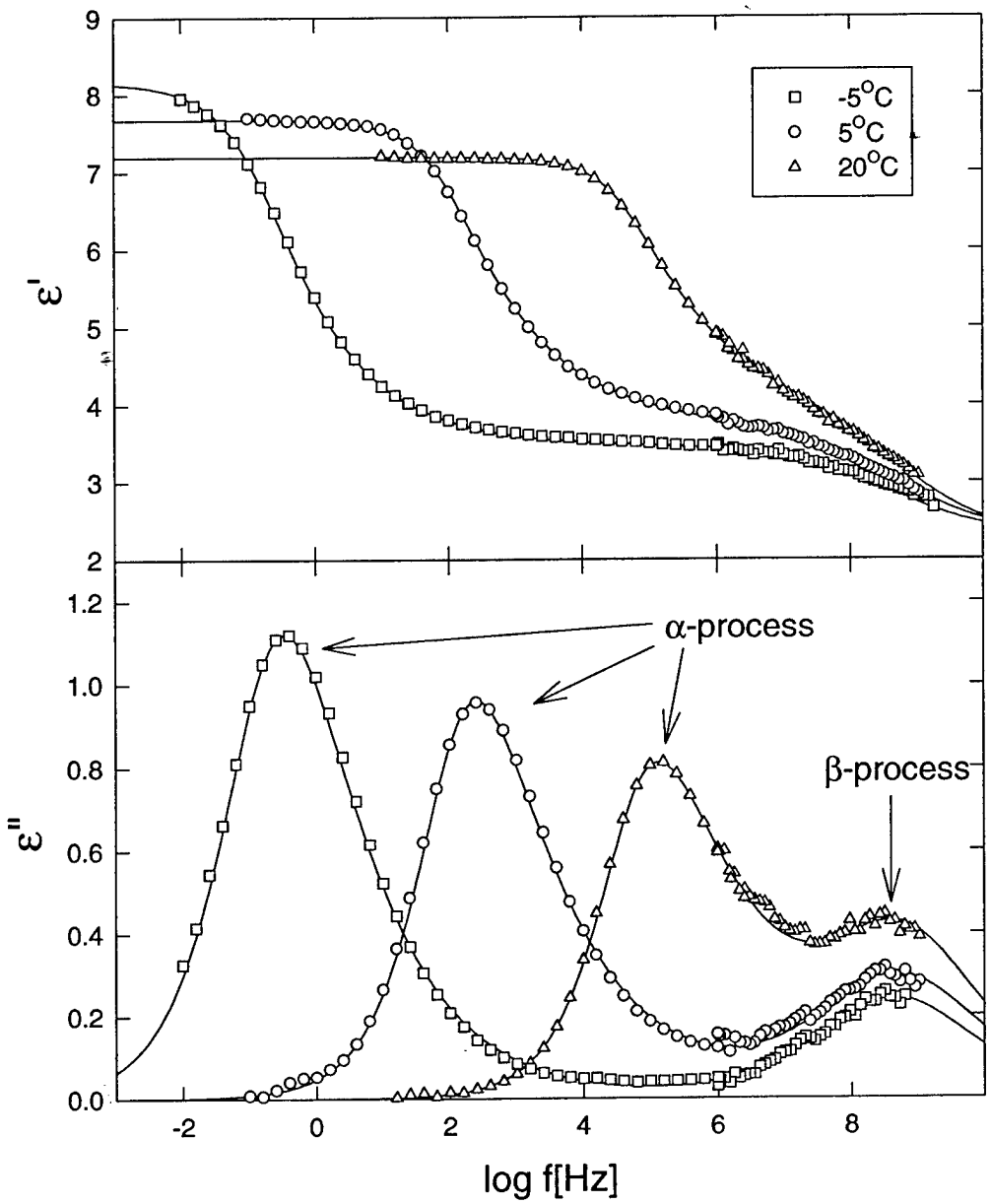

Figure 2.1. **Dielectric permittivity and loss in the frequency domain for uncured DGEBA/MDA mixture with temperature as a parameter. Solid lines are fits to Havriliak-Negami equation.**

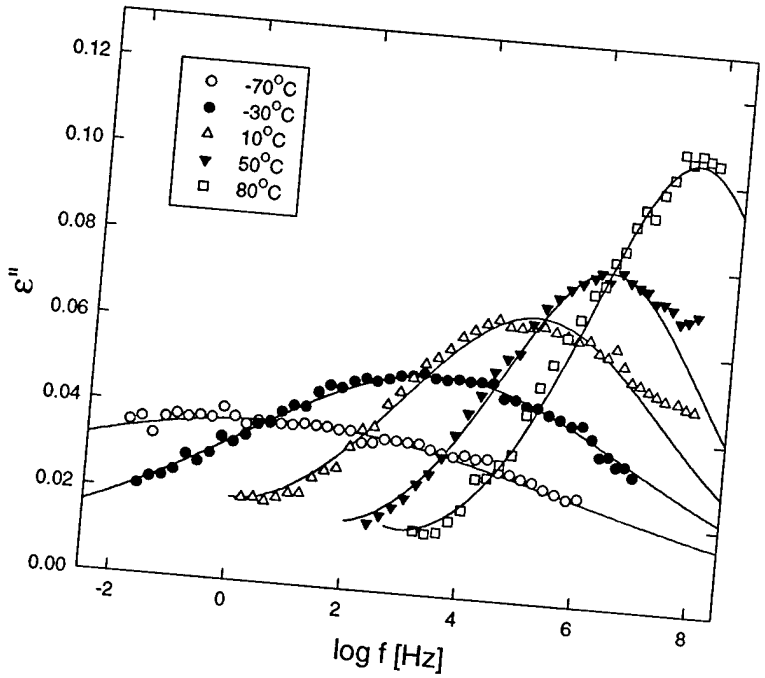

Figure 2.2. Dielectric loss in the frequency domain for fully-cured DGEBA/MDA with temperature as a parameter. Solid lines are fits to Havriliak-Negami equation.

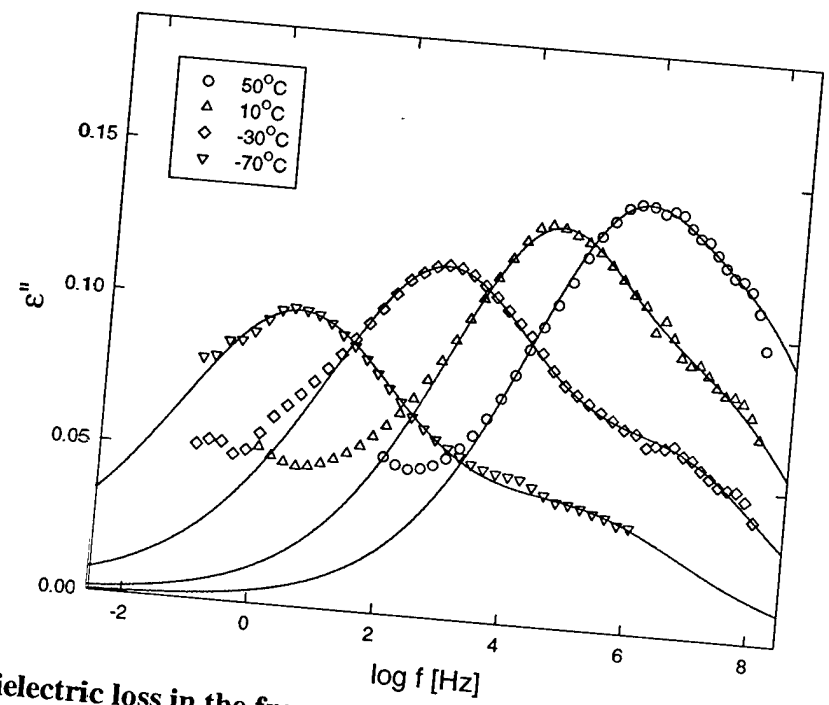

Figure 2.3. Dielectric loss in the frequency domain for fully-cured DGEBA/MDA with temperature as a parameter after 3-day exposure to environment. Solid lines are fits to Havriliak-Negami equation.

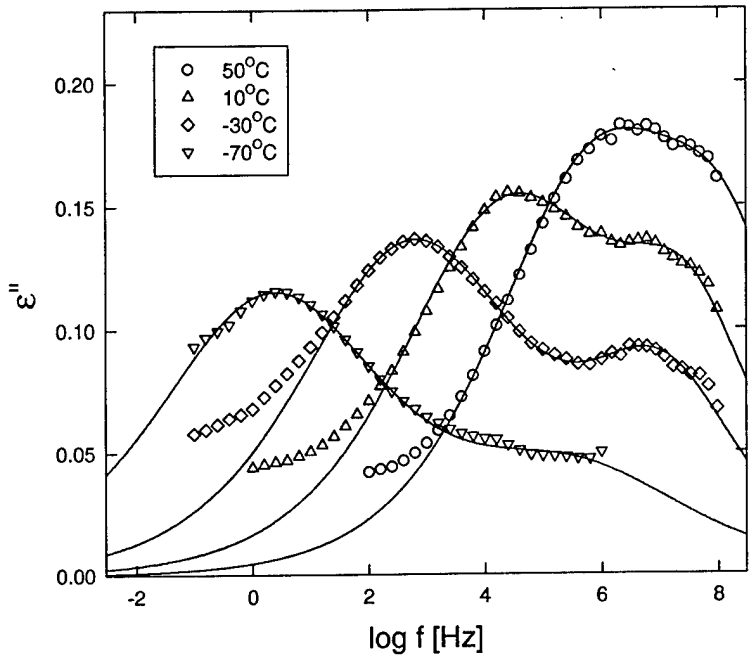

Figure 2.4. Dielectric loss in the frequency domain for fully-cured DGEBA/MDA with temperature as a parameter after 5-day exposure to environment. Solid lines are fits to Havriliak-Negami equation.

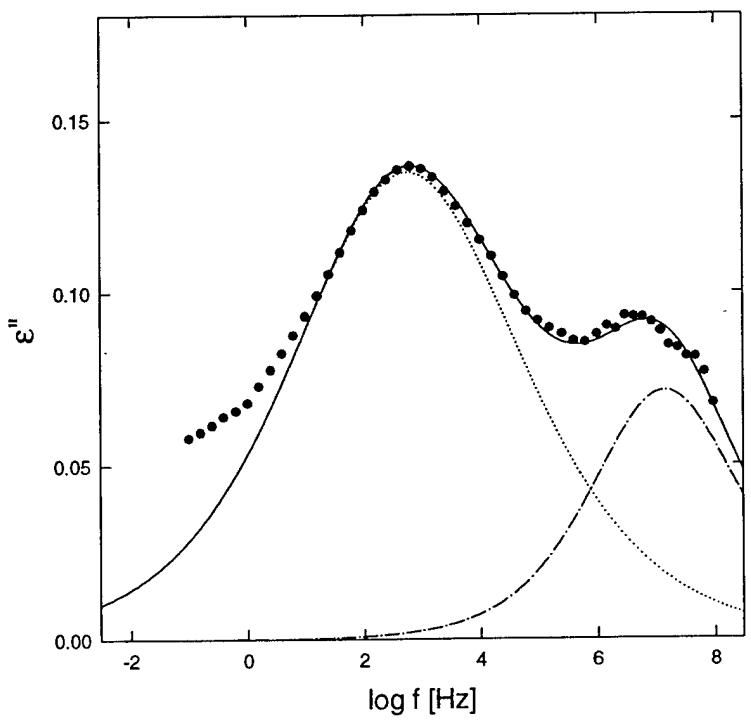

Figure 2.5. Dielectric loss in the frequency domain after 5-day exposure to environment, measured at –30°C. β and γ processes were fit to the Cole-Cole equation.

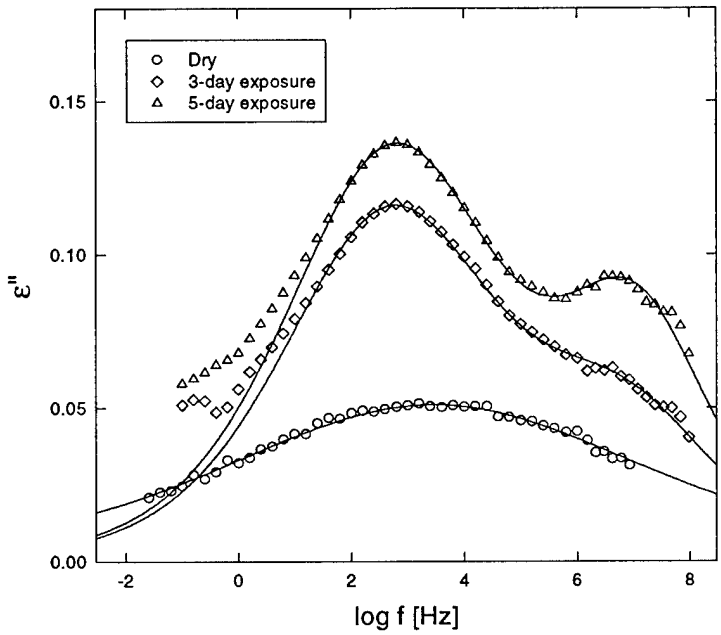

Figure 2.6. Dielectric loss in the frequency for the fully-cured DGEBA/MDA with exposure time as a parameter, measured at –30°C. Solid lines are fits to Havriliak-Negami equation.

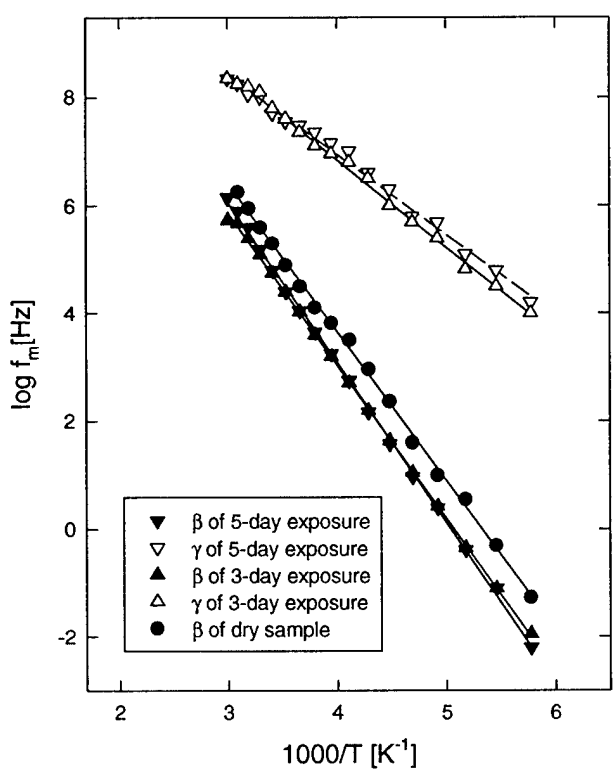

Figure 2.7. Frequency of dielectric loss maximum f_m as a function of reciprocal temperature for dry, and moist DGEBA/MDA.

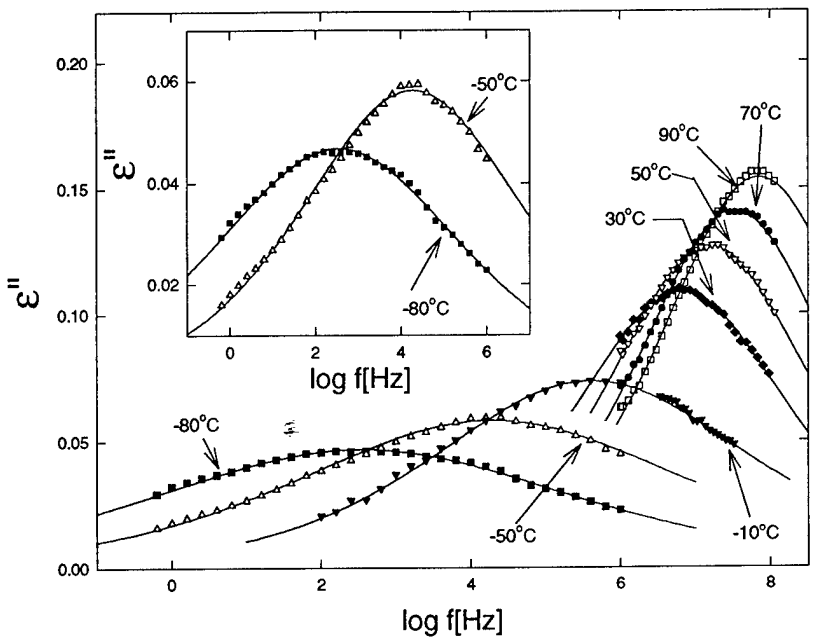

2.8. Dielectric loss in the frequency domain for fully cured FM73U with temperature as a parameter. Solid lines are fits to Havriliak-Negami equation.

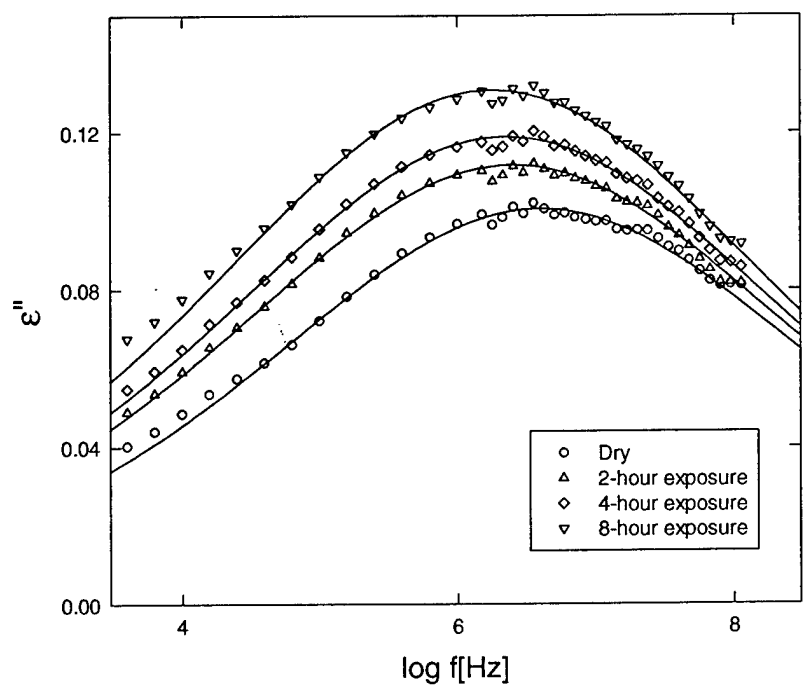

2.9. Dielectric loss in the frequency domain for cured FM73U with exposure time as a parameter. Solid lines are fits to Havriliak-Negami equation.

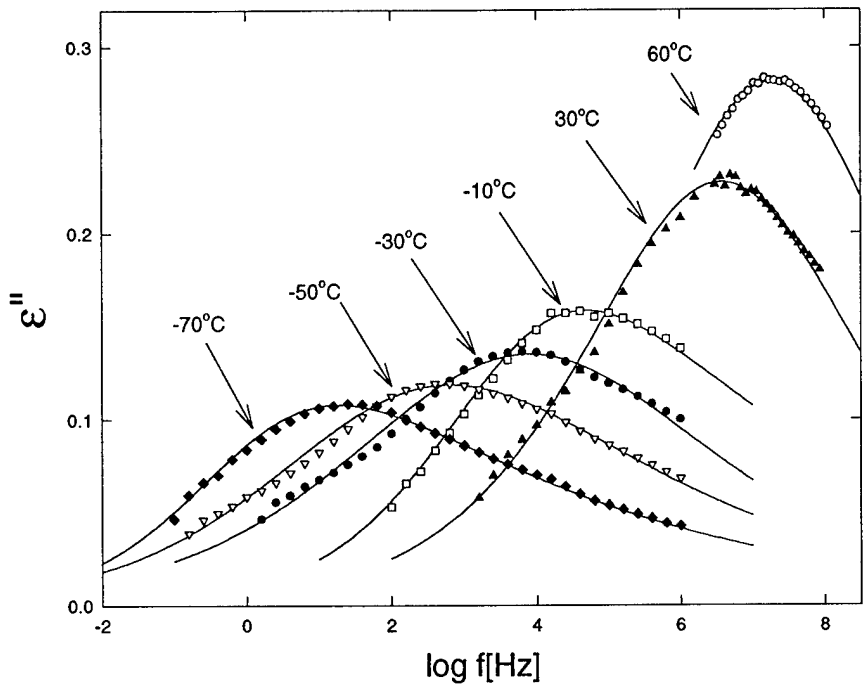

Figure 2.10. Dielectric loss in the frequency domain for FM73U after 10-day exposure, with temperature as a parameter. Solid lines are fits to Havriliak-Negami equation.

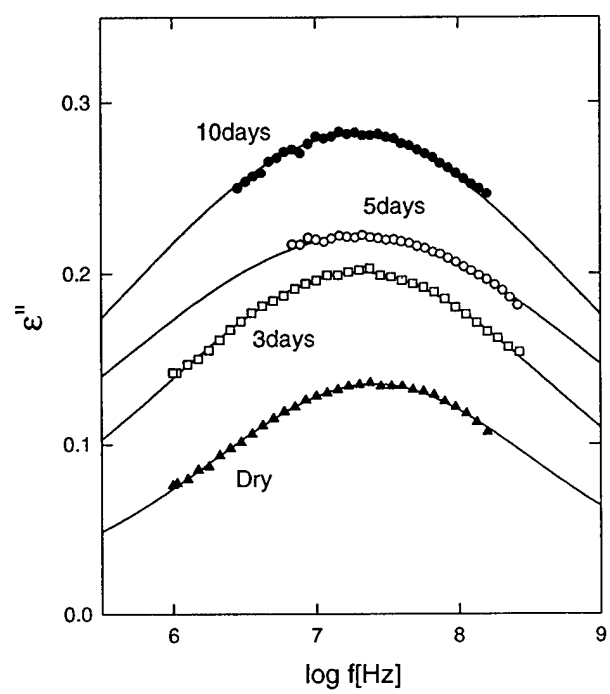

Figure 2.11. Dielectric loss in the frequency domain for FM73U with exposure time as a parameter, measured at 60°C. Solid lines are fits to Havriliak-Negami equation.

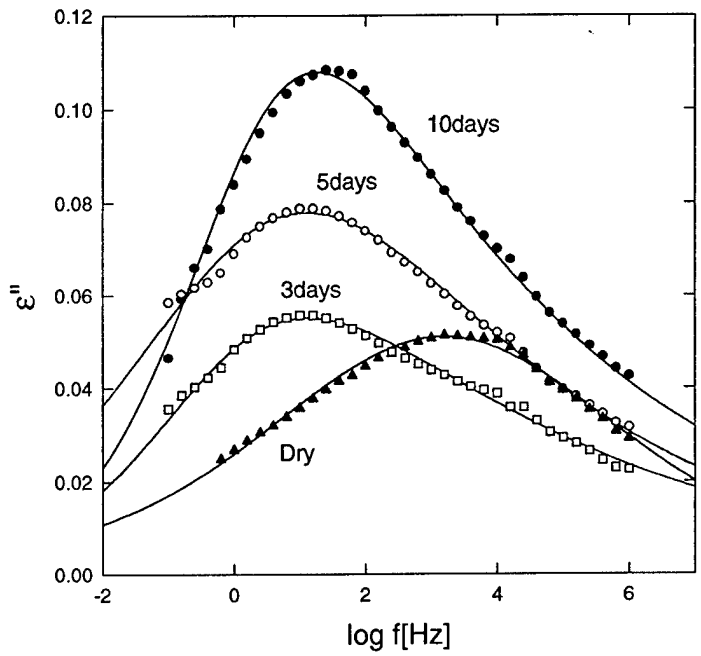

Figure 2.12. Dielectric loss in the frequency domain for FM73U with exposure time as a parameter, measured at -70°C. Solid lines are fits to Havriliak-Negami equation.

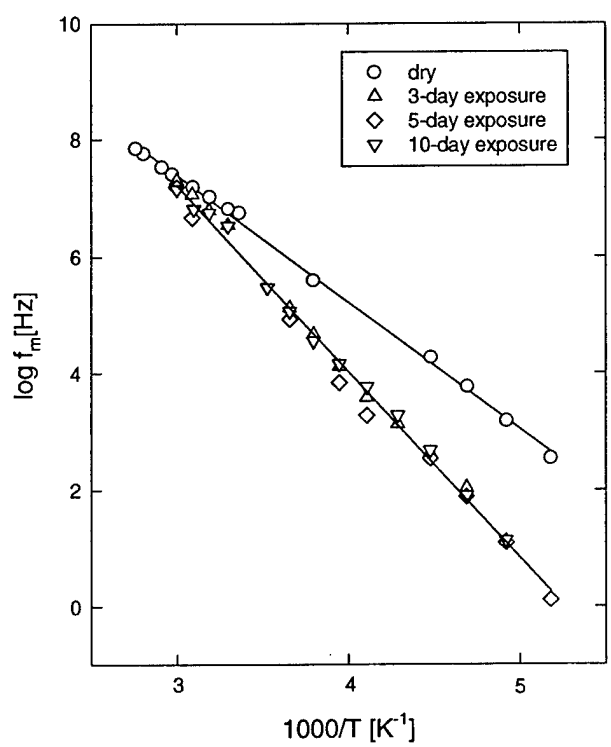

Figure 2.13. Frequency of dielectric loss maximum f_m as a function of reciprocal temperature for dry, and moist FM73U.

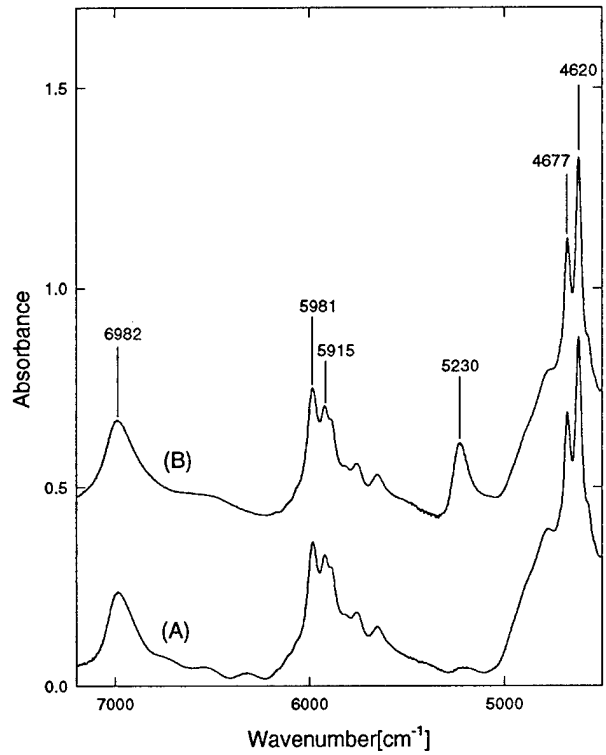

Figure 2.14. Near-IR spectra of DGEBA/MDA: (A)dry and (B) after 1-day exposure.

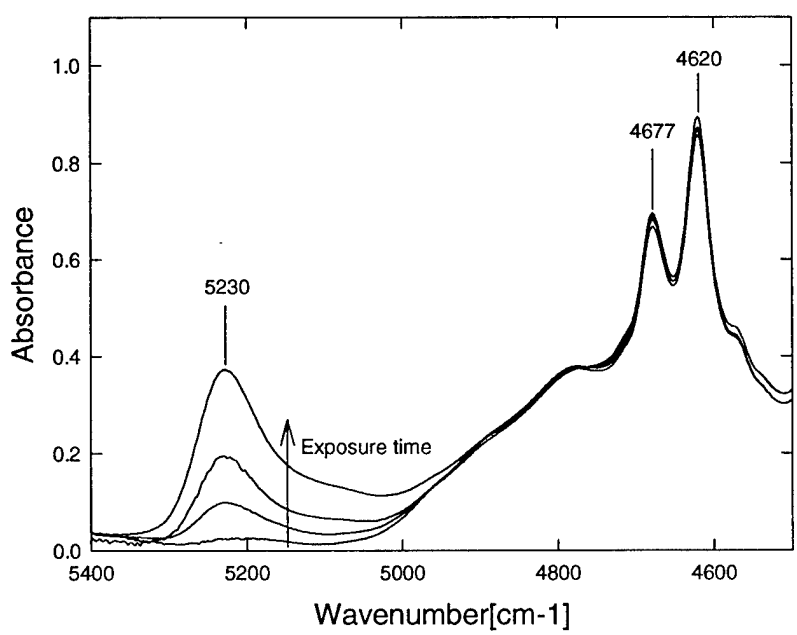

Figure 2.15. Near-IR spectra for DGEBA/MDA at different exposure times: dry, 2 hours, 1 day, 13 days.

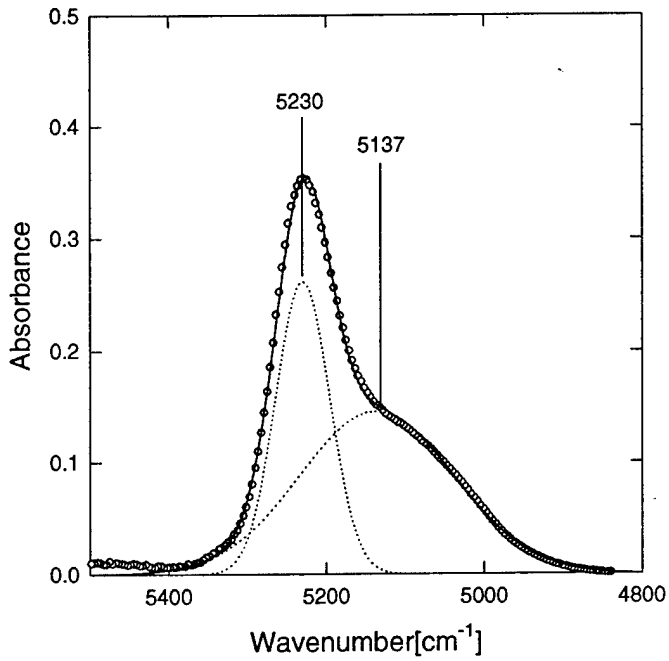

Figure 2.16. Deconvolution of the 5400-4800cm^{-1} range after 13-day exposure. Two separate processes were described by Gaussian function.

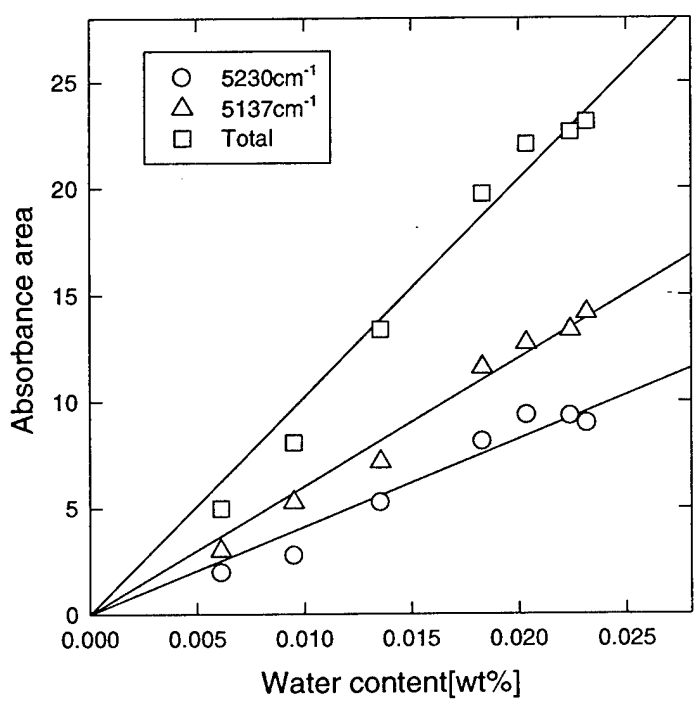

Figure 2.17. Absorbance area as a function of water content for absorbances of 5230cm^{-1}, 5137cm^{-1}, and their sum.

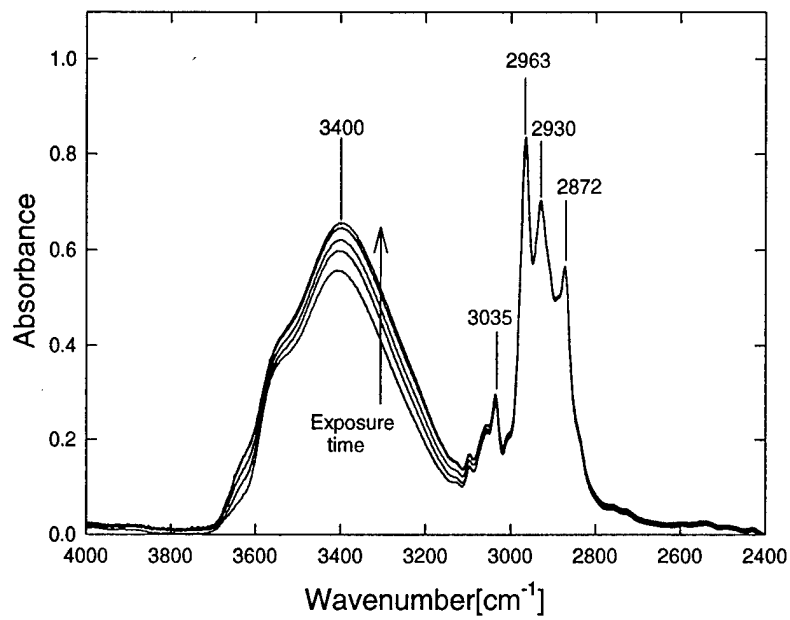

Figure 2.18. Mid-IR spectra for DGEBA/MDA at different exposure times: dry, 10 minutes, 1 hour, 1 day, and 8 days.

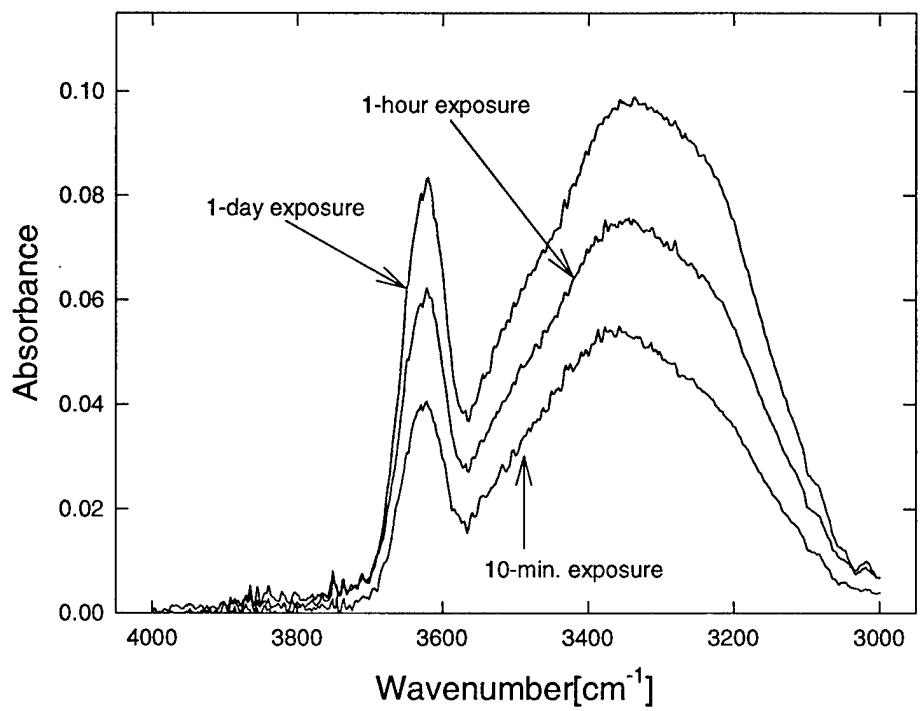

Figure 2.19. Mid-IR difference spectra for DGEBA/MDA at different exposure times: 10 minutes, 1 hour, and 1 day.

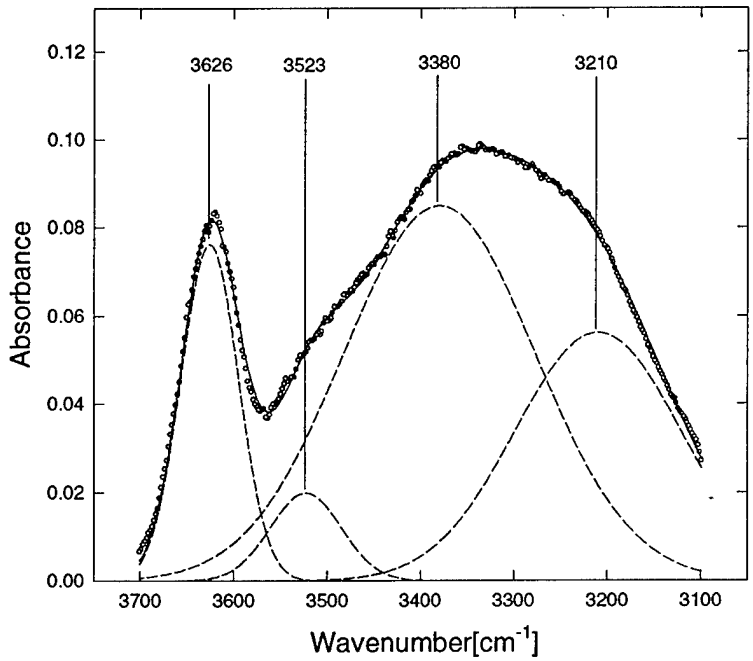

Figure 2.20. Deconvolution of difference spectra in the range of 3700-3100cm^{-1} after 1-day exposure. Each separate peak was described by a Gaussian function.

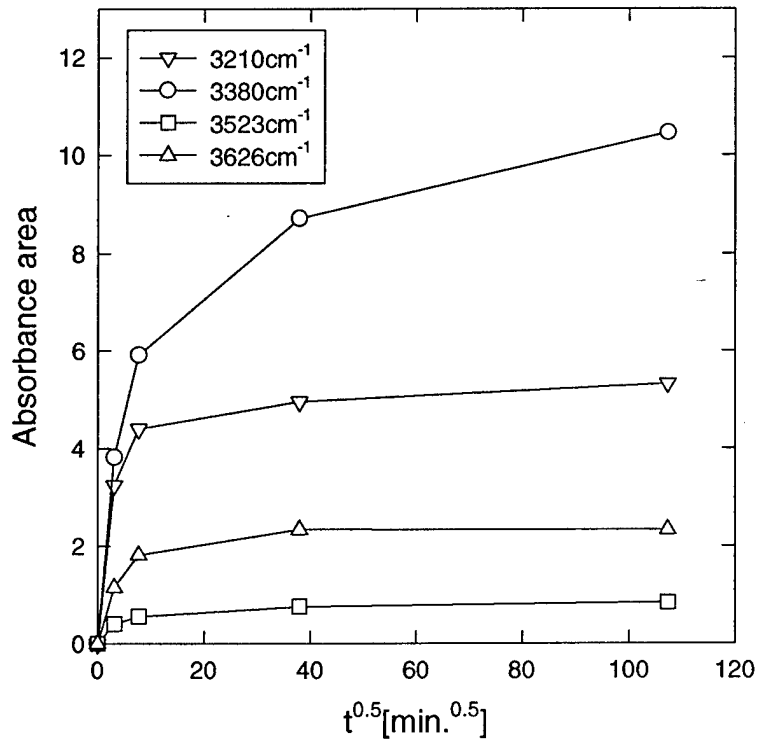

Figure 2.21. Absorbance area of each separated peak as a function of exposure time.

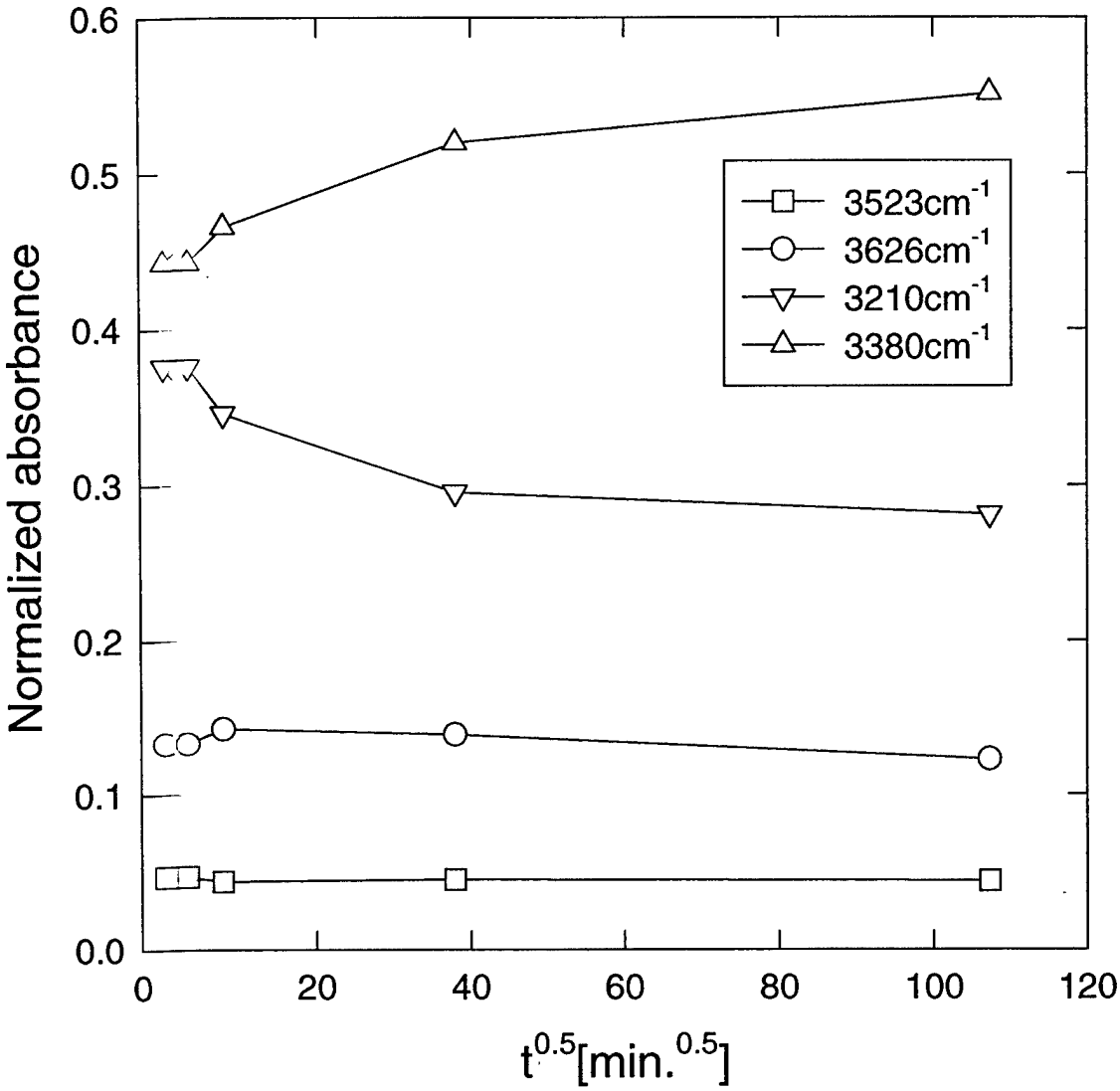

Figure 2.22. Normalized absorbance area of each peak as a function of exposure time.

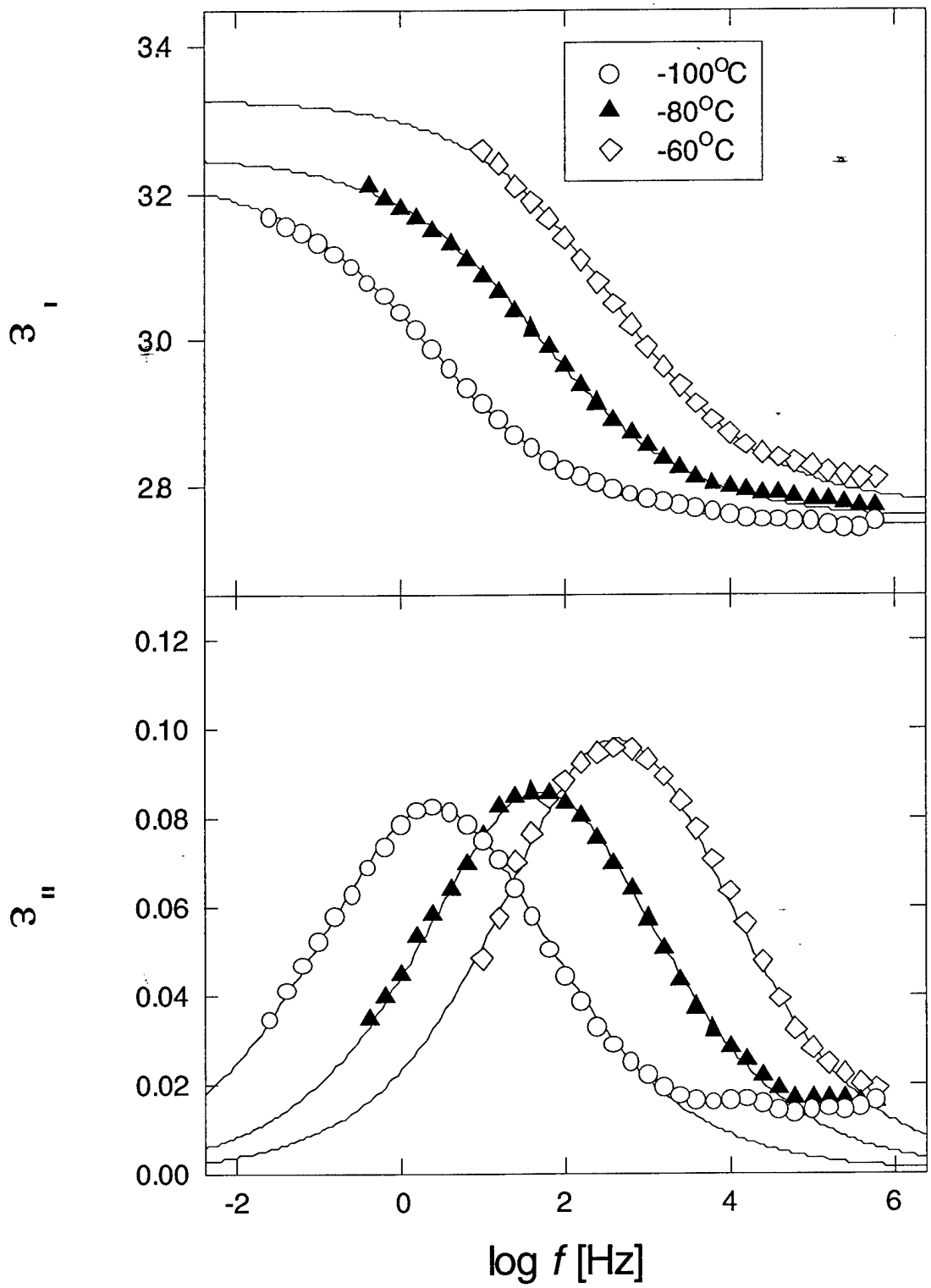

Figure 2.23. Dielectric permittivity and loss in the frequency domain for cured BMI with temperature as a parameter after 1-day exposure to environment. Solid lines are fits to Cole-Cole equation.

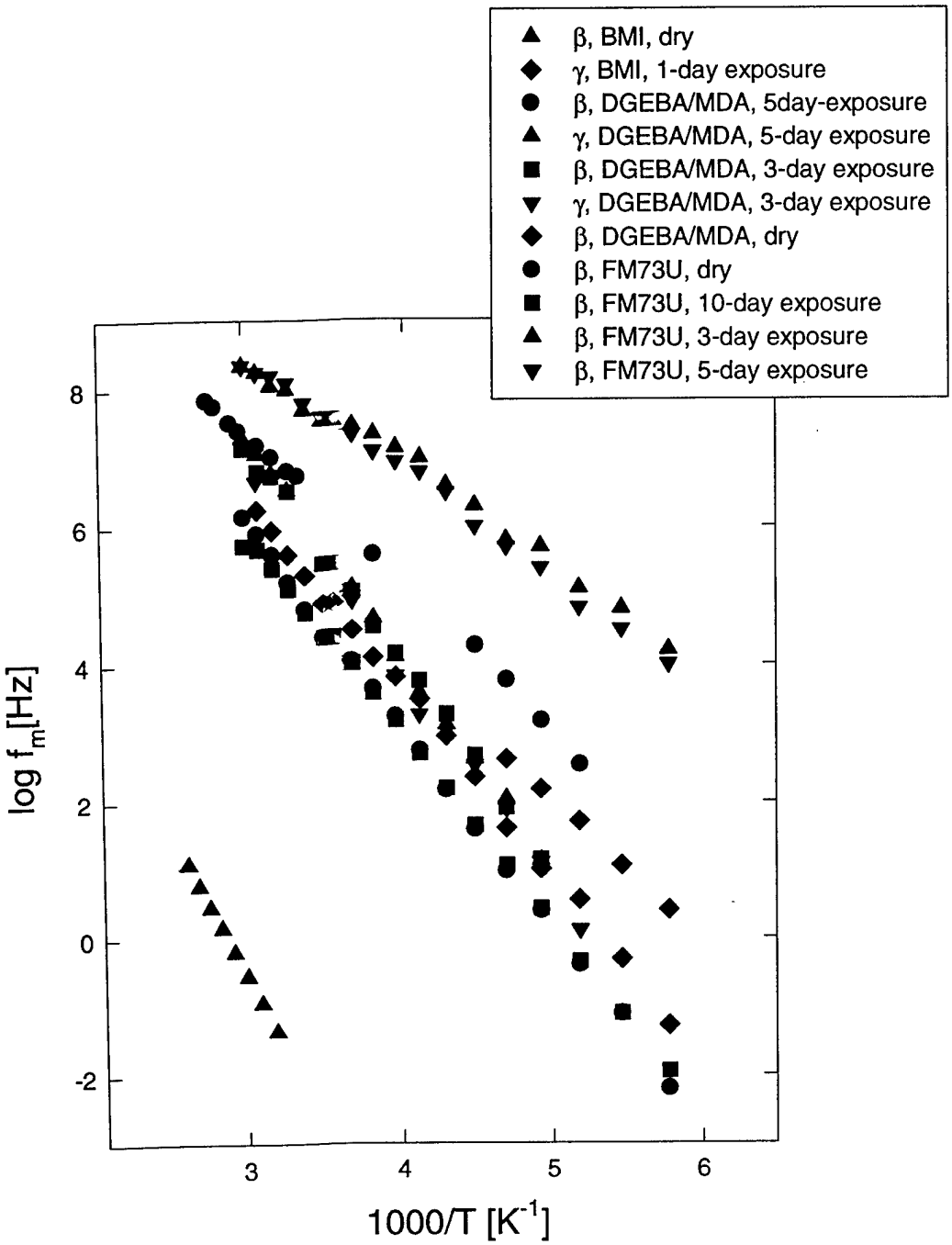

Figure 2.24. Composite plot of frequency of dielectric loss maximum f_m as a function of reciprocal temperature for BMI, DGEBA/MDA and FM73U at various exposure times.

3.0 DIELECTRIC RELAXATION SPECTROSCOPY OF BISMALEIMIDE (BMI)

Molecular aspects of chemical and physical changes in bismaleimide (BMI) adhesive joints caused by absorbed moisture were investigated. The focus was on the early (pre-damage) stage that precedes the formation of voids and microcracks. Local dynamics were investigated by broad-band dielectric relaxation spectroscopy (DRS) and the changes in the chemical state of the matter were monitored by FTIR. Absorbed water interacts with the BMI network and gives rise to a fast relaxation process (termed γ^*), characterized by an increase in the dielectric relaxation strength, an Arrhenius temperature dependence of the average relaxation time and an activation energy of 50 kJ/mol. The γ^* dynamics are slower than the relaxation of bulk liquid water because of the interactions between the absorbed water and various sites on the network (the ether oxygen, the hydroxyl group, the carbonyl group and the tertiary amine nitrogen). One particularly significant finding is that the average relaxation time for the γ^* process above 20^0C is of the order of nanoseconds or less, and hence the detection and monitoring of this process hinges upon the ability to perform high precision DRS at frequencies above 1 MHz. This is an important consideration in the ongoing efforts aimed at the implementation of DRS as non-destructive inspection (NDI) tool for adhesive joints. FTIR spectra reveal the presence of non hydrogen-bonded water and hydrogen-bonded water; the latter bonded to one and/or two sites on the BMI network. A good agreement was found between the calculated ratio of non hydrogen-bonded to total absorbed water from DRS and FTIR data.

3.1 Introduction

The under-utilization of adhesive joints, particularly in the aerospace structures, is a widely recognized phenomenon that is largely ascribed to insufficient fundamental understanding of the

effect of service environment on these joints. The consensus of opinion is that the chemical and physical changes in the adhesive on a *molecular level* during the early (pre-damage) stage of environmental exposure (prior to the formation of voids and microcracks that lead to the degradation of joints) hold the key to the understanding of initiation, propagation and failure.[1] The vast majority of the reported studies,[2-16] however, have been concerned with the effect of moisture on *macroscopic* (bulk) properties and/or the detection of delamination and loss of adhesion that occur when water eventually diffuses through the adhesive and reaches the adhesive/adherend interface/interphase.

There are numerous fundamental questions about the *molecular-level* events in glassy adhesives in the pre-damage stage that remain unanswered. In what form (single molecules, dimers, trimers, hydrogen-bonding complexes) the absorbed water resides in the adhesive? How does water interact with the host matrix and what effect that has on the local network dynamics? What are the effects on dynamics of the temperature, pressure and relative humidity of the environment? The knowledge gained from such studies is expected to contribute further towards the development of a methodology that can predict the course of subsequent degradation and anticipate failure.

The paucity of information about the effect of absorbed moisture on the local dynamics in glassy adhesives is caused to a large measure by the short time scale (as fast as few picoseconds and hence not easily measurable) of these processes. Of a few experimental techniques operable at high frequency (where fast processes are observed) and adaptable to the adhesive joint configuration, broad-band dielectric relaxation spectroscopy (DRS) is rapidly becoming a

dominant tool [17, 18] and is utilized in this study. The great attraction of DRS derives from an unparalleled frequency range available (up to 16 decades) that enables one to conduct fundamental studies of molecular dynamics of condensed matter in various phases and at different temperatures: from amorphous liquids to liquid crystals to an amorphous or crystalline glass; from high temperature, where the dipole relaxation times are of the order of picoseconds, through the vitrification process where relaxation times in the glassy state reach tens to hundreds of seconds. Of course, the interpretation of molecular dynamics obtained from DRS can be greatly aided by the use of a complementary technique capable of providing specific information about the *chemical state* of the matter. Among those techniques, Fourier Transform Infrared Spectroscopy (FTIR) represents the most attractive choice because of 1) the unmatched wealth of the information about the chemical state of the matter contained in the infrared spectrum, 2) the adaptability of near-IR (NIR) to remote (fiber-optic) in-situ real time application and 3) the possibility of using NIR for non-destructive inspection (NDI). The combined use of DRS and FTIR spectroscopy is therefore designed to afford a simultaneous examination of *physical* (DRS) and *chemical* (FTIR) changes at a molecular level in adhesive joints exposed to an aggressive environment.

Our initial efforts along those lines are described in a recent publication that deals with the effect of absorbed moisture on the *chemical and physical* changes in epoxy-amine adhesive joints.[18] Here, we focus attention on the effect of moisture on the local dynamics of a two-component bismaleimide (BMI) formulation.

3.2 Theoretical Background

We describe the theoretical basis of DRS briefly and for further details we refer the interested reader to one of the several excellent reviews in the literature.[19, 20] In an isotropic amorphous system, with negligible internal field factors, complex dielectric permittivity, ε^*, is related to the dipole moment correlation function by:[21]

$$\frac{\varepsilon^*(\omega)-\varepsilon_\infty}{\varepsilon_0-\varepsilon_\infty}=1-i\omega\int_0^\infty\left[\exp(-i\omega t)\right]\Phi(t)dt \qquad (1)$$

where ε_0 is the limiting low-frequency value of the dielectric permittivity, ε_∞ is the limiting high-frequency dielectric permittivity, ω is angular frequency, and $\Phi(t)$ is the relaxation kernel that can be obtained, theoretically, from the dipole moment time-correlation function (TCF).[21] The reorientational motion of dipoles gives rise to a relaxation process in the frequency domain and the physical interpretation of this behavior is understood in terms of the dipole moment TCF. Traditionally, it has been customary to present the results of DRS by fits of ε^* (ε' and/or ε'') in the frequency domain using various empirical functional forms. For example, ε^* may be modeled by a number of empirical functions in the frequency domain; a particularly popular and robust form is the Havriliak-Negami[22] (HN) function given as:

$$\varepsilon^*(\omega)=\varepsilon_\infty+\frac{\varepsilon_0-\varepsilon_\infty}{\left[1+\left(i\omega\tau_{HN}\right)^a\right]^b}+i\frac{\sigma}{\omega\varepsilon_v} \qquad (2)$$

where a and b are the dispersion shape parameters, σ is the conductivity, ε_v is the vacuum permittivity, and the other parameters are defined in eq 1. The HN equation is a generalization of the Cole-Cole (CC) equation, to which it reduces for b=1, and a generalization of the Cole-

Davidson (CD) equation, to which it reduces for a=1. HN and CC functional forms were employed in this study to describe local dynamics in the frequency domain. Alternatively, the dipole moment correlation function can be quantified via a stretched exponential function of the Kohlrausch-Williams-Watts[23] (KWW) type:

$$\Phi(t) = Ce^{-(t/\tau)^{\beta}} \tag{3}$$

where C is a constant, τ is the relaxation time and β is the stretching exponent ranging form 0 to 1 (β=1 for the single exponential decay function). The average relaxation time is defined as $\tau = 1/2\pi f_{max}$, where f_{max} is the frequency of maximum loss. Typically, the temperature dependence of τ is of the Vogel-Fulcher-Tammann (VFT) form for the segmental relaxation (the α process) and of the Arrhenius form for the localized sub-Tg processes.

3.3 Experimental Materials

A two-component bismaleimide (BMI) formulation (Matrimid 5292, courtesy of Ciba-Geigy Corporation), consisting of 4,4' bismaleimidodiphenyl methane (component A) and 0,0' diallyl bisphenol A (component B), was investigated in this study. Chemical structures of components A and B are shown in Figure 3.1. Equimolar amounts of the two components were mixed at 120-125^{0}C and stirred continuously until a clear, homogeneous mixture was obtained. The cure schedule consisted in heating the sample from 20 to 240^{0}C at 5^{0}C/min and maintaining it at 240^{0}C for 30 min. Samples were cured between aluminum adherends and the calorimetric (DSC) glass transition temperature (Tg) was over 220^{0}C. The adherend surface was cleaned with acetone prior to the application of the resin. The bondline thickness was 50μm. The cured

samples were reproducible (DSC and FTIR controls were run) and were subjected to the identical thermal history (by heating above the Tg and then cooling) prior to the exposure to environment in order to factor out the effect of structural relaxation *between* different samples. Two controlled aggressive environments were employed: (1) 60^0C/98% RH, and (2) 80^0C/98% RH. Relative humidity (RH) was maintained with a saturated $NaHSO_4$ solution. Samples were removed from the environment at selected time intervals and tested.

3.4 Techniques

The principal experimental technique we used was broad-band dielectric relaxation spectroscopy (DRS). A brief description of our experimental facility for dielectric measurements follows. More details are given elsewhere[24] and several excellent reviews of experimental methodology for dielectric measurements were recently published.[25,26] In this study we have used Novocontrol's α Analyzer (3 μHz – 10 MHz) and Hewlett-Packard 4291 B RF Impedance Analyzer (1 MHz - 1.8 GHz). Both instruments are interfaced to computers via IEEE 488.2 and are connected to a heating/cooling unit (modified Novocontrol's Novocool System) equipped with a custom-made motor driven arm that can selectively insert into the Novocool cryostat chamber either the low-frequency or the high-frequency sample cell. This setup has the advantage of providing high-precision temperature control over the entire frequency range (3μHz – 1.8 GHz). A photograph of the entire setup (Figure 3.2) shows the mobile unit in the upward position, with the high frequency cell on the left and the low frequency cell on the right. A variety of sample cells were employed, including parallel plates, high precision extension airlines, cells for the simultaneous dielectric/remote fiber optic FTIR tests, etc. Supporting evidence was obtained from Fourier transform infrared (FTIR) spectroscopy, using Nicolet

Instrument's Magna 750 Spectrometer,[27] and differential scanning calorimetry (DSC), using Perkin-Elmer model 7 DSC at a heating rate of 10°C/min.

3.5 Results and Discussion

We begin by presenting the DRS results for the uncured BMI (the initial mixture of components A and B). This system is miscible and has a calorimetric (DSC) Tg of -20^0C prior to the onset of curing reactions. Dielectric permittivity and dielectric loss in the frequency domain (measured over 11 decades of frequency) with temperature as a parameter are shown in Figure 3.3. Because permittivity and loss are related by the Kramers-Kronig transforms, the remaining figures in the text contain only the loss data. The solid lines in Figure 3.3 are fits to the HN functional form (Eq.2) with the low frequency contribution subtracted. The data depict the segmental α process above the calorimetric Tg of the mixture. The temperature dependence of the average relaxation time (Figure 3.4), defined as $\tau=1/2\pi f_{max}$, is of the VFT form. We reiterate that the uncured system is shown only as a reference and all subsequent results pertain to the cured networks with a calorimetric Tg above 220^0C. Dielectric loss in the frequency domain for a cured dry network, with temperature as a parameter, is shown in Figure 3.5. In this temperature range the network is well below its Tg and we measure the loss due to local relaxation processes. We observe a prominent β process that is characterized by (1) an increase in the dielectric relaxation strength ($\Delta\varepsilon$) with increasing temperature and (2) Arrhenius temperature dependence of the average relaxation time, τ. Interestingly, the loss spectra are narrower than usually observed for the so-called Johari-Goldstein β process[28] in molecular or polymeric glass formers. We also note a low but measurable loss at frequencies above 10 kHz, suggesting the presence of a relaxation that is faster (more local) than β. The loss intensity of this relaxation increases with increasing

temperature and we term this process γ. Owing to their local nature, β and γ process are precisely what we are interested in; we shall not be concerned here with the α dynamics because our networks are well into the glassy state at the conditions of this study. The molecular origin of the β process is in the rotation around phenyl-oxygen bonds. The γ process, however, is strongly affected by the absorbed moisture and we shall return to its origin later.

Once the dielectric response of the cured dry network was established, we proceeded with a systematic study of the effect of absorbed moisture on the local dynamics. We preface the presentation and discussion of those results with two comments. First, we stress that we shall not be principally concerned here with the kinetics of moisture absorption (e.g. 29-31). And second, we acknowledge a number of efforts to monitor moisture absorption in polymer networks quantitatively by tracking dielectric permittivity at a constant frequency,[32-36] but hasten to add that the dielectric response of a changing structure is a function of both exposure time *and* frequency. Therefore, when one is interested in dynamics, as we are here, the correct way to track it is by recording the relaxation spectra at selected time intervals over a wide frequency range. Because of the local nature of the sub-Tg relaxations, it was anticipated that the dynamics of such processes would be particularly sensitive to the interactions of absorbed moisture from the very beginning of environmental exposure.

Let us now examine the loss spectra *measured* at select temperatures following exposure to the 60^0C environment for various times. Figure 3.6 shows dielectric loss in the frequency domain measured at 50^0C for samples exposed to the environment for 3 and 5 days. A spectrum of the dry sample is also included as reference. There is a remarkable change in the relaxation spectrum

as a result of the moisture uptake. We observe the emergence of a pronounced relaxation with an average relaxation time of about 8 ns, corresponding to the frequency at loss maximum of ca. 20 MHz. The intensity of this process, which we term γ^*, increases with exposure time. It is clear that the γ^* process *is not* a modified (by absorbed moisture) β process; note that the β process in the dry sample, at the same measuring temperature of 50^0C (Fig. 5), is located at about 0.1 Hz, a full seven decades lower. Apparently, the γ^* process originates in the interactions of the absorbed moisture with the γ process observed in the dry sample. With decreasing measuring temperature the γ^* process moves to lower frequency, as exemplified in Figure 3.7a-c measured at –20, -60 and –100^0C, respectively. Analogous observations were made in the samples exposed to the 80^0C environment for various times between 30 minutes and 2 days, as seen in Figure 3.8a-c measured at 20, -20 and –60^0C, respectively. The gradual emergence of a loss peak is noted in each figure. Interestingly, the frequency of maximum loss increases initially (the average relaxation time gets shorter) and then levels off, while loss intensity increases continuously with exposure time. When samples exposed to 60 and 80^0C environments for the same duration are compared at the same measuring temperature, we note an increase in intensity for the latter batch. All fits in Figures 3.7 and 3.8 are to the CC functional form. We have also generated KWW fits but have not observed a systematic variation in the KWW β parameter for those samples. The calculated average value of β_{KWW} of about 0.3 is below that for the segmental α process, but slightly above a typical value for the localized β process in molecular and polymeric glass-formers.

An alternative way of displaying the effect of absorbed moisture on the local dynamics is to plot the loss spectrum at a fixed exposure time and with measuring temperature as a parameter. An

shown in Figure 3.9a-c, for the 60^0C environment and exposure times of 1 (9a), 3 (9c) days, respectively. Note a systematic shift of the γ^* process to lower frequency sing measuring temperature.

te plot of the frequency of maximum loss for different relaxation processes and ıts is shown as a function of reciprocal temperature in Figure 3.10. Both the β process I) and the γ^* process are Arrhenius, with activation energy of about 80 kJ/mol and 50 pectively. Data in Figure 3.10 for the γ^* process correspond to the exposure times ıer moisture absorption does not affect the average relaxation time. We observe that r the 60 and 80^0 C environments fall on the same line and yield the same activation

xamined the dielectric relaxation strength, $\Delta\varepsilon$, of the γ^* process. $\Delta\varepsilon$ is an important aracteristic because it depends on the chemical structure and molecular architecture. strength is defined as $\Delta\varepsilon=\varepsilon'_0-\varepsilon'_\infty$, where ε'_0 and ε'_∞ represent the limiting low- and ɜncy dielectric permittivity, respectively, and is proportional to the concentration of d the mean-squared dipole moment per molecule. The possibility of analyzing elaxation strength in terms of component contributions, and for each component, in ıolecular dipole moments, is of particular interest to us. If the concentration of each ɔup could be obtained from, say, the FTIR measurements, then the change in the ıolecular architecture during moisture absorption could be monitored in-situ by DRS. nformation, the classic Onsager (or appropriately modified) model could be used as a

starting point in the attempt to develop a relationship between chemical and physical changes in moisture-absorbing networks. The Onsager model[37] is written as:

$$\frac{(\varepsilon_0 - \varepsilon_\infty)(2\varepsilon_0 + \varepsilon_\infty)}{\varepsilon_0(\varepsilon_\infty + 2)^2} = \frac{\sum N_i \langle \mu_i^2 \rangle}{9kT\varepsilon_v} \tag{4}$$

where ε'_0 and ε'_∞ are the limiting low and high-frequency permittivities, Ni is the dipole concentration of species i (in dipoles/cm^3), $\langle\mu_i^2\rangle$ is the ensemble average dipole moment squared of molecule i, T is the temperature, and ε_v is the vacuum permittivity. The ability to identify and measure precisely the concentration of a particular dipole group (or an interactive hydrogen-bonded complex) raises interesting possibilities as regards the correlation between vibrational and dielectric spectroscopy. In Figure 3.11 we show a composite plot of dielectric relaxation strength as a function of exposure time at 60 and 80^0 C, with measuring temperature as a parameter. The data reveal that (1) $\Delta\varepsilon$ increases with exposure time in both aggressive environments, and (2) $\Delta\varepsilon$ increases faster at a higher exposure temperature. It is clear that moisture absorption is accompanied by an increase in the concentration of dipoles, suggesting a correlation between $\Delta\varepsilon$ and molecular composition (an investigation is currently underway in our laboratory).

An important question is what can be learned from the DRS data about the molecular origin of sub-Tg relaxations and the γ^* process in particular. Although the precise nature of the interactions between the network and the absorbed moisture could be studied only in conjunction with the FTIR data, it is immediately clear that the γ^* process is strongly affected by water. What is not clear from DRS data is 1) in what form (e.g. isolated single molecules, dimers, trimers)

water resides within the adhesive, 2) at what network sites water forms hydrogen bonds, and 3) in how many hydrogen bonds a water molecules participates? We briefly discuss the first point; a more detailed examination of all these questions is offered later in the text. An attempt to elucidate the form in which water initially resides in the network was made in an earlier study of moisture absorption in epoxy networks,[18] where a dynamics simulation study was conducted with the aid of a commercial software package (Cerius 2). A stoichiometric DGEBA/MDA mixture composed of twenty-six molecules of DGEBA and thirteen molecules of MDA was constructed first. Then, nine molecules of water were introduced into the network, bringing the water content to 1.6% by weight (a reasonable value considering that the maximum water content at the condition of that study was ca. 3% by weight). Although that simulation was limited to a relatively small network fragment, interesting observations were made: 1) fluctuations involving network atoms and water molecules were seen, and 2) only single molecules of absorbed water were detected; no dimers or trimers were observed. These observations were mostly in agreement with the excellent work of Musto et al.[38, 39], though our simulations have revealed that a water molecule participates in hydrogen bonding to only one site on the network. If and to what extent these simulation results are relevant to BMIs is not yet known and we are currently conducting a larger simulation study on BMI networks.

Notwithstanding the form in which water resides in the adhesive, a comparison with the dynamics of liquid water is warranted. For example, at 50^0C liquid water has a dielectric loss peak at about 25 GHz (corresponding to an average relaxation time of about 9 picoseconds)[40], while the relaxation time of the γ^* process at the same temperature is longer by about three decades on the frequency scale. Whether the reason for this is physical (e.g. steric hindrance due

to neighboring moieties, such as benzene rings) and/or chemical (hydrogen bonding interactions with specific network sites) is not apparent from DRS. The findings reported by Jelinski et al.[41, 42] in their study of epoxy networks by solid state NMR spectroscopy are similar. These authors also argue that the "free" water (defined as isotropically mobile with the same relaxation time as liquid water) is not present in the network. The γ^* process in BMIs, with an average relaxation time of 160 ps at 20^0C, is slower than the γ process in moist epoxy-amine networks, but faster than the β process in these networks.[18]

Formation of hydrogen bonds throughout the network is expected to affect the dynamics. Identification of the network sites that could form hydrogen bonds with absorbed moisture requires the knowledge of molecular architecture, which, in turn, requires an understanding of the reaction mechanism that leads to network formation. While only a few such studies have been reported, the complexity of BMI cure is widely recognized.[43-49] Suffice it to say that a number of polymerization and cross-linking routes have been claimed, including homopolymerization of BMI via the reaction of maleimide C=C double bond that results in the formation of four member rings, homopolymerization of BMI via the reaction of maleimide C=C that involves three BMI molecules, reaction between the maleimide double bonds and allyl groups, homopolymerization of allyl double bonds, etherification (dehydration) involving hydroxyl groups of the allyl component, etc. Based upon the earlier investigations of the effect of cure conditions on the reaction kinetics, mechanism and structure of BMI networks,[48] we can say that the thermal history used in this study will give rise to a network schematically shown (characteristic fragment) in Figure 3.12. An examination of this figure reveals several possible sites (hydroxyl group, ether oxygen, carbonyl group, tertiary amine nitrogen) that could

participate in hydrogen bonding with absorbed moisture (shown in bold, Fig. 12). In examining this issue further, we raise two important questions. First, is there an order of preference, as regards the network site, for hydrogen bond formation? And second, is it possible to determine the number of network sites to which each water molecule bonds? It was anticipated that further insight into these queries would be obtained from the FTIR study; thence we turn attention to the results of near-IR (NIR) and mid-IR (MIR) analysis of our networks. We acknowledge the use of conventional FTIR spectroscopy to detect moisture in polymers,[50-53] but are not aware of any study of adhesive joints by a combined NIR, MIR and DRS approach.

NIR and MIR spectra of the individual components (A and B) of our BMI formulation have been documented elsewhere [48] and will not be described here. A NIR spectrum of the cured dry network is shown in Figure 3.13. All major peaks of relevance in cured BMI networks are present, including hydroxyl absorption around 7000 cm^{-1}, allyl and maleimide double bond absorption at 6112 cm^{-1} and a doublet due to the –CH stretching (4627, 4676 cm^{-1}). The broad absorption between ca. 5750 and 5900 cm^{-1} has been shown[48] to contain three peaks characteristic of the homopolymerized maleimide (component A). A series of NIR spectra of moist samples taken at select time intervals during exposure to the 80^0C environment are shown in Figure 3.14a. Difference spectra obtained by subtraction, using the 5500–6200 cm^{-1} range as internal standard, are shown in Figure 3.14b. Water uptake causes pronounced changes in the 4950–5400 cm^{-1} and 6200–7500 cm^{-1} range; we examine the former first. There is a progressive increase in the intensity of the absorption band centered at 5225 cm^{-1} that has been associated with the combination band due to bending (deformation) (1600-1650 cm^{-1}) and asymmetric stretching (3100-3800 cm^{-1}) of (the absorbed) water. A careful inspection of the data also reveals

a consistent increase in the absorption intensity at the lower wavenumber (lower frequency) side of the 5225 cm^{-1} peak, suggesting a gradual development of a parallel absorption mechanism. This is an interesting finding. Deconvolution of the broad absorption was carried out and two absorption peaks were clearly detected, as exemplified in Figure 3.15. Both peaks were Gaussian; initially, the first was centered at 5225 cm^{-1} and the second at 5116 cm^{-1}. During exposure, the second peak exhibited a slight shift to higher wavenumber (frequency). Interestingly, the area under each peak is a linear function of water content, as shown in Figure 3.16. Unfortunately, identification of each peak with specific interactions (although of considerable interest) is difficult because the NIR absorption in this range is associated with the overtones of a combination of bending and stretching vibrations that are affected oppositely by hydrogen bonding; therefore, no further attempts were made along those lines.

Additional information was obtained from the consideration of the characteristic hydroxyl absorption in the 6200-7500 cm^{-1} region. Deconvolution of the spectra[54] reveals the presence of three absorption bands (following a 2-hour exposure to 80^0C) centered at 7088, 6804 and 6445 cm^{-1}, as seen in Figure 3.17. Similar observations were reported in other systems, including the liquid mixtures of water with non-polar and polar solvents, and cross-linked thermoset networks.[55, 39] An explanation was offered by postulating the existence of three spectroscopically distinguishable forms of hydrogen bonding, termed S_0, S_1 and S_2, where subscripts zero, one and two denote the number of hydrogen atoms of the water molecule that participate in hydrogen bonding. Based on the changes in the breadth and the full width-at-half-height (fwhh) of the peaks at 7088, 6804 and 6445 cm^{-1}, an argument can be put forward to associate these absorption bands with S_0, S_1 and S_2, respectively. Although the fwhh of each

peak did not change with water uptake, the fwhh of the 6445 cm^{-1} band was about two-three times greater that the other two. This further supports the assignment of the 6445 cm^{-1} band to strong hydrogen bonding interactions likely to be encountered in S_2 complexes.

An important consideration is the proportion of non hydrogen-bonded (S_0) to hydrogen-bonded ($S_1 + S_2$) water absorbed in the network. We have monitored the increase in the peak area of the corresponding absorption bands during moisture uptake and have calculated the S_0 / S_t ratio, where $S_t = S_0 + S_1 + S_2$. The absorbance area, A, is related to the concentration of the absorbing species, C, by A=aC, where a is the absorption coefficient. We extended Choppin's findings[55] that the absorption coefficient for S_0, S_1 and S_2 in water-solvent systems did not vary with the type of solvent to our BMI network and utilized his values for a_1, a_2 and a_3. The following equation was then used to calculate the relative concentration of each species (i = 0, 1 or 2):

$$\frac{C_{Si}}{C_{tot}} = \frac{A_i / a_{S_i}}{A_{7088} / a_{S_0} + A_{6804} / a_{S_1} + A_{6445} / a_{S_2}} \qquad (5)$$

The relative ratios of various forms of absorbed water are plotted as a function of water content in Figure 3.18. It is very interesting to note that about 70% of the absorbed water is in the S_0 form and that the ratio of any absorbed species (S_0, S_1 or S_2) to the total absorbed water changes very little with moisture uptake.

We have also utilized the DRS data for an analogous calculation. Let us assume that the γ^* process represents the dynamics associated with the S_1 and S_2 forms, while a faster (higher frequency) process, termed δ, represents the dynamics of the non hydrogen-bonded water (S_0). The value of ε' at 0.1 Hz was taken as the limiting low-frequency permittivity that encompasses

δ processes (i.e., 0.1 Hz << $\omega_{max\gamma}$ [illegible] $\omega_{max\gamma^*}$; Fig. 7). The value of ε' at 1 MHz was taken to limiting low-frequency permittiv[illegible]tivity for the δ process (i.e., 1 MHz << $\omega_{max\delta}$). Thus the changes in ε' at 0.1 and 1 M[illegible] MHz during moisture uptake one gets information ıcrease in the total (S_t = S_0 + [illegible] + S_1 + S_2) and non hydrogen-bonded (S_0) water, The S_0/ S_t ratio can then be calcu[illegible]culated from the following equation:

$$\frac{\varepsilon'(dry)\big)_{1MHz}}{\varepsilon'(dry)\big)_{0.1Hz}} = \frac{S_0}{S_t} \qquad (6)$$

, the values of S_0 /S_t calculated fr[illegible] from eq. 6 (shown in Figure 3.19 as filled symbols) ange between 0.6 and 0.8 and did[illegible] did not vary systematically with exposure time. This lels the result of the analysis base[illegible]ased on the NIR data, shown in Figure 3.18. We also e S_0 /S_t ratio from the DRS data[illegible]ata by manipulating the left-hand side (LHS) of the ation (eq. 4) into the following for[illegible]orm:

$$\frac{\left[\frac{(\varepsilon'_{1MHz}-\varepsilon_\infty)(2\varepsilon'_{1MHz}+\varepsilon_\infty)}{\varepsilon'_{1MHz}(\varepsilon_\infty+2)^2}\right](m) - \left[\frac{(\varepsilon'_{1MHz}-\varepsilon_\infty)(2\varepsilon'_{1MHz}+\varepsilon_\infty)}{\varepsilon'_{1MHz}(\varepsilon_\infty+2)^2}\right](dry)}{\left[\frac{(\varepsilon'_{0.1Hz}-\varepsilon_\infty)(2\varepsilon'_{0.1Hz}+\varepsilon_\infty)}{\varepsilon'_{0.1Hz}(\varepsilon_\infty+2)^2}\right](m) - \left[\frac{(\varepsilon'_{0.1Hz}-\varepsilon_\infty)(2\varepsilon'_{0.1Hz}+\varepsilon_\infty)}{\varepsilon'_{0.1Hz}(\varepsilon_\infty+2)^2}\right](dry)} = \frac{S_0}{S_t} \qquad (7)$$

values of ε' at 0.1 Hz and 1 MH[illegible]Hz have the same physical significance as described e value of ε_∞, the limiting high fr[illegible] frequency permittivity for our network, was set at ε_∞ [illegible]0 /S_t values calculated from eq. [illegible]q. 7, shown as open symbols in Figure 3.19, are in eement with the values obtained [illegible]d from eq. 6 (filled symbols).

A MIR spectrum of a dry BMI network is shown in Figure 3.20. Again, all major peaks that characterize BMI networks are present. Of major interest here is the range between approximately 3000 and 3700 cm^{-1}, where vibrational modes due to the various forms of hydrogen bonding are located. A close-up of that spectral range in a dry sample is shown in Figure 3.21. Deconvolution of the spectrum of Figure 3.21 results in a weak absorption band at 3652 cm^{-1} and three more bands at lower frequencies. Moisture uptake has a dramatic effect on the intensity of all absorption peaks, as exemplified in the spectrum shown in Figure 3.22. A series of difference spectra (obtained by subtracting the spectrum of a dry sample from that of each moist sample) with exposure time at 60^0C as a parameter, are shown in Figure 3.23. Two distinct regions are observed: a relatively sharp absorption between 3600 and 3700 cm^{-1} and a broad, irregularly shaped absorption between about 3600 and 3100 cm^{-1}. An example of deconvoluted spectrum of a sample exposed to the 60^oC environment is shown in Figure 3.24. The intensity of those absorption bands increases with exposure time and the important question is what is the molecular origin of these changes? We first consider the narrow absorption band at higher frequency that was fit to a Gaussian function with a peak at 3639 cm^{-1}. There is little doubt that this absorption is due to the previously defined S_0 species and that it corresponds to the 7088 cm^{-1} NIR band assigned to a combination of symmetric and asymmetric stretching of non-hydrogen bonded water. This absorption was observed in polymer networks and water-solvent mixtures, and has been attributed to non-hydrogen-bonded water.[56-58] In our BMI network, this absorption is assigned to water molecules located in the pockets surrounded by hydrophobic moieties, such as benzene rings, where the likelihood of hydrogen bonding is low.

We next proceeded with attempts to deconvolute the broad absorption range between 3600 and 3100 cm^{-1}. The best results were obtained using three Gaussian functions, as shown in Figure 3.21 for dry BMI, with peaks initially centered at 3599, 3470 and 3238 cm^{-1}. The absorption intensity (defined by the area under the peak) increases with increasing exposure time. The presence of several absorption bands confirms that 1) the absorption mechanism is complex and 2) the often-invoked but seldom justified concept of two types of absorbed moisture, lumped under "loosely" and "strongly" bound water, is an oversimplification of the actual situation. But what can we say about the molecular origin of absorption bands at 3599, 3470 and 3238 cm^{-1} ? It is evident that these three bands are associated with hydrogen bonded water, though it is not clear from the MIR spectra: 1) what specific atoms/sites on the network participate in these interactions, 2) in what order of preference (if any), and 3) how many hydrogen atoms on a given water molecules form a bond. In a BMI network, as argued earlier, the absorbed water could (possibly) form a hydrogen bond at several sites on the network, including the hydroxyl group, the ether oxygen, the carbonyl group and the tertiary amine nitrogen. But while the strength of hydrogen bonding interactions (and the corresponding frequency shift) is known to depend on the nature of the donor-acceptor pair, the identification of an absorption band with a particular type of hydrogen bond (i.e. between water hydrogen and one of the above specified network sites) is not straightforward. The quantitative interpretation of MIR spectra is further complicated by difficulties associated with a precise measurement of the (frequency dependent) molar absorptivities for various interacting pairs. Nonetheless, Musto et al.[39] , in their study of water absorption in epoxy, networks have tentatively assigned the 3599 cm^{-1} band to the stretching mode of hydrogen bonded water hydroxyl. But the identity of an epoxy or BMI network site that participates in hydrogen bonding, in either S_1 or S_2 form, remains unspecified. Moreover, if the

absorbed water forms dimers or trimers, there will also be a possibility of hydrogen bonding between the adjacent water molecules (S_3). It is therefore fair to say that although a water molecule can participate in one (S_1) or two hydrogen bonds (S_2), an outright quantitative identification of a MIR absorption band with a specific complex form (S_1, S_2, S_3) warrants further research. We do anticipate that the ongoing simulation study on a larger BMI network will provide additional information.

A final comment regards our efforts aimed at the development of fundamental quantitative correlation between FTIR and DRS data. That, in effect, would provide a link between the chemical (FTIR) and physical (DRS) phenomena that accompany water absorption into the network. Specifically, we are seeking to correlate a dielectric material parameter (such as the average relaxation time, dielectric strength or a shape parameter of the dielectric spectrum) with a fundamental parameter deduced from the FTIR spectra (e.g., absorption strength, dipole type and concentration). This will be the subject of a forthcoming publication.

3.6 Conclusions

The results of this investigation provide new insight into the local molecular dynamics and the chemical interactions between bismaleimide (BMI) networks and absorbed water. Near-IR (NIR) and mid-IR (MIR) analyses revealed the presence of non hydrogen-bonded and hydrogen-bonded water. A quantitative analysis of NIR and DRS data revealed that about 70% of the absorbed water is non hydrogen-bonded.

The non hydrogen-bonded water, termed S_0, is represented by the NIR and MIR absorption bands at 7088 and 3639 cm^{-1}, respectively. Characteristic absorption bands in the NIR and MIR spectra were deconvoluted and attempts were made to match absorption bands with water molecules that participate in one (S_1) or two (S_2) hydrogen bonds. But the identification of an absorption band with a specific atom/site on the BMI network that participates in hydrogen bonding (e.g., ether oxygen, hydroxyl group, carbonyl group, tertiary amine nitrogen) was not straightforward and more should be learned before such assignments are made.

The absorbed water molecules contribute to the development of a local relaxation process, termed γ^*. The dielectric relaxation strength of this process was observed to increase with increasing moisture uptake. Like most sub-Tg relaxations, the γ^* process is Arrhenius, with activation energy of 50 kJ/mol. The γ^* dynamics are slower that those of liquid water, the probable cause being the steric hindrance imparted by the surrounding network. One particularly important finding is that the average relaxation time for the γ^* process at temperatures above 25^0C is of the order of nanoseconds and hence its detection hinges on the ability to perform high precision dielectric measurements in the frequency range above 1 MHz. This is an important consideration in the ongoing efforts aimed at the implementation of DRS as non-destructive inspection tool for adhesive joints.

Acknowledgement This material is based on work supported by the AFOSR, Polymer Matrix Composites Program (Contract No. F49620-99-C-0057, Dr. Charles Y-C Lee, Program Director). One of the authors (JM) is most grateful to Professor Radomir Kovacevic for helpful comments.

References and Notes

[1] A strong initiative has emerged in recent years aimed at identifying and monitoring the underlying chemistry and physics on a *molecular level.* Most recent discussion meeting on this subject was held during the Annual Review of the AFOSR Polymer Matrix Composites Program (Dr. Charles Y-C Lee, Director), Long Beach, CA, May 11-12, 2001.

[2] Gledhill, R. A. and Kinloch, A. J. *J. Adhesion* **6**, 315 (1974).

[3] Browning, C. E., *Polym. Eng. Sci.* **18**, 16 (1978).

[4] Keenan, J. D., Seferis, J. C. and Quinlivan, J. T., *J. Appl. Polym. Sci.* **24**, 2375-2387 (1979).

[5] Rowland, S. P., Ed., *Water in Polymers* (ACS Symposium Series 127, American Chemical Society, Washington, DC, 1980).

[6] Sedlacek, B. and Kahovec, J. Eds., *Crosslinked Epoxies* (Walter de Gruyter, Berlin, 1987).

[7] Kaelble, D. H., Moacanin J. and Gupta, A., in *Epoxy Resins Chemistry and Technology* (Marcel Dekker, New York, 1988), May, C. A., Ed., Chap. 6, 603.

[8] Apicella, A., in *International Encyclopedia of Composites* (VCH Publishers, New York, 1990), Lee, S. M. Ed., Vol. 2.

[9] Nairn, B. J., Dickstein, P. A., Plausinis D. J. and Spelt, J. K., *J. Adhesion* **48**, 121-136 (1995).

[10] de Neve, B. and Shanahan, M. E. R., *J. Adhesion* **49**, 165-176 (1995).

[11] Maggana, C. and Pissis P., *J. Polym. Sci. Part B: Polym. Phys.* **37**, 1165-1182 (1999).

[14] Soles, C. L., Chang, F. T., Gidley, D. W. and Yee, A. F., *J. Polym. Sci. Part B: Polym. Phys.* **38**, 776-791 (2000).

[15] Grave, C., McEwan, I. and Pethrick, R. A., *J. Appl. Polym. Sci.* **69**, 2369-2376 (1998).

[16] Affrossman, S., Banks, W. M., Hayward, D. and Pethrick, R. A., *Proc. Inst. Mech. Eng.* **214**, Part C, 87-102 (2000).

[17] Williams, G., in *Keynote Lectures in Selected Topics of Polymer Science* (CSIC, Madrid, 1997), Riande, E., Ed., Chap. 1, 1-40.

[18] Mijovic, J., Miura, N. and Soni, S. *J. Adhesion* **76(2),** 123 (2001).

[19] Williams, G., Dielectric Properties, in *Comprehensive Polymer Science* (Pergamon, Oxford, 1989), Eds., Allen G., Bevington J. C., Vol. 2, Chap. 7, 601-632.

[20] Williams, G., Theory of Dielectric Properties, in *Dielectric Spectroscopy of Polymeric Materials* (American Chemical Society, Washington, DC, 1997), eds. Runt, J. P., and Fitzgerald, J. J., Chap. 1, 3-65.

[21] Williams, G., Molecular Aspects of Multiple Dielectric Relaxation Processes in Solid Polymers, in *Advances in Polymer Science* (Springer-Verlag, Berlin, 1979), Eds., Cantow, H.-J. et al., Vol. 33, 59-92.

[22] Havriliak, S. Jr. and Negami, S., *Polymer* **8**, 161 (1967).

[23] Williams, G., Watts, D. C., *Trans. Faraday Soc.* **66**, 80 (1970).

[24] Fitz, B., Andjelic, S. and Mijovic, J., *Macromolecules* **30**, 5227-5238 (1997).

[25] Kremer, F. and Arndt, M., in *Dielectric Spectroscopy of Polymeric Materials* (American Chemical Society, Washington, DC, 1997), Eds. Runt, J. P., and Fitzgerald, J. J., Chap. 5, 139.

[26] Kranbuehl, D. in *Dielectric Spectroscopy of Polymeric Materials* (American Chemical Society, Washington, DC, 1997), Eds. Runt, J. P., and Fitzgerald, J. J., Chap. 11, 303.

[27] Mijovic, J. and Andjelic, S., *Macromolecules* **29**, 239-246 (1996)

[28] Johari, G. P. and Goldstein, M., *J. Chem. Phys.* **53**, 2372 (1970).

[29] Frisch, H. L. *Polym. Eng. Sci.* **20**, 1 (1980).

[30] Mikols, W. J., Seferis, J. C., Apicella, A. and Nicolais, L. *Polym. Comp.* **3**, 118 (1982).

[31] Apicella, A., Nicolais, L. and de Cataldis, C. *Adv. Polym. Sci.* **66**, 189 (1985).

[32] Bellucci, F. and Nicodemo, L. *Corrosion* **49**, 235 (1993).

[33] Bellucci, F., Nicodemo, L., Monetta, T., Kloppers, M. J. and Latanision, R. M. *Corrosion Sci.* **8**, 1203 (1992).

[34] Casalini, R., Corezzi, S., Fioretto, D, Livi, A. and Rolla, P. A., *Chem. Phys. Lett.* **258**, 470 (1996).

[35] Corezzi, S., Capaccioli, S., Gallone, G., Livi, A. and Rolla, P. A., *J. Phys.: Condens. Matter* **9**, 6199 (1997).

[36] Fitz, B. D., Mijovic, J., *Macromolecules* **32**, 4134-4140 (1999).

[37] Onsager, L. *J. Amer. Chem. Soc.* **58**, 1486 (1936).

[38] Musto, P., Mascia, L., Ragosta, G., Scarinzi, G., Villano, P., *Polymer* **41**, 565-574 (2000).

[39] Musto, P., Ragosta, G. and Mascia, L., *Chem. Mater.* **12**, 1331-1341 (2000).

[40] Barthel, J., Bachuber, K., Buchner, R., Hetzenauer, H., *Chem. Phys. Lett.* **195**, 369-373 (1990).

[41] Jelinski, L. W., Dumais, J. J., Stark, R. E., Ellis, T. S. and Karasz, F. E., *Macromolecules* **18**, 1019 (1985).

[42] Jelinski, L. W., Dumais, J. J., Cholli, A. L., Ellis, T. S. and Karasz, F. E., *Macromolecules* **18**, 1091 (1985).

[43] King, J. J., Chaudhari, M. and Zahir, S. *Int. SAMPE Symp.* **29**, 394 (1984).

[44] Lee, B., Chaudhari, M. and Galvin, T. *Int. SAMPE Tech. Conf.* **17**, 172 (1985).

[45] Lind, A. C. and Fry, C. G. *ACS Proc. Div. Polym. Mater. Sci. Eng.* **59**, 466 (1988).

[46] Brown, I. M. and Sandreczki, T. C. *ACS Proc. Div. Polym. Mater. Sci. Eng.* **59**, 612 (1988).

[47] Morgan, R. J., Jurek, R. J. and Yen, A., Donnellan, T. *Polymer* **34**, 835 (1993).

[48] Mijovic, J. and Andjelic, S. *Macromolecules* **29**, 239 (1996).

[49] Rozenberg, B. A., Shin, E. E. and Morgan, R. J. *Polymer* **38**, 639 (1997).

[50] Antoon, M. K., Koenig, J. L. and Serafini, T. *J. Polym. Sci. Polym. Phys. Ed.* **19**, 1567 (1981).

[51] Skrovanek, D. J., Painter, P. C. and Coleman, M. M., *Macromolecules* **19**, 699-705 (1986).

[52] Ngono, Y., Marechal, Y. and Mermilliod, N., *J. Phys. Chem. B* **103**, 4979-4985 (1999).

[53] Ngono, Y. and Marechal, Y., *J. Polym. Sci. B: Polym. Phys.* **38**, 329-340 (2000).

[54] Three absorption bands are resolved using Lorentzian function, yielding an excellent fit. The use of best-fit Gaussian function yields a fourth (low-intensity, high-frequency) peak, but the locations of the other three peaks are practically identical to those in the Lorentz fits.

[55] Choppin, G. R., Violante, M. R. *J. Chem. Phys.* **56**, 5890 (1972) and references therein.

[56] Harris, D. C., Bertolucci, M. D., *Symmetry and Spectroscopy* (Dover Publications, New York, 1989), Chap. 3, 93-224.

[57] Luck, W. A. P., Infrared Studies of Hydrogen Bonding in Pure Liquids and Solution, in *Water, A Comprehensive Treaties* (Plenum Press, New York, 1973), F. Franks Ed., Vol. 2, Chap. 4.

[58] Gragson, D. E. and Richmond, G. L., *J. Phys. Chem. B* **102**, 569-576 (1998).

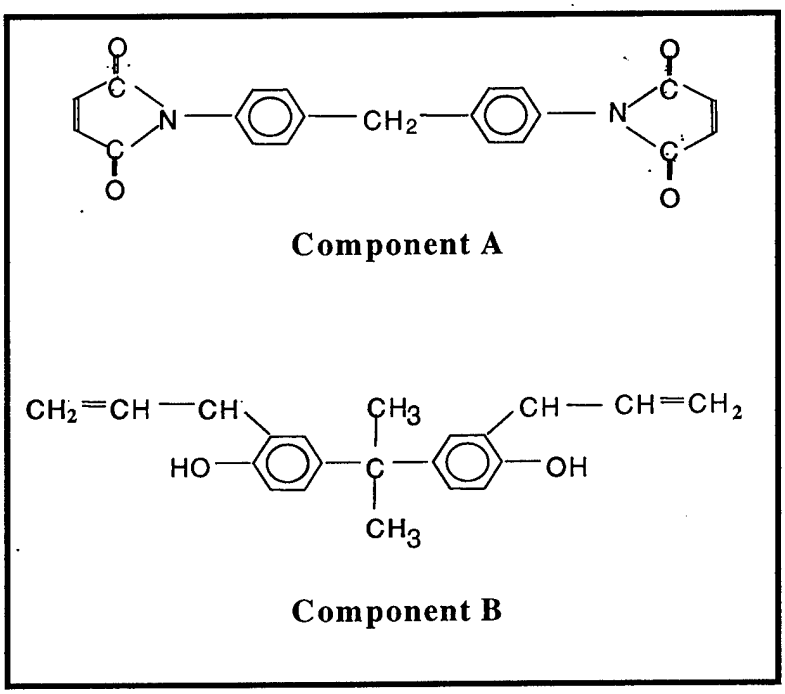

Figure 3.1. Chemical composition of the BMI formulation.

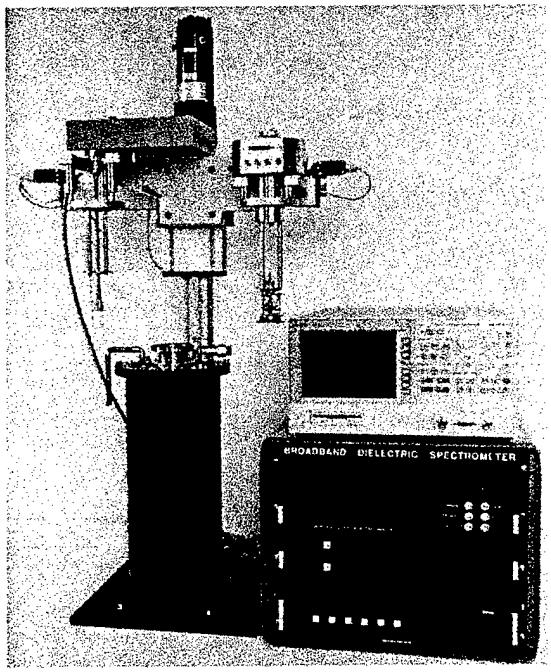

Figure 3.2. Photographs of our setup for dielectric measurements. On the right is Novocontrol's Alpha analyzer, and a 4291 RF impedance analyzer on top of it. On the left is the cryostat with the mobile unit behind it and the two cells in their uppermost (high frequency – left and low frequency – right).

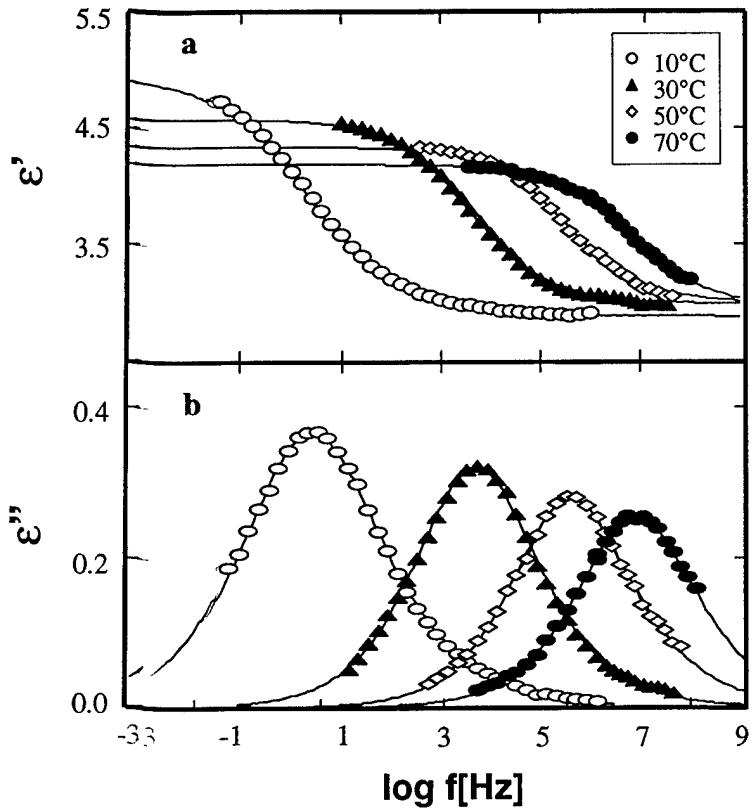

Figure 3.3. Dielectric permittivity (a) and loss (b) in the frequency domain for uncured BMI with temperature as a parameter. Solid lines are fits to the Havriliak-Negami equation.

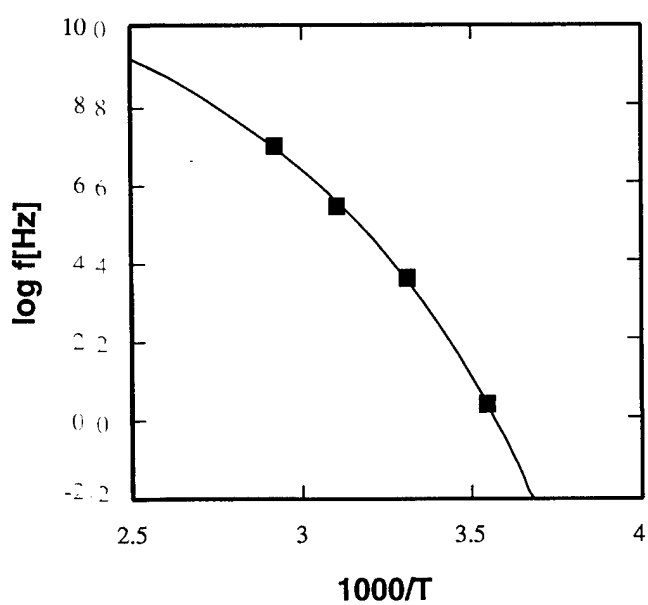

Figure 3.4. Log frequency at maximum loss as a function of reciprocal temperature for uncured BMI. Solid line is a VFT fit.

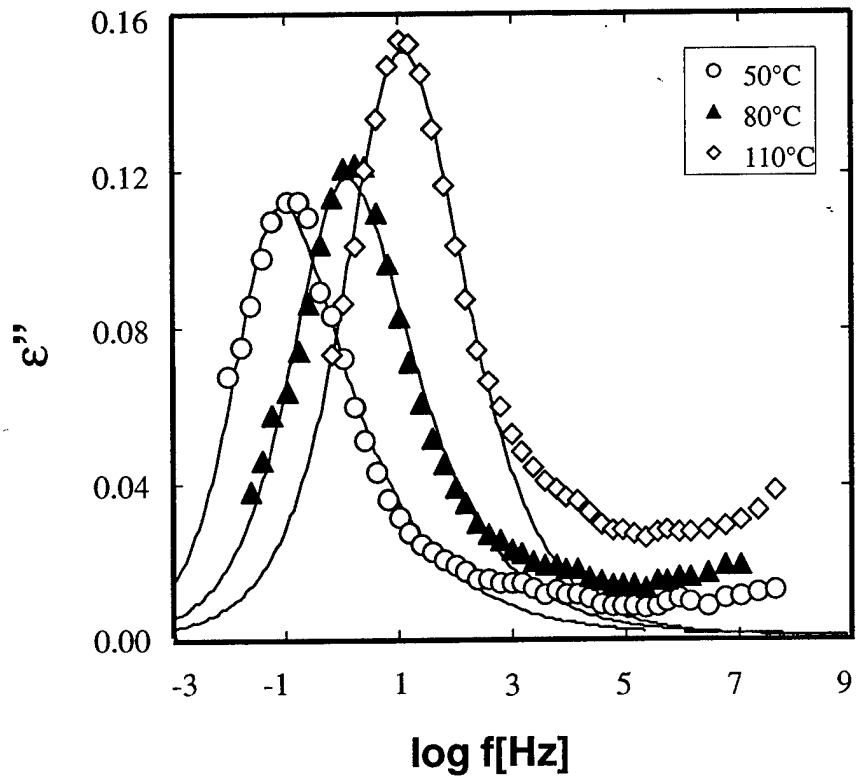

Figure 3.5. Dielectric permittivity and loss in the frequency domain for cured BMI with temperature as a parameter. Solid lines are fits to the Havriliak-Negami

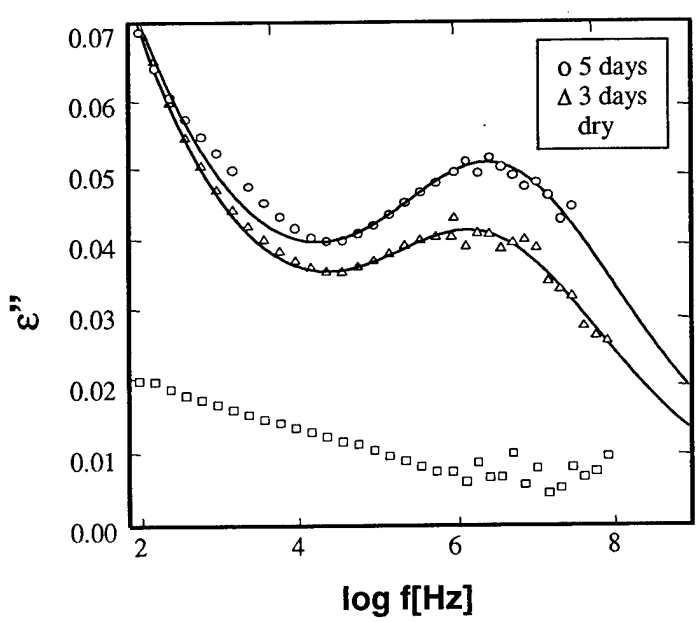

Figure 3.6. Dielectric loss in the frequency domain measured at 50°C for 0, 3 and 5-day exposure to 60°C/98% RH.

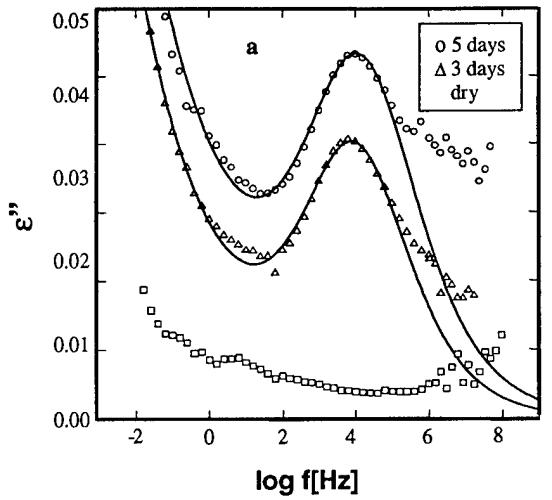

(a)

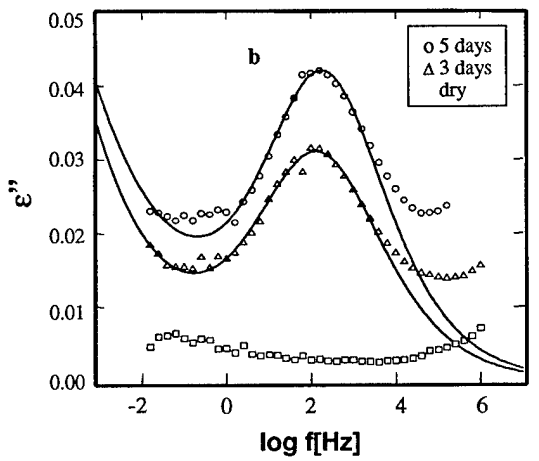

(b)

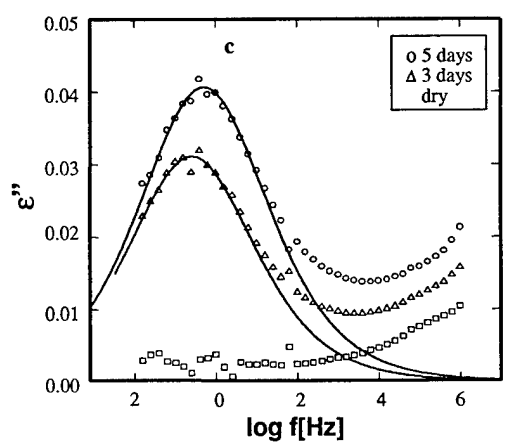

(c)

Figure 3.7. Dielectric loss in the frequency domain for cured BMI exposed to 60°C/98% RH with exposure time as a parameter, measured at (a) -20°C, (b) -60°C and (c) -100°C.

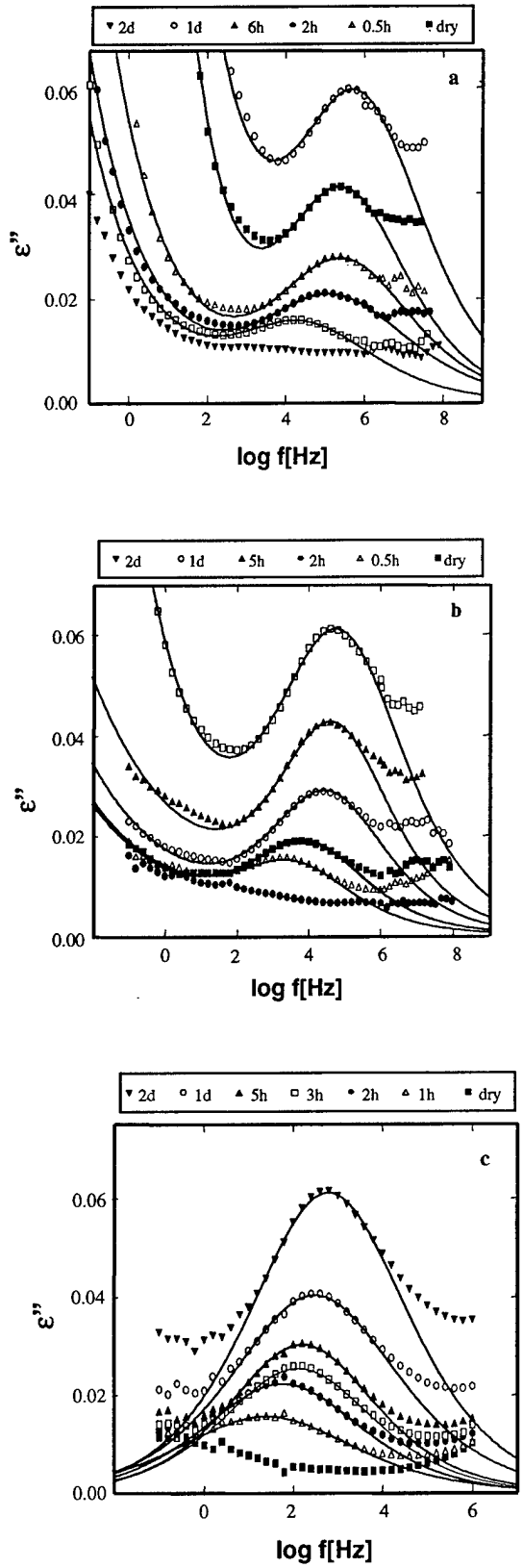

(a)

(b)

(c)

Figure 3.8. **Dielectric loss in the frequency domain for cured BMI exposure to 80°C/98% RH with exposure time as a parameter, measured at (a) 20°C, (b) –20°C and (c) -60°C.**

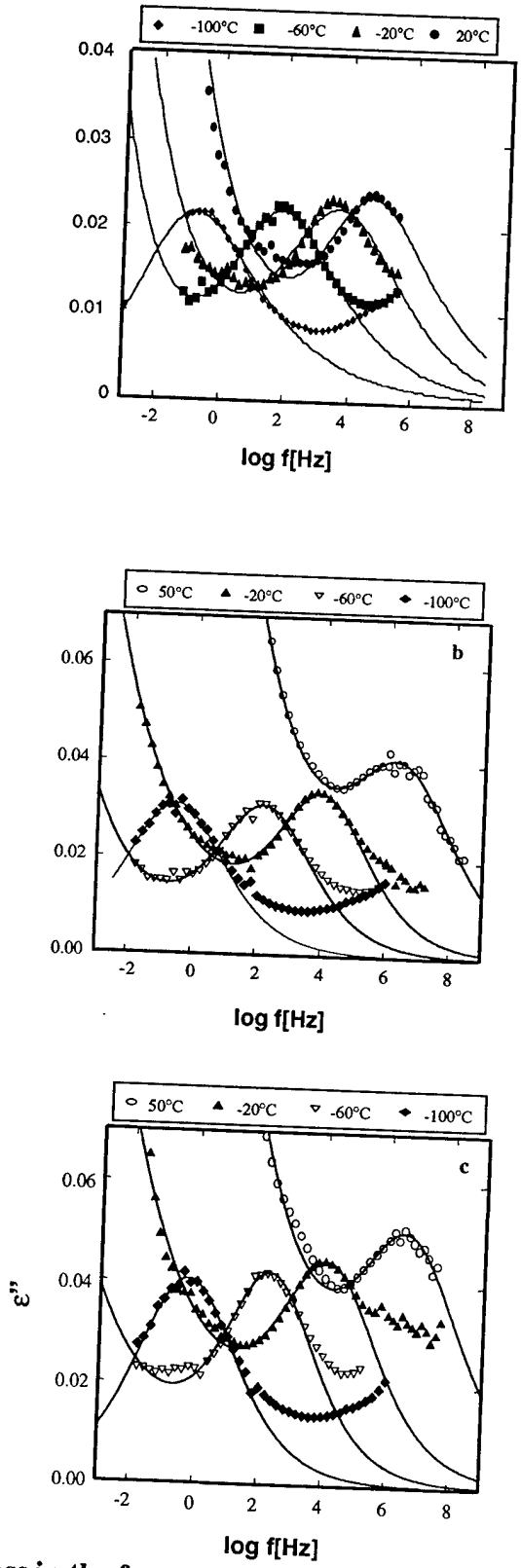

Figure 3.9. **Dielectric loss in the frequency domain for cured BMI after (a) 1day, (b) 3days and (c) 5days exposure at 80°C/98% RH, with measuring temperature as a parameter.**

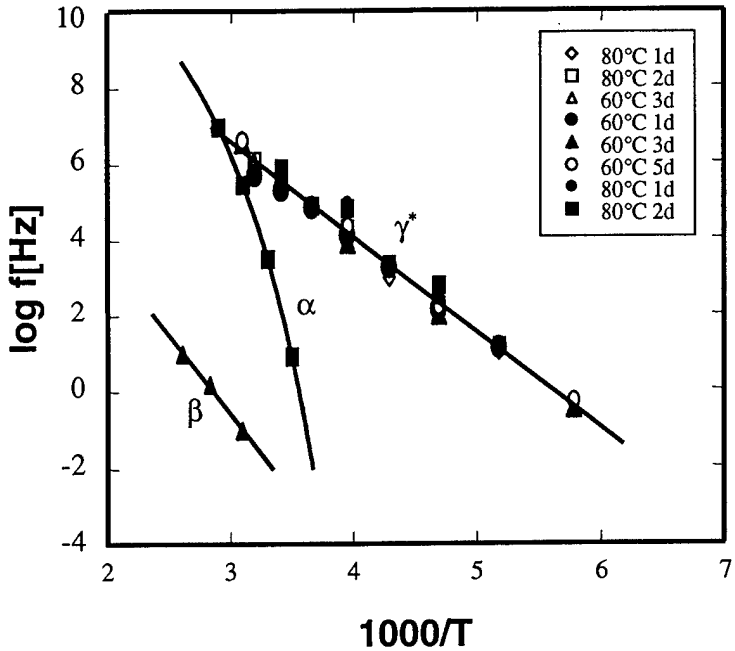

Figure 3.10. **Log frequency at maximum loss as a function of reciprocal temperature for different exposure times in dry and moist BMI.**

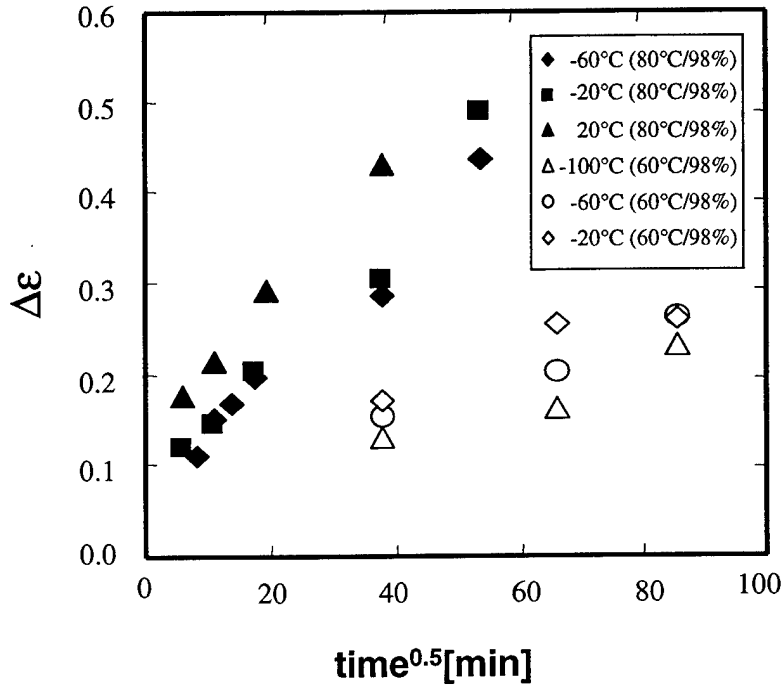

Figure 3.11. **Dielectric relaxation strength of cured BMI after exposure to 60°C and 80°C environments as a function of exposure time.**

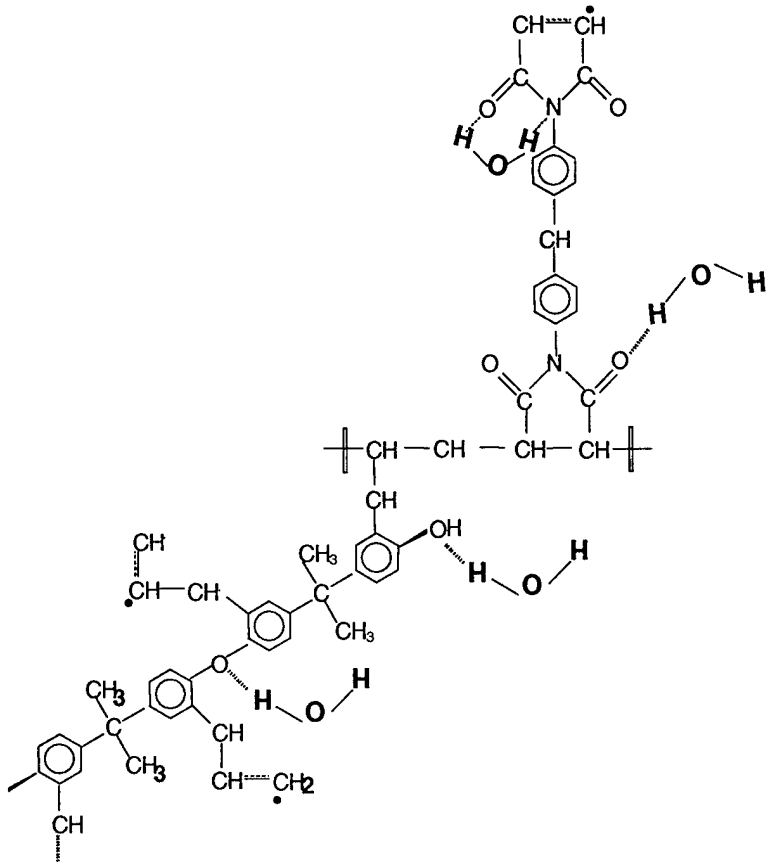

Figure 3.12. Chemical structure of a fragment of cured BMI network. Note: Different network sites that could participate in hydrogen bonding with absorbed water (shown in bold).

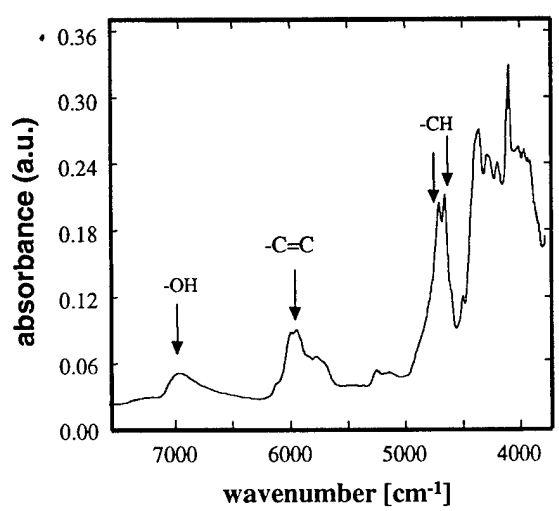

Figure 3.13. NIR spectrum of cured BMI.

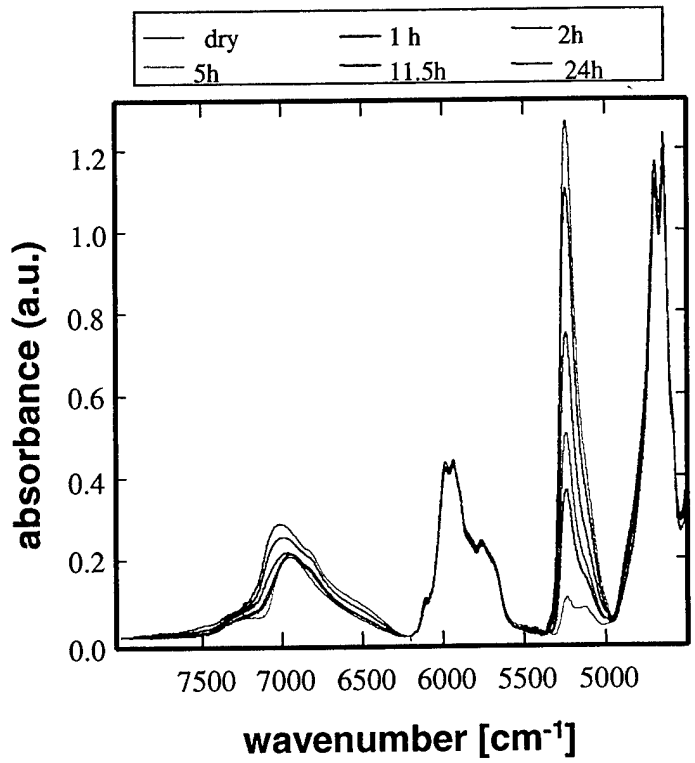

(a)

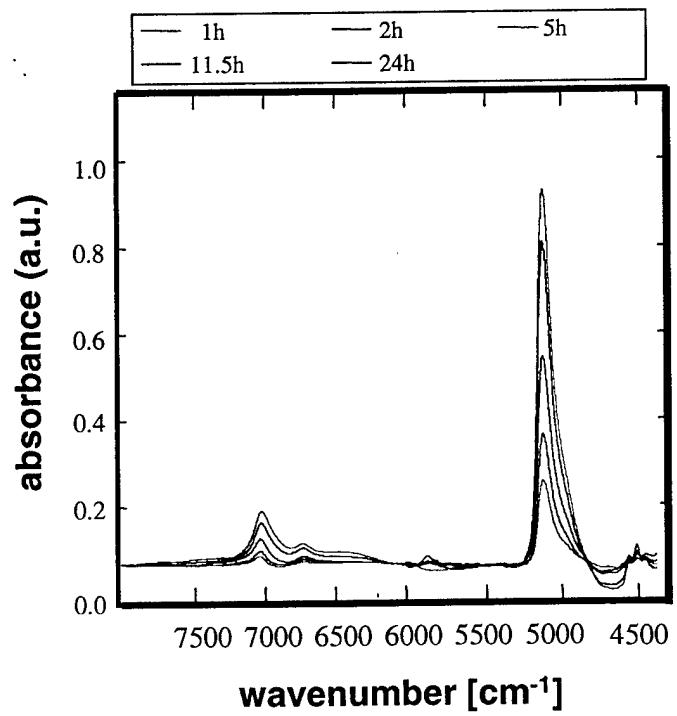

(b)

Figure 3.14. **a - NIR spectra of BMI at different exposure times: dry, 2hrs, 1day, 4 days and 23 days; b – difference spectra.**

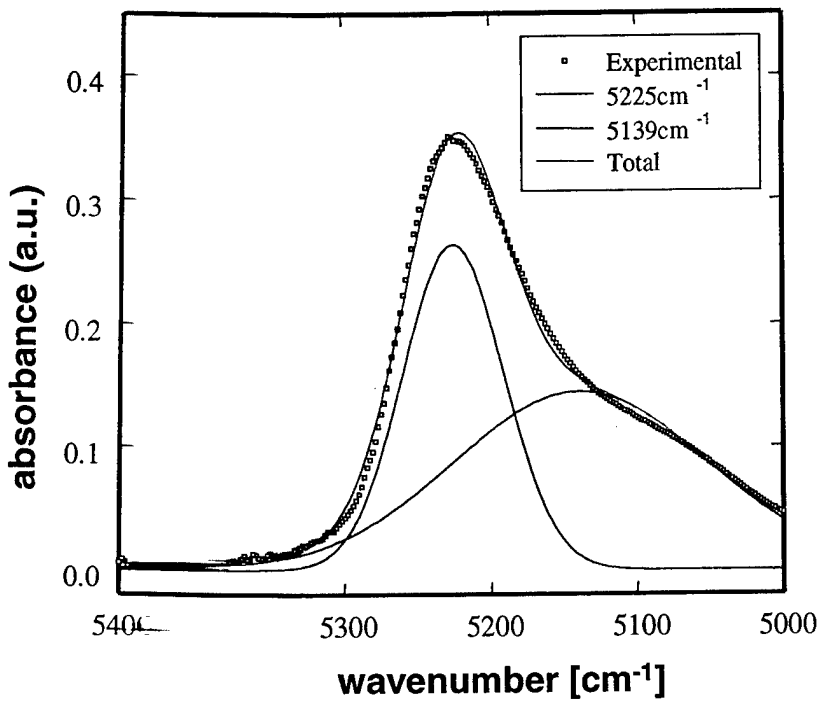

Figure 3.15. Deconvoluted difference spectra in the 5000-5400 cm-1 range after a 4-day exposure to 60°C /98%RH.

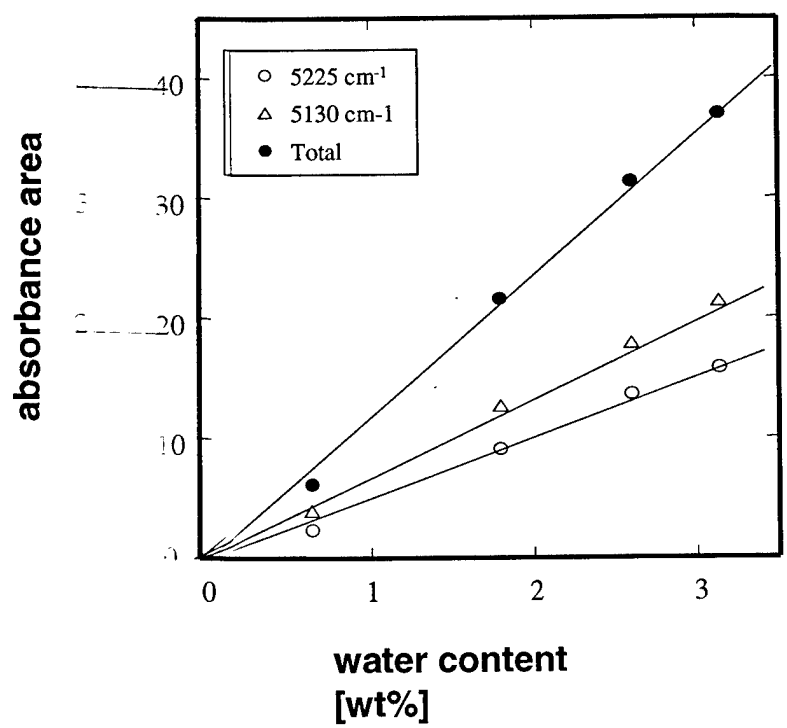

Figure 3.16. Absorbance area as a function of water content.

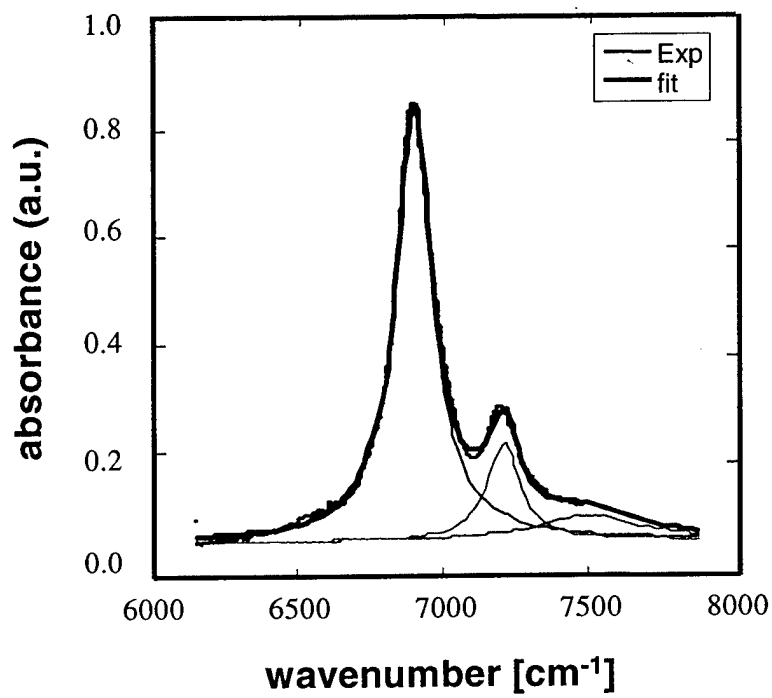

Figure 3.17 Deconvoluted NIR spectrum of cured BMI after exposure to 80°C for 5h.

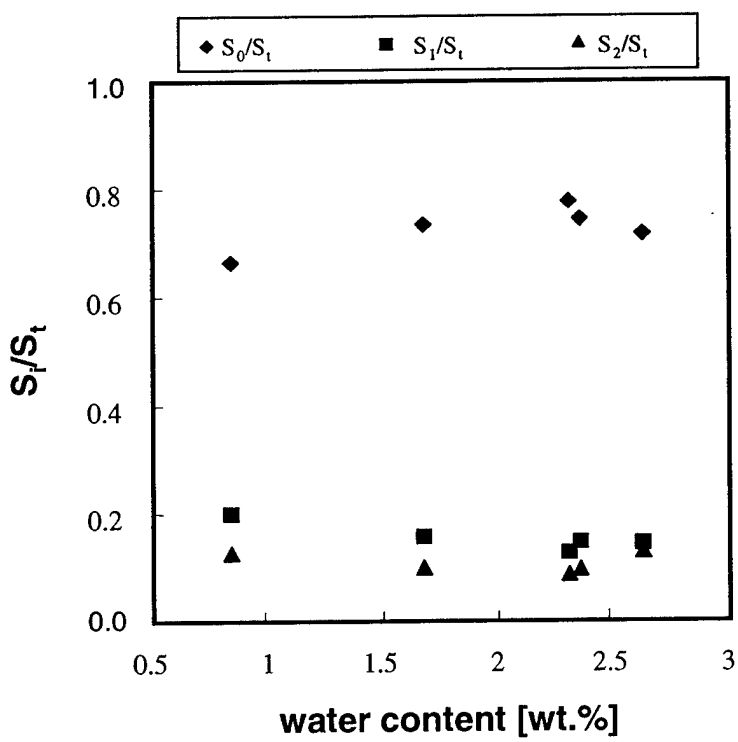

Figure 3.18. Ratio of non hydrogen-bonded (S_0) to total (S_t) absorbed water as a function of water content, calculated from the NIR data.

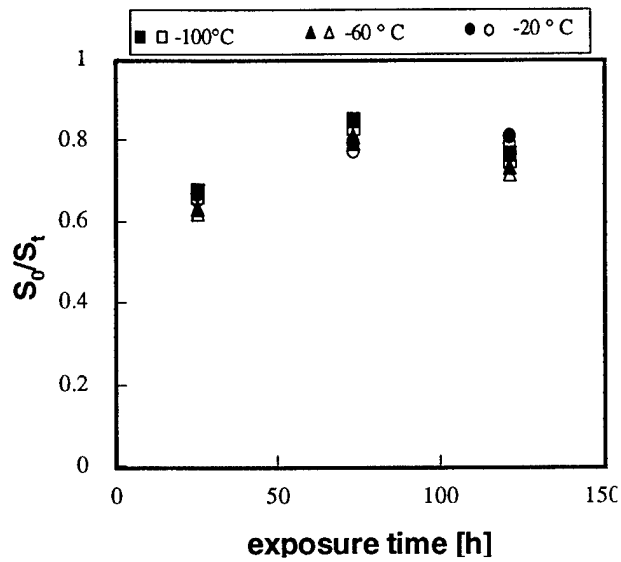

Figure 3.19 **Ratios of non hydrogen-bonded (S_0) to total (S_t) absorbed water as a function of water content, calculated from the DRS data; filled symbols (eq. 6); open symbols (eq. 7).**

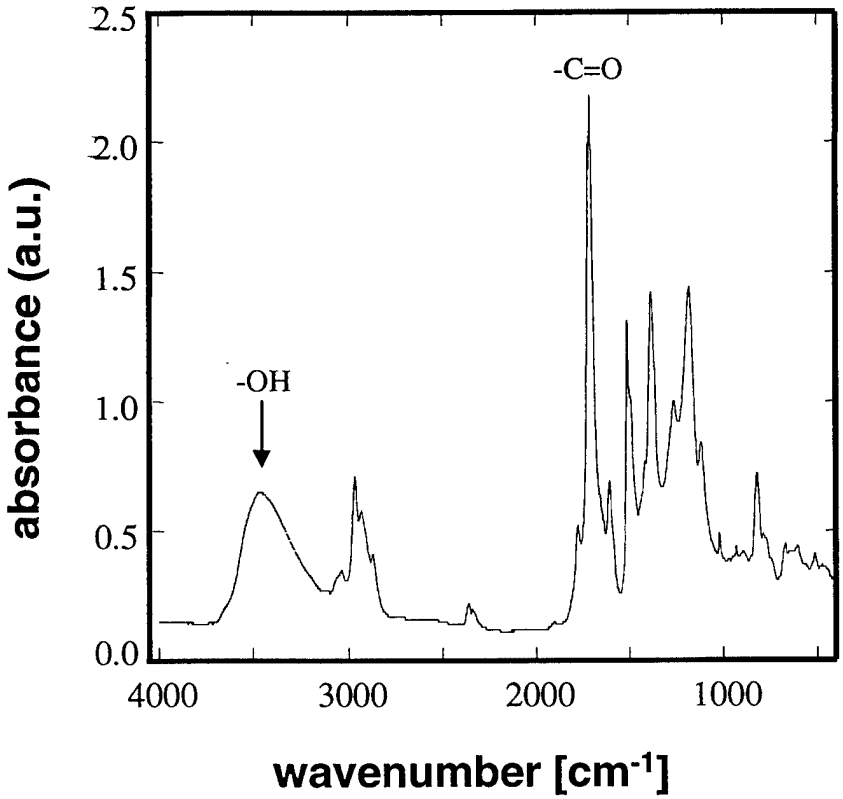

Figure 3.20. MIR spectrum of cured BMI.

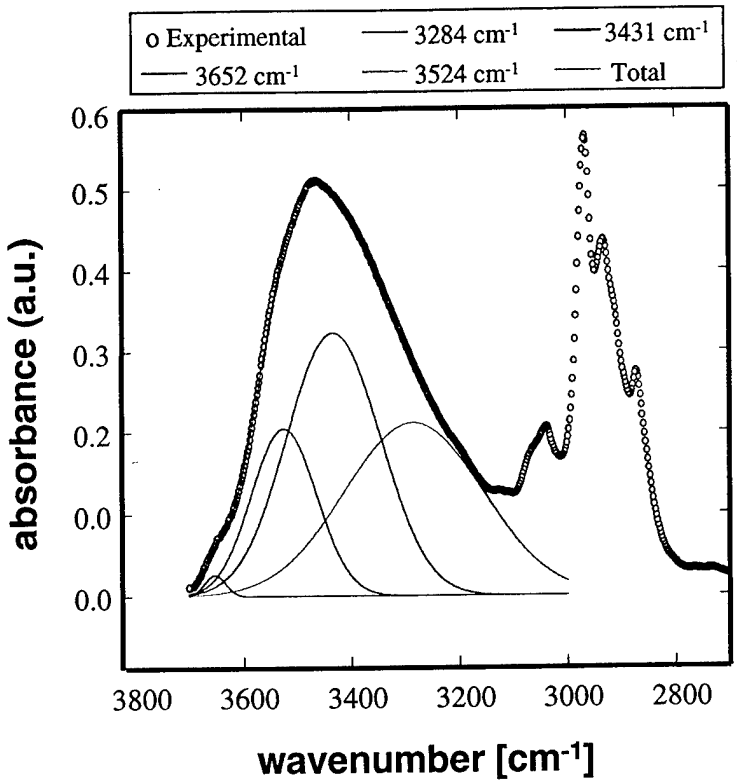

Figure 3.21. Deconvoluted MIR spectrum of cured BMI in the 3700-2800cm^{-1} region.

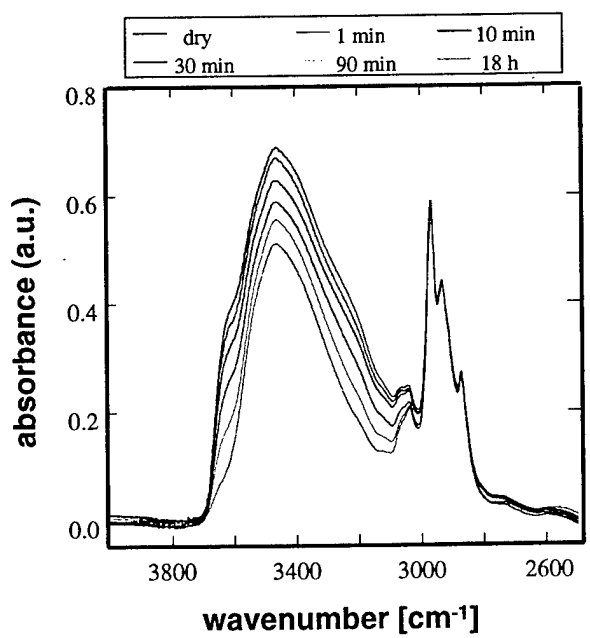

Figure 3.22. MIR spectra of cured BMI after exposure to different periods of time.

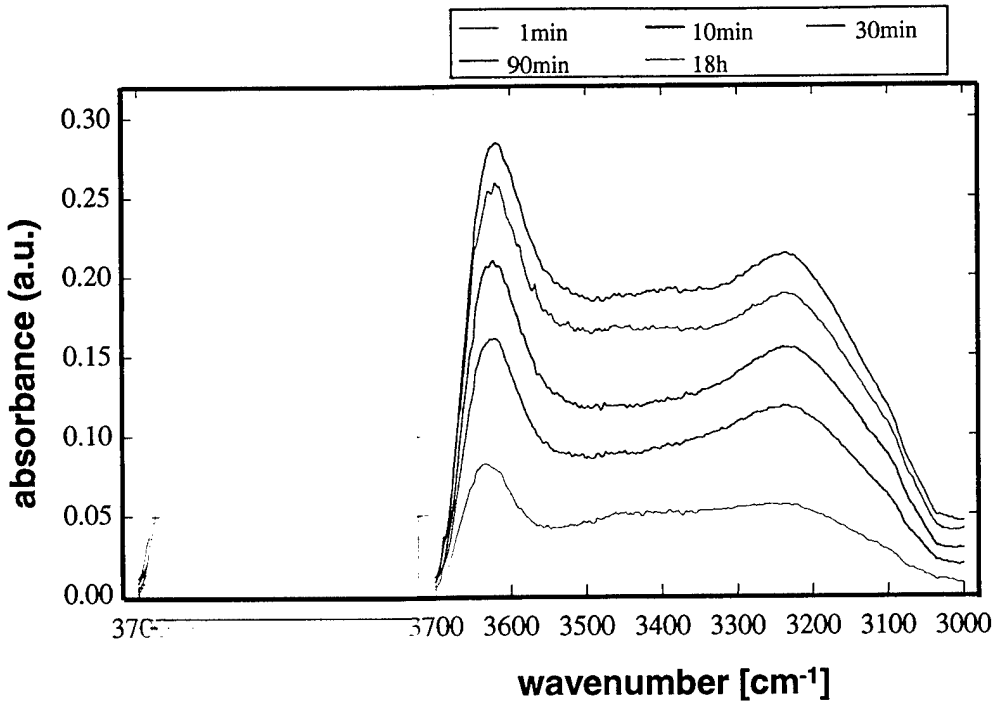

.23. Difference s[redacted]e spectra of cured BMI in the 3700-3000cm^{-1} range after exposure to [redacted]o 60°C/98 %RH for different time.

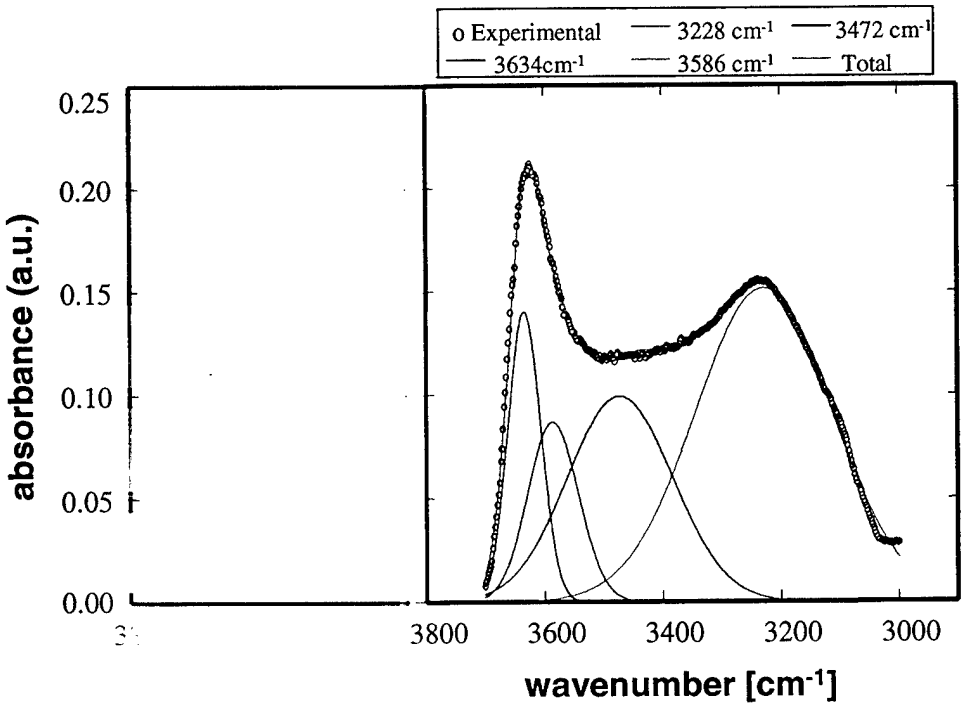

. Deconvoluted [redacted]d MIR spectrum of cured BMI in the 3700-2800cm^{-1} region, following expo[redacted]posure to 60°C/98 %RH environment for 30min.

4.0 THE STRENGTH AND DURABILITY OF ADHESIVELY BONDED JOINTS

4.1 Introduction

Adhesive bonding has always been a desirable method of joining two or more components and bonding is often used in structural applications for aircraft, automobile and many other industries. Bonded joints have a better strength-to-weight ratios and stress distribution compared to mechanical fastners [1]. Bonded joints, however, are susceptible to moisture and temperature-induced degradation. Absorption of moisture by adhesives is usually one of the main factors behind degradation of the joint strength.

All organic adhesives absorb water to some extent and as a result, the mechanical behavior of adhesives is changed. The change in mechanical properties of adhesive due to water absorption is the result of physical and/or chemical interactions of the adhesive with ingressing water molecules. Most of the modern adhesives are not easily hydrolyzed (good chemical resistance to water), however, physical interaction in the form of plasticization is common.

The primary objective of this work is to understand the microscopic physical and/or chemical changes occurring in the adhesive upon exposure to a hygrothermal environment, and to correlate that information to the changes in the macroscopic mechanical properties.

4.2 EXPERIMENTAL

4.2.1 Test Equipment, Materials and Supplies

The environmental test chamber (temperature/humidity chamber) was purchased from Associated Environmental Systems, Ayer, MA. The de-ionized water (resistivity ~ 18.0 MΩ) system (E-pure system, Barnstead/Thermolyne Corporation) was purchased from Fisher Scientific. A direct current power supply unit (model LM30-6, Sorensen), required for phosphoric acid anodization, was purchased from Elgar Electronics Corporation, San Diego, CA. An analytical balance (model HR-120) was purchased from Precision Weighing Balances, Bradford, MA. The balance is accurate to 0.0001 grams.

Aluminum (2024-T3) plates and rods were obtained from Copper and Brass Sales, Cleveland, Ohio for making wedge, double notch shear (DNS) and DRS test specimens. The wedge test specimens were made from 3.175 mm thick, 152.4 x 127 mm aluminum plates, while DNS test specimens were made from 4.064 mm thick, 114.3 x 88.9 mm aluminum plates. The plates were saw cut to size by the manufacturer to help ensure flatness. The stainless steel shim (Precision Brand) having a thickness of 0.127 mm, used for maintaining bondline thickness in bonded joints in DNS and wedge test configurations, was purchased from Innovative Distributor Group, Inc. (IDG), Dayton, Ohio.

The unsupported (without scrim) FM-73U epoxy film (0.0889 mm thick) was obtained from Cytec Fiberite. The FM73U film adhesive was stored in the freezer (≈-20°C) until required. The model epoxy system consisted of diglycidyl ether of Bisphenol A (DGEBA) and methylene dianiline (MDA) were obtained from Sigma Aldrich Chemical Corporation. A two-component bismaleimide (BMI) formulation (Matrimid 5292) consisting of 4, 4' bismaleimidodiphenyl

methane (component A) and 0, 0' diallyl bisphenol A (component B) were obtained from Ciba-Geigy Corporation.

Chemicals such as O-phosphoric acid (certified ACS grade), nitric acid (certified ACS plus grade) and sodium hydroxide pellets (certified ACS grade) were purchased from Fisher Scientific and used without further purification.

The adhesively bonded aluminum plates were machined to prepare DNS and wedge test specimens. The bonded plates were machined by BITEC or CNC Production Machining or Stafford Gage and Tool, Dayton, Ohio.

4.2.2 Surface Pretreatment

The surfaces of the DNS and wedge test specimens were prepared for bonding using ASTM Standard D 2651-90 "Practice for Preparation of Metal Surfaces for Adhesive Bonding" and ASTM Standard D 3933-88 "Guide for the Preparation of Aluminum Surfaces for Structural Adhesive Bonding (Phosphoric Acid Anodizing)". The PAA surface treatment of aluminum plate was carried out for 20 minutes at 10 volts. The PAA surface treatment was utilized on all aluminum adherends prior to adhesive bonding. Phosphoric acid anodization (PAA) was carried out in phosphoric acid solution (7% v/v) bath for 20 minutes at 10 0.1 volts. The PAA surface treated adherends were stored in desiccator until bonding. The PAA treated adherends were bonded within 3 days after the surface preparation. The PAA treated adherends were inspected prior to bonding using the polarizing filter.

4.2.3 Adhesive Bonding

The appropriate bonding procedure and cure schedule for FM-73U, model epoxy and bismaleimide adhesives are given below.

For FM-73U adhesive system, two layers of adhesive film were sandwiched between two PAA treated aluminum adherends. The bond line thickness of 0.127 mm was maintained by placing two stainless steel shim (0.127 mm thick) on either sides of the plate. The plates were then placed in a hot press and cured. The cure schedule involved heating the plates from 20°C to 110°C at the rate of 5°C/min and maintaining it at 110°C for 60 minutes under pressure (0.10 MPa).

For model epoxy, the stoichiometric amounts of epoxy groups and amine hydrogen were used and the components were mixed until a clear mixture was obtained. The mixture was then spread on PAA treated aluminum adherends, and the two plates were pressed together. The cure schedule involved heating the sample from 20°C to 180°C at the rate of 5°C/min and maintaining it at 180°C for 30 minutes under pressure (0.10 MPa).

The two components of bismaleimide formulation were mixed in equimolar ratio at 120-125°C and stirred continuously until a clear, homogeneous mixture was obtained. The mixture was then spread on PAA treated aluminum adherends, and the two plates were pressed together. The cure schedule involved heating the sample from 20°C to 240°C at the rate of 5°C/min and maintaining it at 240°C for 30 minutes under pressure (0.10 MPa). The adhesively bonded plates were then machined to make wedge and DNS test specimens. However, for bismaleimide this cure schedule produced a highly brittle adhesive; almost all of the adhesively bonded plates failed while they were machined to produce wedge and DNS test specimens. So, mechanical test data could not be obtained for the aluminum/bismaleimide system.

For each adhesive system, the adhesively bonded test specimens were subjected to the identical thermal history (by heating 10°C above the T_g and then cooling to room temperature) prior to the exposure to environment in order to factor out the effect of structural relaxation between different test samples. The DSC Tg_α of cured FM73U and model epoxy adhesives was 93°C and 170°C, respectively.

4.2.4 Double Notch Shear (DNS) Test:

The FM73-U/aluminum DNS specimens were exposed to 95% relative humidity at 50°C, 60°C and 80°C for various times. The model epoxy/aluminum DNS specimens were exposed to 95% relative humidity at 60°C, and at room temperature in 20% relative humidity for various times. At each exposure condition, test specimens were removed from the environmental chamber at regular intervals and weighed after allowing them to cool to room temperature (approximately after 10 minutes). At the end of the environmental exposure period, specimen was removed from the environmental chamber and a mechanical test was performed within one hour. Some of FM-73U/aluminum specimens that were exposed to 95% relative humidity at 50°C and 80°C for 14 days were vacuum dried at 70°C for 0.5 hr prior to mechanical testing. For each DNS specimen, the average thickness and width of the bonded region were recorded prior to mechanical testing. The DNS specimens were subjected to axial compression load as per ASTM D 3846-94. The specimen was loaded edgewise in a supporting jig of the same description as referenced in ASTM D 695. For each specimen, load versus stroke data was recorded. The ultimate failure load was noted for each test specimen. The shear strength was then calculated from the knowledge of ultimate failure load and area of the bonded region. An average shear strength value was obtained by testing four or five specimens per condition. The debonded DNS specimens were visually inspected to determine the mode of failure.

4.2.5 Wedge Test:

The wedge test specimens were prepared as per ASTM D 3762-79 standard. Generally, the ASTM test procedure was followed except that the size of the wedge specimen was shortened from 203.2 × 25.4 mm to 127 x 25.4 mm. The FM-73U/aluminum wedge specimens were exposed to 95% relative humidity at temperatures 40°C, 50°C, 60°C, 70°C and 80°C. Some FM-73U/aluminum test specimens were also exposed to boiling water. The model epoxy/aluminum wedge specimens were exposed to 95% relative humidity at 60°C and 80°C, and at room temperature in 20% relative humidity. For each environmental condition, a total of five wedge specimens were tested. The wedge test specimen was periodically removed from the test chamber and crack length was measured and recorded as a function of time. The initial crack length a_0, crack extension Δa, and crack extension failure mode were recorded in accordance with the ASTM standard. At the end of the test exposure-period, wedge specimens were forced open and visually inspected to determine the mode of failure.

4.3 RESULTS AND DISCUSSION

4.3.1 Adherend Surface Characterization

The PAA treated aluminum surface was characterized using X-ray photoelectron spectroscopy (XPS), Auger Electron Spectroscopy (AES) and Scanning Electron Microscopy (SEM). The elemental composition of PAA treated aluminum surface, as determined by XPS technique, is given in Table 4.1. The elements carbon, oxygen, aluminum and phosphorous were detected on PAA treated aluminum surfaces. The binding energy of phosphorous (134.0 eV) suggests that it is in the oxidized form, most likely in the form of PO_4^{-3} or P_2O_5. The binding energy of aluminum (74.4 eV) is consistent with that of aluminum in the form of oxide (Al_2O_3). The

oxygen binding energy value is 531.7 eV. When phosphorous is present in the form of $AlPO_4$ and the contribution of this is subtracted off, the O/Al ratio for what remains is about 1.6, which is close to what is expected for Al_2O_3. The source of carbon on the PAA-treated aluminum surface is from the hydrocarbon contamination from the atmosphere. The hydrocarbon contamination is difficult to avoid since hydrocarbons are adsorbed inadvertently on the metal surfaces when exposed to the atmosphere.

The AES depth profile of a PAA treated aluminum surface is shown in Figure 4.1. The sputter rate for AES depth profile is 150 Å/min. The AES depth profile of a PAA-treated aluminum shows that the aluminum oxide layer is about 1400 Å thick.

The SEM photomicrograph of as anodized (PAA treated) aluminum surface is shown in Figure 4.2. The oxide surface of a PAA-treated aluminum has a microscopically rough morphology. The micro-rough oxide morphology provides a better means for mechanical keying between the oxide surface and the adhesive that is desired for improved strength and durability of an adhesively bonded joint.

4.3.2 DNS Test Results for FM73U/aluminum Joints

Figure 4.3 shows a representative load versus stroke trace of a control specimen (as bonded, unexposed DNS specimen). The average maximum failure shear strength for unexposed DNS specimens is 64.0 ± 3.0 MPa. The load versus stroke data exhibits a nonlinear stress-strain behavior that can be adequately represented by a bilinear curve, which is typical of ductile materials. In general, the bilinear behavior can be conveniently divided into two parts: an elastic zone with corresponding elastic shear modulus and elastic shear strain component, and a plastic

zone with corresponding plastic shear modulus and plastic shear strain component. The DNS test results can be interpreted in terms of shear stress-strain curves, which is a material property. The visual inspection of debonded control specimen showed bond failing primarily within the adhesive (cohesive failure mode).

Figures 4.4-4.6 shows a representative load versus stroke data for DNS specimens exposed to 95% relative humidity at 50°C, 60°C and 80°C, respectively, for various times. A representative load versus stroke data for an unexposed specimen is also included in the figure for comparison purposes. The shear strength, as a function of various test environments and exposure time for FM-73U/aluminum bonded joints, is summarized in Table 4.2. The standard deviations from the average values are given at 95% confidence limit. The average shear strength values increased slightly for specimens exposed to 95% relative humidity for a day (24 hours) at 50°C and 60°C compared to the control specimen (no-exposure specimen), however, the strength values are within the experimental errors of margin. An increase in an initial joint strength could be attributed to the relief of shrinkage stresses in the adhesive due to the presence of moisture [2]. A similar behavior has been reported in the literature for various adhesively bonded joints where an initial increase in joint strength with time in a wet environment is observed [3,4]. The shrinkage stresses develop in the adhesive during the bonding and curing process. However, for specimens exposed to 95% relative humidity at 80°C, the shear strength decreases as the exposure time is increased. Compared to a control specimen, specimens exposed to 95% relative humidity at 80°C didn't exhibit an increase in shear strength after 24 hours of exposure. This could be due to accelerated plasticization of the adhesive at 80°C that negates the advantage due to relief of shrinkage stresses in the adhesive. In general, the DNS test result shows that the average shear strength decreases with an increase in exposure time at various temperatures.

Compared to a control specimen, the average shear strength decreased by 17%, 9% and 36% for specimens exposed to 95% relative humidity at 50°C for 3 days, 7 days and 14 days, respectively. For specimens exposed to 95% relative humidity at 60°C for 3 days, 7 days and 14 days the average maximum shear strength decreased by 7%, 5% and 34%, respectively. The average shear strength decreased by 11%, 31% and 40% for specimens exposed to 95% relative humidity at 80°C for a day, 3 days and 7 days, respectively. Compared to unexposed specimens, the load corresponding to yield point is reduced for specimens exposed to 95% relative humidity at 50°C, 60°C and 80°C for various times. The adhesive is increasingly plasticisized as the exposure time is increased at any given temperature.

Figure 4.7 shows the photographs of failure surfaces of representative specimens exposed to 95% relative humidity at 50°C for various times. The visual inspection of failure surfaces revealed that the failure mode becomes increasingly interfacial (bond fails at the adhesive/metal interface) as the exposure time is increased. Interfacial failure is observed around the edges of the bonded region, which moves towards the center of the bonded region as the exposure time is increased. The interfacial failure pattern is obvious since moisture enters from all four sides of the bonded region and diffuses towards the center of the bonded region, and with time, moisture eventually reaches the adhesive/metal interface and degrades the oxide layer at the interface. A similar failure pattern was observed for DNS specimens exposed to 95% relative humidity at 60°C and 80°C. However, the interfacial (metal/adhesive) degradation process is accelerated at higher temperatures.

Specimens that were exposed to 95% relative humidity for 14 days at 50°C regains a part of the lost strength when they were vacuum dried prior to mechanical testing, see Figure 4.4. The

specimens that were exposed to 95% relative humidity at 80°C for 14 days and vacuum dried prior to mechanical testing exhibited the similar behavior. The result suggests that only a part of the strength could be recovered by drying the specimen. The unrecoverable strength could be due to a permanent degradation of the adhesive/metal interface.

4.3.3 Wedge Test Results for FM73U/aluminum Joints

Figure 4.8 shows the average crack length as a function of exposure time for specimens exposed to 95% relative humidity at 40°C, 50°C, 60°C, 70°C and 80°C. The initial crack length upon wedge insertion is about 43.2 mm for all wedge specimens. The crack propagation for wedge specimens exposed to various temperatures at 95% relative humidity follows the order: 80°C>70°C>60°C>50°C>40°C. The average crack growth is less than 2.5 mm for wedge specimens kept in desiccator (relative humidity < 15%) at room temperature for about 400 hours. The visual examination of failure surfaces of debonded wedge specimens revealed that the failure is within the adhesive for specimens exposed to a low humidity atmosphere (<15% relative humidity) in the desiccator at 20°C. The failure mode due to environmental exposure to 95% relative humidity becomes increasingly interfacial as the exposure temperature is increased from 40°C to 80°C.

The average crack length as a function of exposure time for specimens exposed to boiling water is shown in Figure 4.9. The average crack length is 45.7 mm for wedge specimens exposed to boiling water for about 18 hours. A relatively higher crack growth for specimens exposed to boiling water is not surprising since a hot-wet environment is considered to be one of the harshest conditions for adhesively bonded joints. The failure mode was largely cohesive within the adhesive (visual inspection only).

Since the average crack growth for specimens exposed to 95% relative humidity at various temperatures is much smaller than for specimens exposed to boiling water for an equivalent time, the mechanism of bond degradation could be different in two cases or the degradation process is simply accelerated in boiling water. The stresses, mechanical and/or environmental, that an adhesively bonded joint experiences during environmental exposure, in general, accelerates the bond degradation processes. For example, the hydrolysis of epoxies by water was observed for stressed bonded joints exposed to 80°C, but unstressed joints were unaffected for up to 3 months [5,6]. The presence of stresses in bonded joint lowers the activation energy for breaking chemical bonds in the polymers and/or chemical bonds between polymer and metal oxides, and thus a bonded joint becomes susceptible to environmental attacks [7,8].

4.3.4 Wedge Test Results for Model Epoxy/aluminum Joints

Figure 4.10 shows the average crack length as a function of exposure time for specimens exposed to 95% relative humidity at 60°C and 80°C, and for specimens exposed to <15% relative humidity (in desiccator) at room temperature (20°C). The initial crack length upon wedge insertion is 86.5 mm, 86.1 mm and 84.5 mm for specimens exposed to 20°C, 60°C and 80°C, respectively. However, no significant crack propagation was observed for specimens exposed to 20°C/15% RH and 60°C/95% RH for more than 500 hrs and for specimens exposed to 80°C/95% RH for about 280 hrs. The wedge test result thus suggests that no significant deterioration of bonded joints have occurred as a result of hygrothermal environmental exposure. The post failure examination of failed bonded joints revealed that for each exposure condition the failure is entirely within the adhesive (cohesive failure). This is in sharp contrast to FM-73U/aluminum bonded joints, where increasingly interfacial failure was observed for wedge specimens exposed to 95% relative humidity as the exposure temperature was increased from 40°C to 80°C. This result suggests that

the model epoxy is comparatively a better moisture resistant adhesive system than a commercial epoxy adhesive, FM-73U epoxy. This is understandable, since FM-73U adhesive contains a variety of fillers and additives that could make it less moisture resistant.

4.3.5 DNS Test Results for Model Epoxy/aluminum Joints

Figure 4.11 shows a representative load versus stroke data for DNS specimens exposed to 95% relative humidity for 3 days, 7 days and 10 days. A representative load versus stroke data for an unexposed specimen is also included in the figure for comparison purposes. The shear strength as a function of exposure time is summarized in Table 4.3. The standard deviations from the average values are given at 95% confidence limit. The average shear strength value for a control specimen (no-exposure specimen) is 64.7 ± 2.0 MPa. The average shear strength values for specimens exposed to 95% relative humidity at 60°C for 3 days, 7 days and 10 days are 63.3 ± 0.8, 60.5 ± 1.5 and 59.7 ± 2.0 MPa. The visual inspection of failure surfaces of model epoxy/aluminum DNS specimens revealed that the bonded joints failed within the adhesive (cohesive failure). For model epoxy/aluminum DNS specimens exposed to 95% relative humidity at 60°C for various times the decrease in shear strength values with exposure time is not large compared to FM-73U/aluminum system under a similar exposure condition. This could be due to the fact that the model epoxy adhesive is comparatively more moisture resistant than the FM-73U adhesive.

4.3.6 Mechanical strength – Dielectric Relaxation Data Correlation

Since DRS studies and mechanical tests were performed on two different test specimens having different specimen geometry and bondline thickness, a methodology was developed to normalize the data so that DRS data could be correlated to mechanical test data. First, the dielectric

relaxation strength, measured at any given temperature, was calculated from the DRS test data for various exposure time for a given humidity/temperature exposure condition. The relaxation strength was then plotted against the square root of exposure time divided by the adhesive bondline thickness to obtain a calibration line. The test data was normalized with respect to bondline thickness to take into account the different bondline thickness used in DRS and mechanical tests. From calibration plot (relaxation strength versus exposure time plot), the relaxation strength values were estimated for those exposure-time for which corresponding shear strength (mechanical test) data was obtained. The estimated relaxation strength was then correlated with the shear strength data for the corresponding exposure condition. A similar correlation was also made between dielectric loss maximum and shear strength.

The dielectric loss maximum and relaxation strength (measured at 10°C and 50°C) versus exposure time plots for model epoxy/aluminum DRS specimens exposed to 98% relative humidity at 60°C are shown in Figures 4.12 and 4.13. A linear relationship was obtained. The shear strength as a function of dielectric relaxation strength (measured at 10°C and 50°C) for model epoxy/aluminum bonded joints exposed to 60°C/95% relative humidity is shown in figure 4.14. Figure 4.15 shows the plot of shear strength as a function of dielectric loss max. (measured at 10°C and 50°C) for model epoxy/aluminum bonded joints exposed to 60°C/95% relative humidity. A reasonably good linear relationship was observed between shear strength and dielectric loss max. data, and between shear strength and relaxation strength data. Since, for model epxoy/aluminum system the failure was entirely within the adhesive for specimens exposed to 60°C at 95% relative humidity the correlation between mechanical test data and DRS test data is meaningful. A good correlation between measured shear strength and dielectric properties (loss

maximum and relaxation strength) would thus suggest that DRS could be potentially used as a NDI technique to monitor the integrity of adhesively bonded joints.

Figures 4.16 shows a linear plot of dielectric loss maximum as a function of exposure time for FM-73U/aluminum bonded joints after exposure to 60°C/95% relative humidity. The dielectric loss maximum was measured at 50°C. The shear strength versus dielectric loss maximum plot for FM-73U/aluminum bonded joints exposed to 60°C/95% relative humidity is shown in figure 4.17. Although, for FM-73U/aluminum bonded joints exposed to 60°C/95% relative humidity the bond failure was not entirely within the adhesive, the mechanical test data correlated reasonably well with DRS data.

4.4 CONCLUSIONS

The shear strength of FM-73U/aluminum joints decreases with an increase in exposure time at 95% relative humidity at constant temperatures. The bonded DNS joint fails increasingly in the metal/adhesive interface as the exposure temperature and duration is increased for FM-73U/aluminum bonded joints. The wedge test result shows that the durability of FM-73U/aluminum bonded joint decreases with the increase in temperature. The durability of FM-73U/aluminum joints in 95% relative humidity at various temperatures follows the order: 40°C > 50°C > 60°C > 80°C. Boiling water was the most aggressive environment among all environments tested for bond durability. The wedge test and shear strength data for model epoxy/aluminum bonded joints suggests that the model epoxy is a better moisture resistant adhesive than the commercial FM-73U epoxy.

A reasonably good correlation between measured shear strength data and measured dielectric response was observed for model epoxy/aluminum joints and FM-73U/aluminum joints.

REFERENCES

1. A.J. Kinloch, "*Adhesion and Adhesives Science and Technology*", Chapman and Hall, New York, 1987, p.2.

2. M.R. Bowditch, *Int. J. Adhesion and Adhesives* **16**, 73 (1996).

3. J.D. Minford, in: *Durability of Structural Adhesives*, ed. A.J. Kinloch, Applied Science, London, 1983, p135-214.

4. J.L. Cotter in: *Developments in Adhesives*, ed. W.C. Wake, Elsevier Applied Science, London, 1977, p1.

5. M.K. Antoon, J.L. Koenig and T. Serafini, *J. Polymer Sci. Phys. Edn.* **19**, 1567 (1981).

6. M.K. Antoon and J.L. Koenig, *J. Polymer Sci. Phys. Ed.* **19**, 197 (1981).

7. J. Comyn, in: *Durability of Structural Adhesives,* ed. A.J. Kinloch, Applied Science, London, 1983, p.85-131.

8. A.J. Kinloch, in: *Durability of Structural Adhesives*, ed. A.J. Kinloch, Applied Science, London, 1983, p.1-39.

Table 4.1. XPS analysis results of a PAA treated non-bonded aluminum surface.

Element	Concentration (atomic %)	Binding Energy, eV
Carbon	22.5	285.0 (C 1s)
Oxygen	48.8	531.7 (O 1s)
Aluminum	26.6	74.4 (Al 2p)
Phosphorous	2.2	134.0 (P 2p)

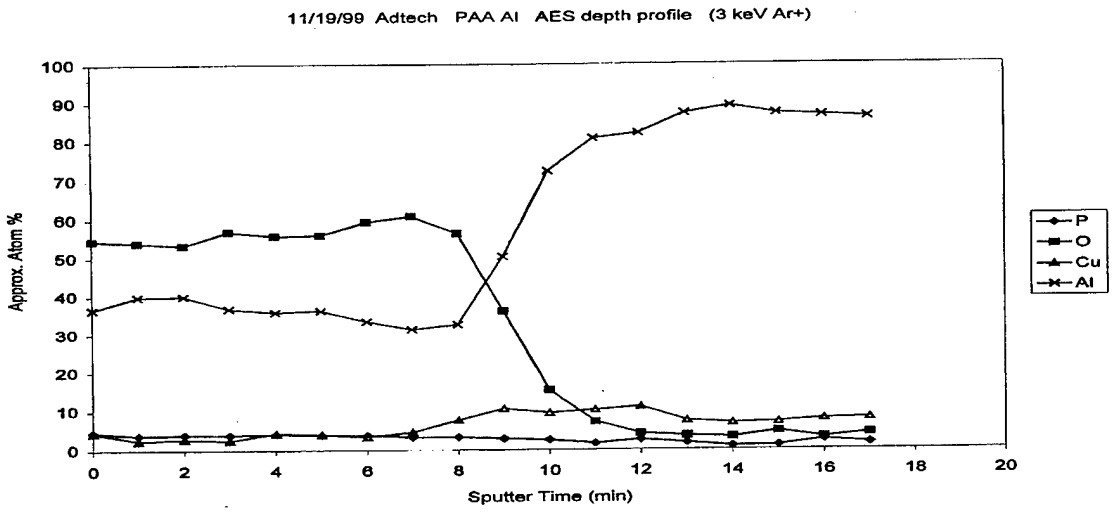

Figure 4.1. AES depth-profile of a PAA treated non-bonded aluminum surface.

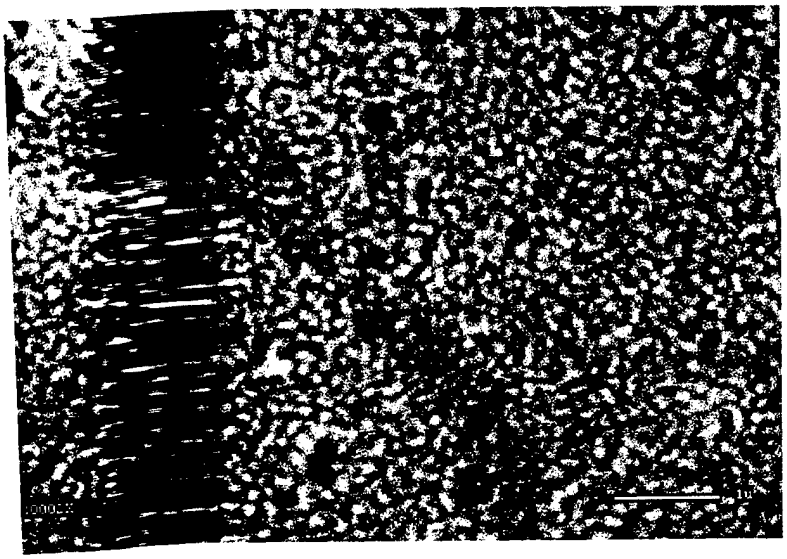

Figure 4.2. SEM photomicrograph of a PAA treated aluminum surface.

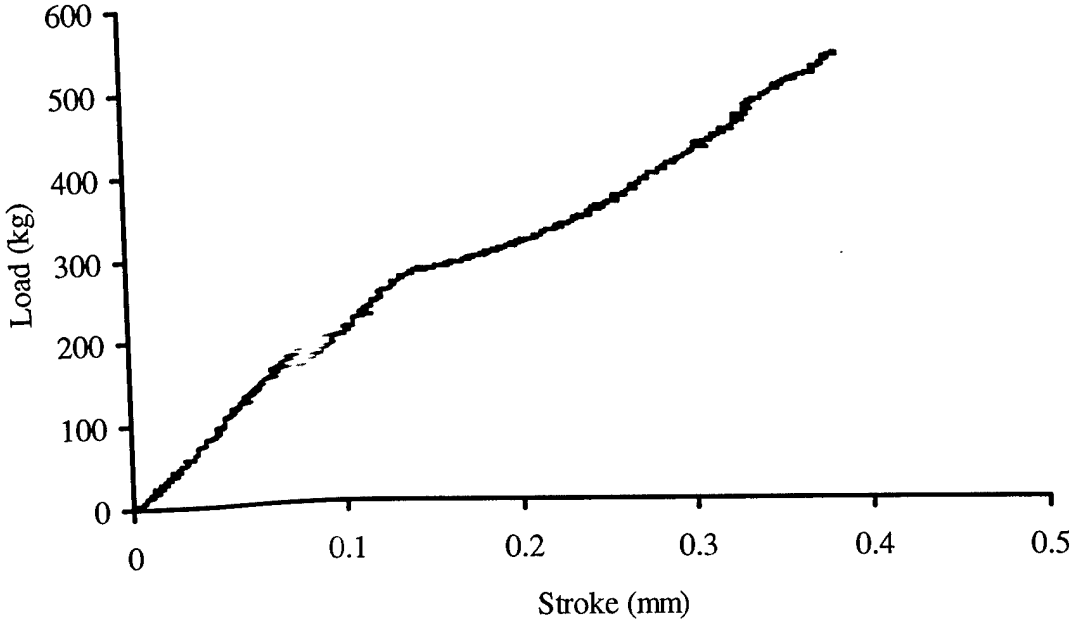

Figure 4.3. Load versus stroke trace for bonded (no-exposure) DNS specimen.

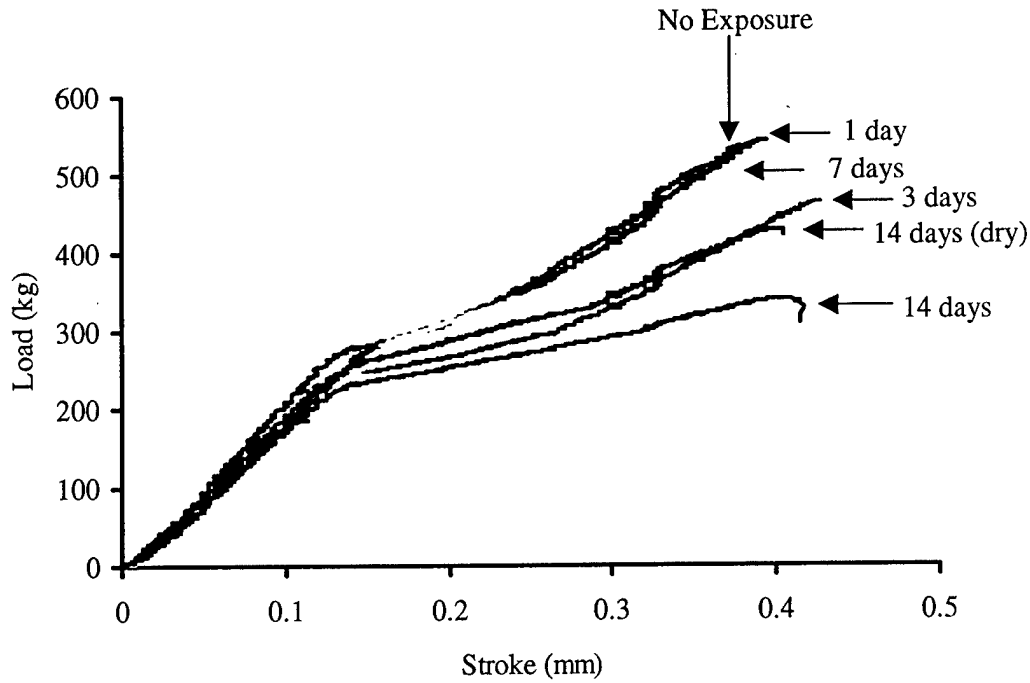

Figure 4.4. Load versus stroke data for DNS specimens exposed to 95% relative humidity at 50°C for various times.

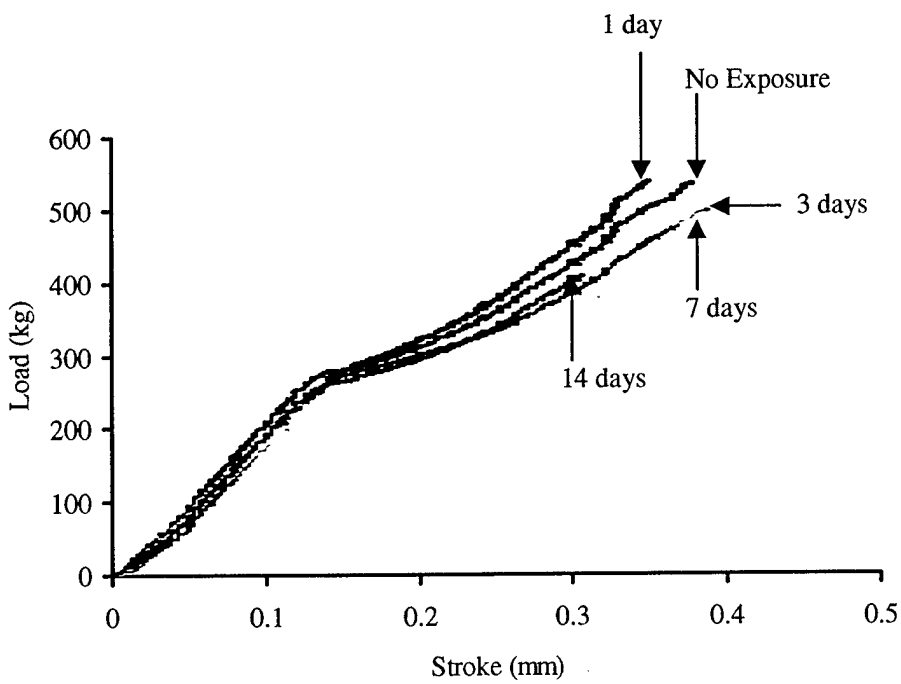

Figure 4.5. Load versus stroke data for DNS specimens exposed to 95% relative humidity at 60°C for various times.

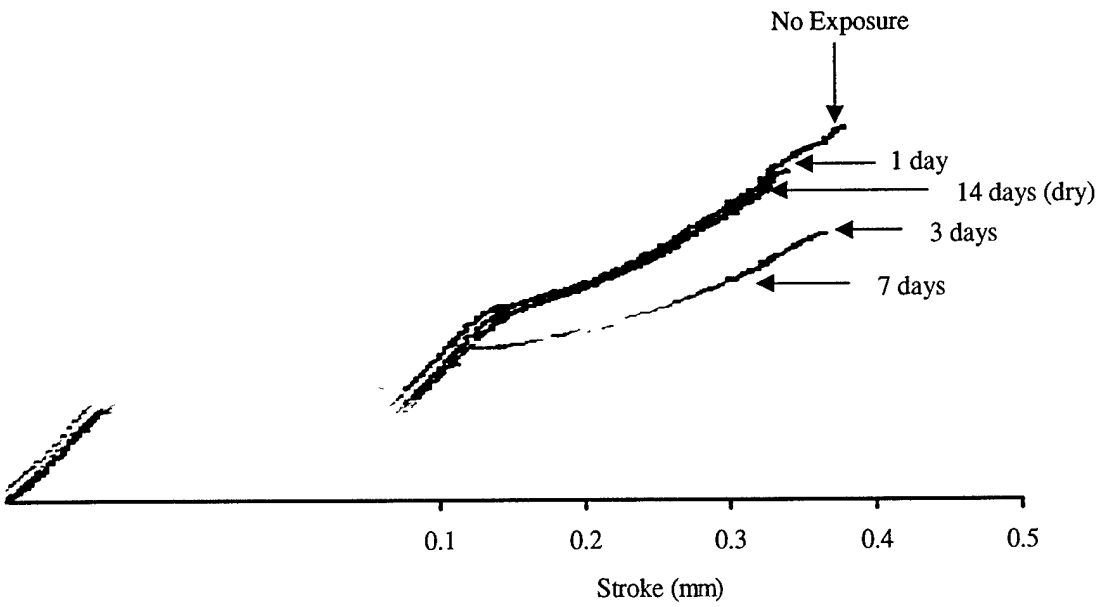

Load versus stroke data for DNS specimens exposed to 95% relative humidity at 80°C for various times.

Shear strengths (MPa) as a function of exposure time in various temperature/humidity environments for FM-73U/Aluminum DNS bonded joints. Standard deviations are given at 95% confidence limit.

osure, days	50°C/95%R.H.	60°C/95%R.H.	80°C/95%R.H.	No Exposure
1	68.0 ± 2.3	66.6 ± 2.1	57.3 ± 0.7	64.0 ± 3.0
3	53.1 ± 3.5	59.5 ± 2.7	44.2 ± 3.8	
7	58.7 ± 5.7	61.0 ± 5.8	38.4 ± 1.4	
14	41.3 ± 7.3	42.2 ± 12.3		
14 (dry)	50.6 ± 2.1		52.6 ± 7.6	

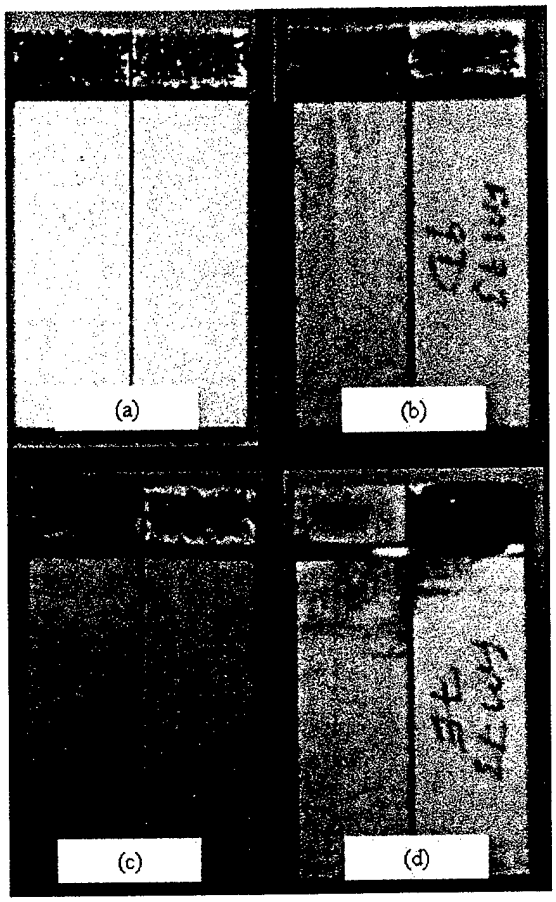

Figure 4.7. Photographs of failure surfaces of DNS specimens exposed to 95% relative humidity at 50°C for (a) 1 day, (b) 3 days, (c) 7 days and (d) 14 days.

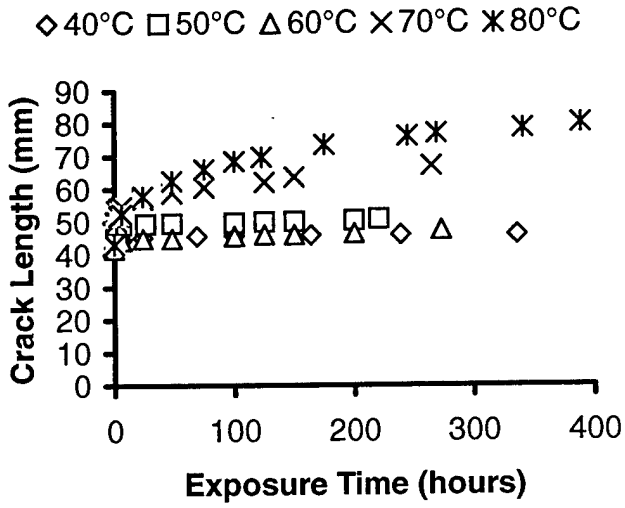

Figure 4.8. Wedge test crack length vs. exposure time for FM73U/aluminum bonded specimens exposed to 95% relative humidity at 40°C, 50°C, 60°C and 80°C.

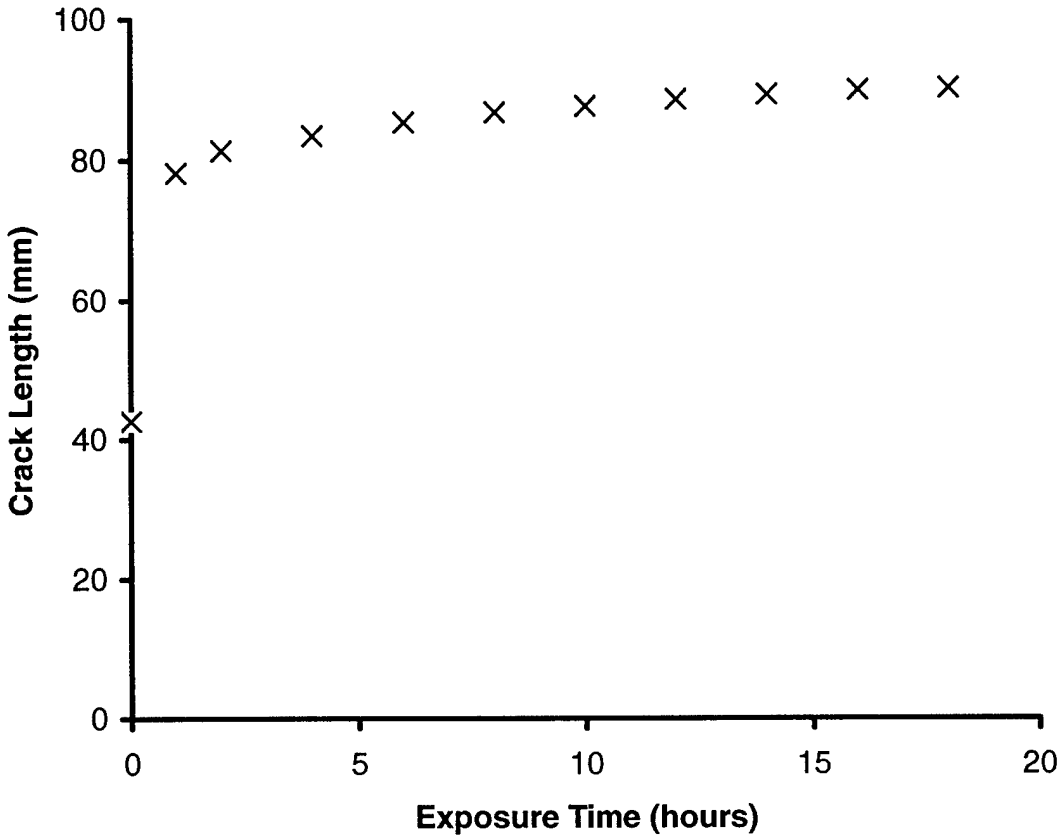

Figure 4.9. Wedge test crack length vs. exposure time for FM73U/aluminum bonded specimens exposed to boiling water.

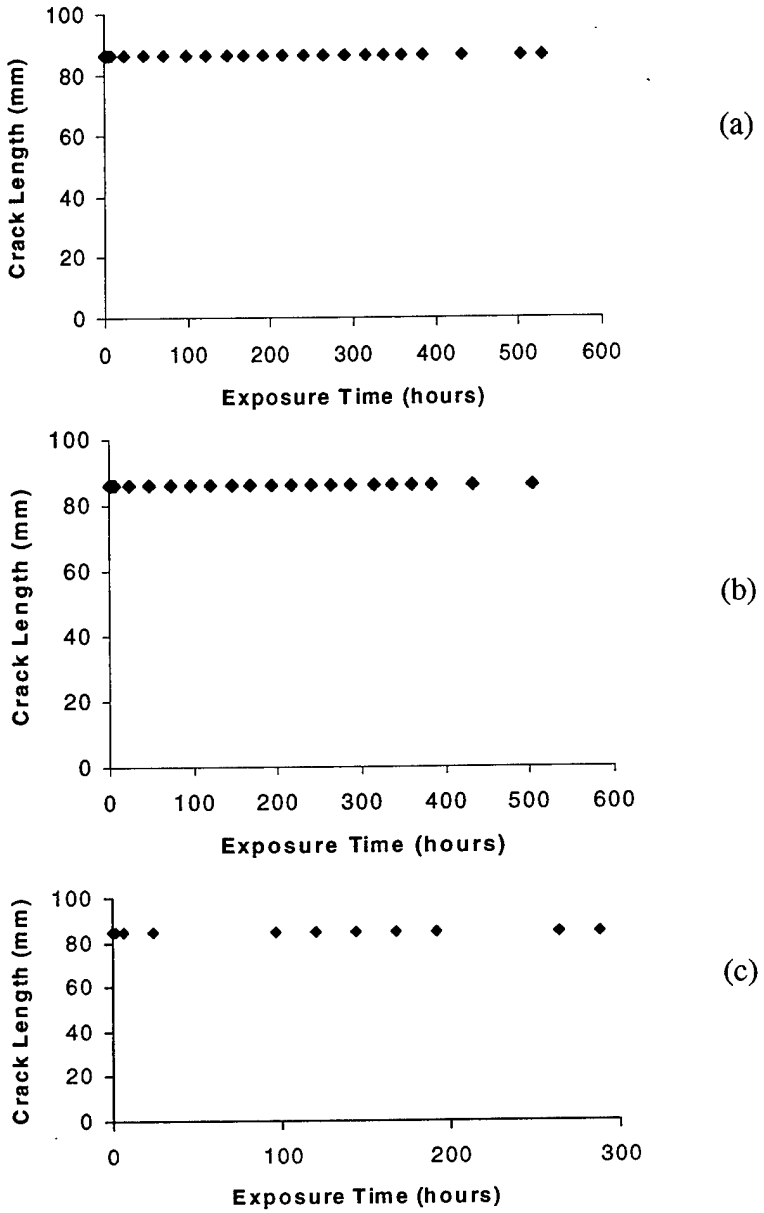

Figure 4.10. **Wedge test crack length vs. exposure time for model epoxy/aluminum bonded specimens exposed to (a) <15% relative humidity at 24°C in desiccator, (b) 95% relative humidity at 60°C and (c) 95% relative humidity at 80°C.**

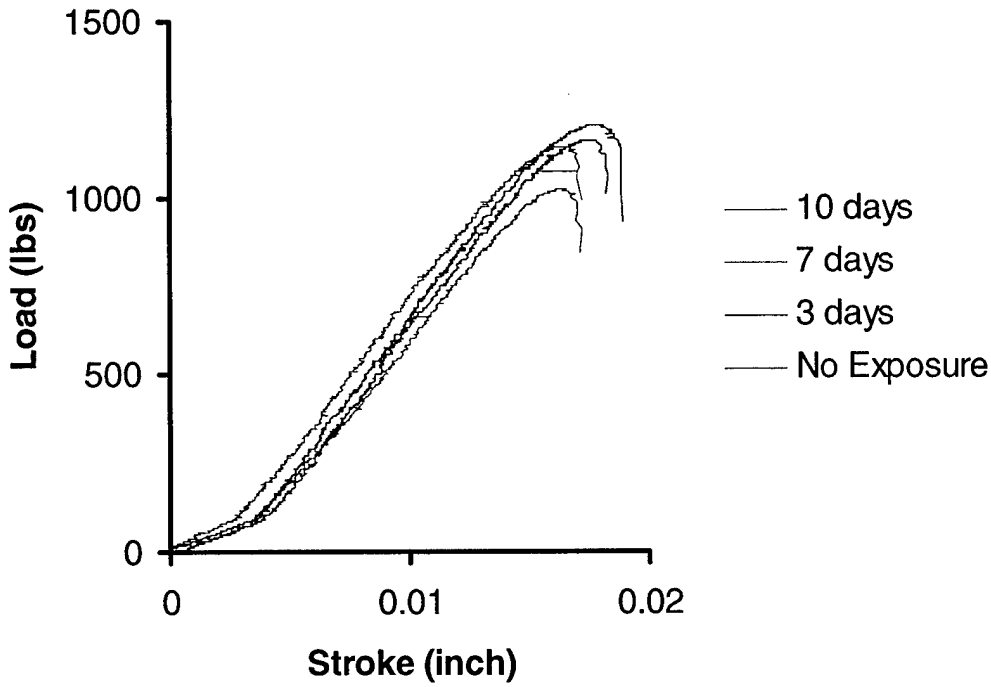

Figure 4.11. Load versus stroke data for model epoxy/aluminum DNS specimens exposed to 95% relative humidity at 60°C for various times.

Table 4.3. Shear strengths (MPa) for model epxoy/aluminum DNS bonded joints exposed to 95% relative humidity at 60°C for various times. Standard deviations are given at 95% confidence limit.

Exposure, days	Shear Strength (MPa)
No exposure	64.7 ± 2.0
3	63.3 ± 0.8
7	60.5 ± 1.6
10	59.7 ± 2.0

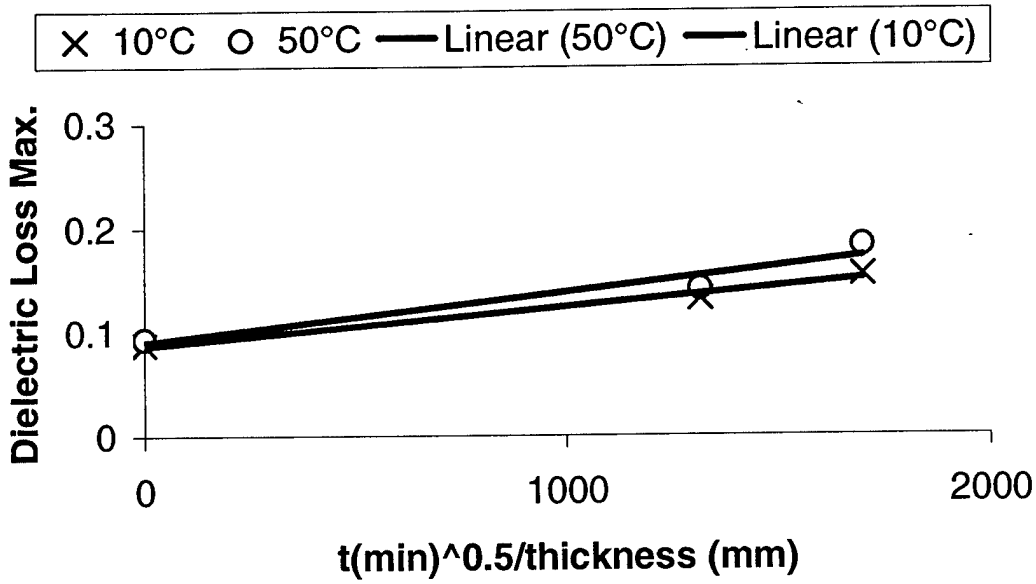

Figure 4.12. Dielectric loss maximum as a function of exposure time (t) for cured model epoxy after exposure to 60°C at 95% relative humidity. Dielectric loss maximum was measured at 10°C (X) and 50°C (o). Straight lines are the least-squares fits from the regression analyses.

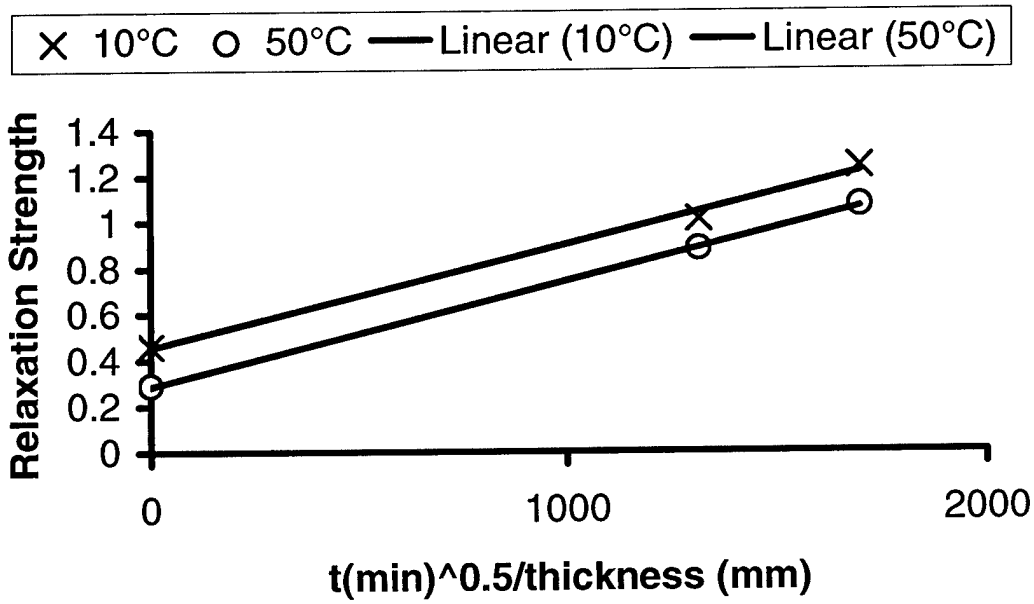

Figure 4.13. Relaxation strength as a function of exposure time (t) for cured model epoxy after exposure to 60°C at 95% relative humidity. Relaxation strength was measured at 10°C (X) and 50°C (o). Straight lines are the least-squares fits from the regression analyses.

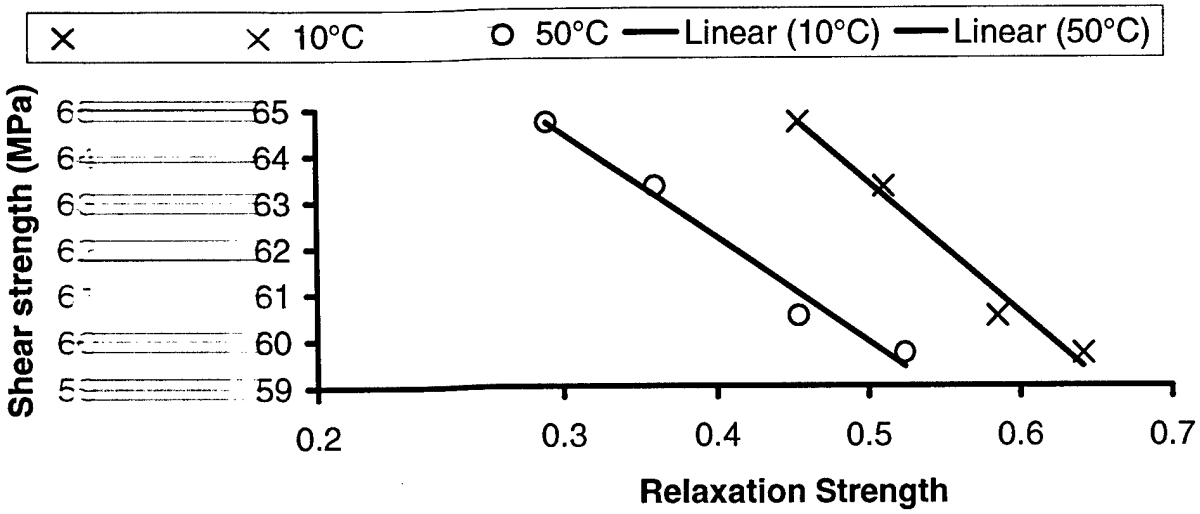

4. Shear strength as a function of dielectric relaxation strength, measured at 10°C (X) and 50°C (o), for model epoxy/aluminum bonded joints exposed to 60°C/95% relative humidity for various times. Straight lines are the least-squares fits from the regression analyses.

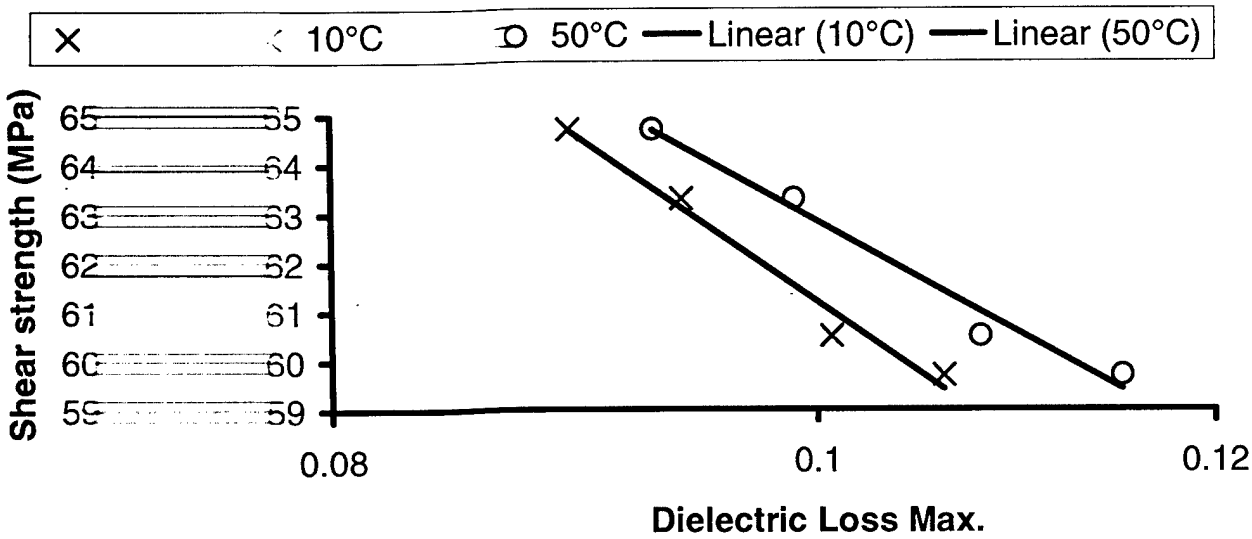

5. Shear strength as a function of dielectric loss max., measured at 10°C (X) and 50°C (o). for model epoxy/aluminum bonded joints exposed to 60°C/95% relative humidity for various times. Straight lines are the least-squares fits from the regression analyses.

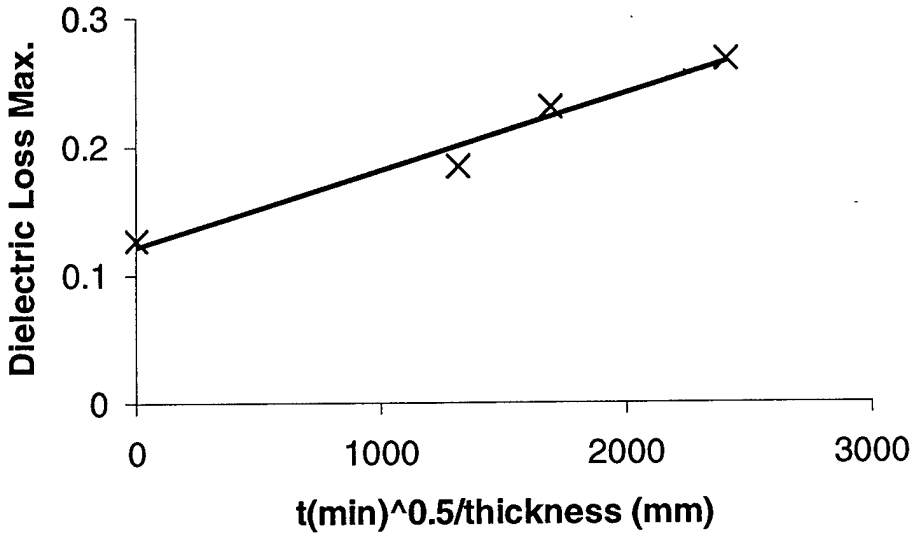

Figure 4.16. Dielectric loss maximum as a function of exposure time (t) for cured FM-73U adhesive after exposure to 60°C at 95% relative humidity. Dielectric loss maximum was measured at 50°C (X). Straight line is the least-squares fits from the regression analysis.

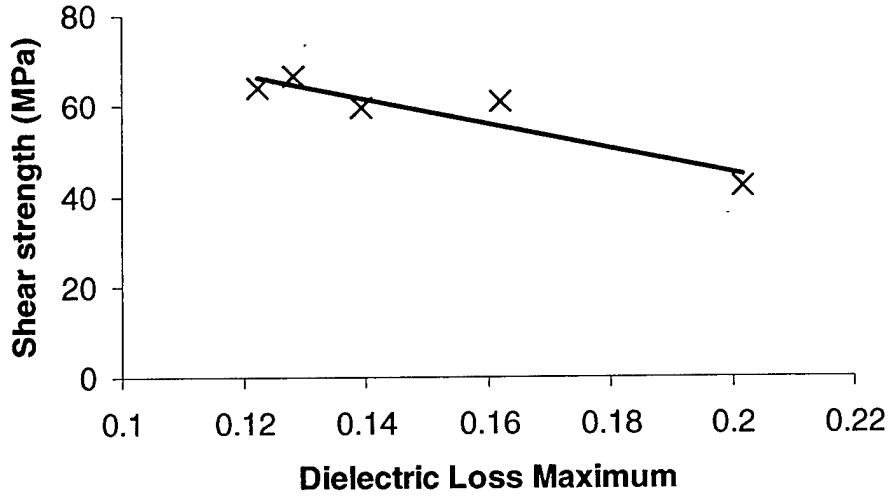

Figure 4.17. Shear strength as a function of dielectric loss max., measured at 50°C (X), for FM-73U/aluminum bonded joints exposed to 60°C/95% relative humidity for various times. Straight line is the least-squares fits from the regression analysis.

5.0 FINITE ELEMENT ANALYSIS OF DOUBLE NOTCH SHEAR TEST SPECIMENS

The mechanical properties of the adherend and adhesive must be known before a mathematical analysis of a joint geometry could be carried out to deduce the strength and nature of the stresses present in a joint. The mechanical properties of bonded joints are influenced not only by the test environments in which they are exposed but also by the stress concentrations arising due to geometrical features of the joints such as bondline thickness and the condition of the free edges of the adhesive layer.

An elastic finite-element method was used to analyze the stress distribution in DNS specimens having a bond line thickness of 5 mils and 10 mils. The effect of bond line thickness on the stress distribution along the bond overlap was analyzed. The influence of adhesive material present beyond the bonded region in the form of a spew or continuous film on the stress distribution along the bond overlap was also analyzed. The SDRC I-DEAS software was used to perform the finite element analysis. The geometry of the DNS test specimen is shown in Figure 5.1. The material properties used in the analysis are listed below:

Adherend: Aluminum 2024 T3

Young's modulus:	10.5×10^6 psi
Poisson's ratio:	0.33

Adhesive: FM-73U epoxy

Young's modulus:	0.337×10^6 psi
Poisson's ratio:	0.40

The adhesively bonded DNS test specimen was modeled using 4560 three-dimensional parabolic brick elements. The bond line was modeled as four layers at the bond overlap. Finer mesh was used near the free edges of the overlap. The boundary conditions used in the analysis are as follows:

- The end face at one end of the specimen was fixed in all directions
- The specimen was loaded in compression along its length. This was achieved by applying a constant pressure on the free end face of the specimen. The value of the pressure was such that the average shear stress in the overlap area equaled 1 psi.
- The specimen was prevented from moving in the transverse direction (perpendicular to the overlap area) by restraining the top and bottom free surfaces of the adherends.

The finite element mesh and the boundary conditions used are shown in Figure 5.2. A three-dimensional contour plot of the shear stress distribution in the overlap areas is shown in Figure 5.3. The effect of bond line thickness on the stress distribution along the overlap is shown in Figure 5.4. The thinner bond line (5 mil) gives a wider stress distribution along the overlap than the thicker bond line (10 mil). The peak stress close to the free edges is higher and the minimum stress at the middle is lower for the thinner bond line.

While the ideal specimen is expected to have square adhesive layer edges, some amount of adhesive remains on the specimen beyond the edges of the overlap. To evaluate the effect of this residual adhesive, the adhesive layer was modeled as a continuous layer of constant thickness throughout the length of the specimen. A schematic of DNS test specimens having an ideal square edge adhesive layer and a continuous adhesive layer are shown in Figure 5.5. The effect of the continuation of the adhesive layer beyond the overlap on stress is shown in Figure 5.6. It

is seen that the continuous layer reduces the peak stresses near the overlap edges compared to the square edge layer. The normalized shear stress along the complete overlap is lower for the continuous layer than the square edge layer. As the adhesive layer of the actual DNS test specimen is not totally continuous across the notches and not totally square, its stress distribution is expected to lie between these two curves.

A two-dimensional contour plot of the maximum principal stress distribution in the overlap area is shown in Figure 5.7. To show the maximum principal stress distribution along the bond overlap and thickness of the adhesive, the maximum principal stress is plotted as a function of bond overlap for the top, middle and bottom adhesive layers, see Figure 5.8. For the bottom adhesive layer it is seen that the maximum principal stress peaks at the left edge and drops to negative value (compressive) at the right edge. The pattern is reversed for the top adhesive layer, while it is symmetric for the middle. The finite element analysis result shows that the adhesive/adherend interface at the free edge of the adherend is subjected to the largest maximum principal stress. As a result, failure of the joint is expected to initiate at the adhesive/adherend interface near the free edge of the adherend.

The visual observations of the failure surfaces of an unexposed FM-73U/aluminum DNS specimen are consistent with the results obtained above from the finite element analysis of a bonded joint. The unexposed DNS specimen fails cohesively within the adhesive except in the area near the free edge of the adherends, see Figure 5.9. The bonded joint fails at the adherend/adhesive interface (interfacial failure) along the free edge of the adherends on both sides of the failure surfaces.

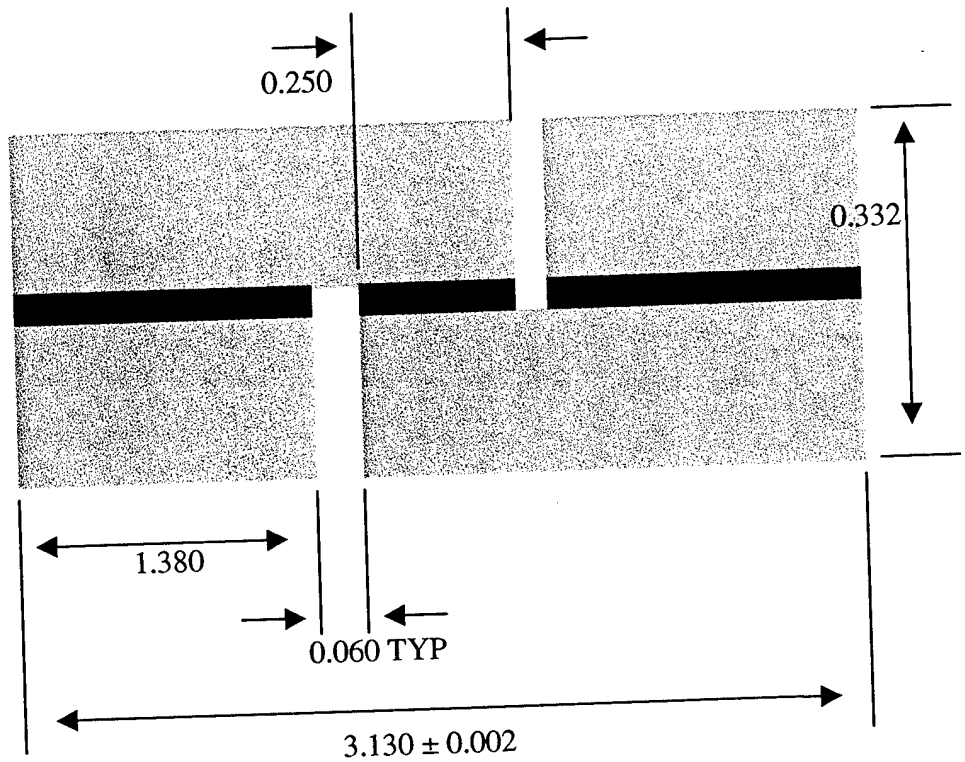

Figure 5.1. Geometry of DNS specimen.

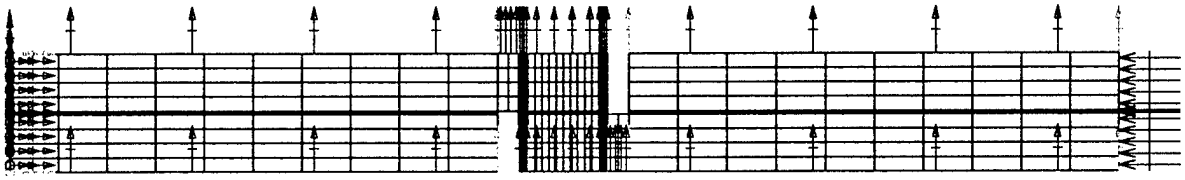

Figure 5.2. Boundary Conditions for a DNS specimen.

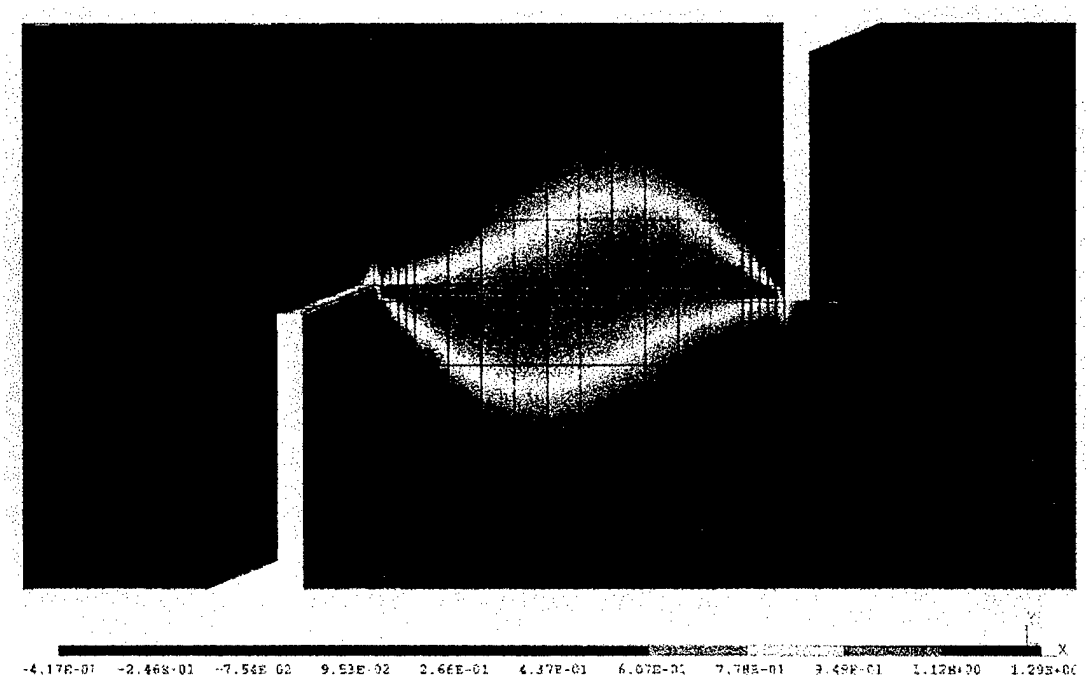

Figure 5.3. Three-dimensional contour plot of shear stress distribution in the overlap regions.

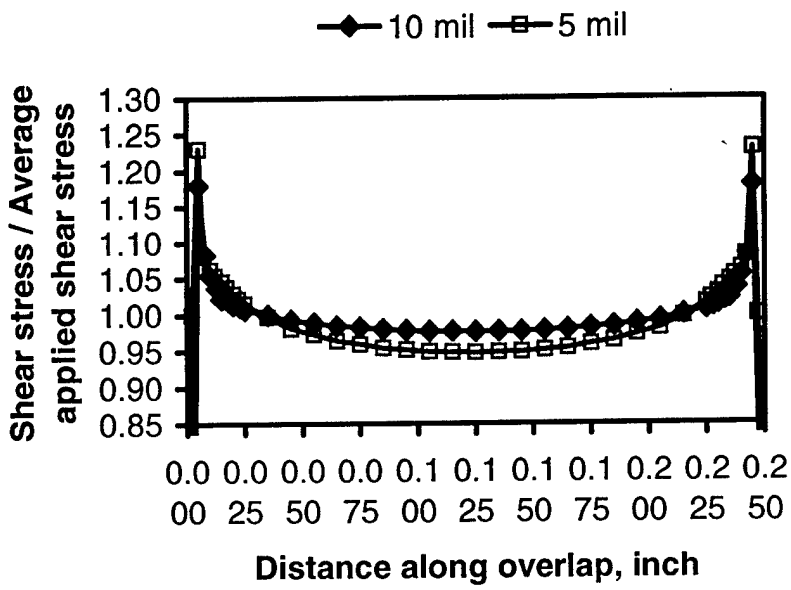

Figure 5.4. The influence of bond line thickness on the stress distribution along the bonded joint overlap.

(a) Square Edge Adhesive Layer

(b) Continuous Adhesive Layer

Figure 5.5. A schematic of DNS test geometry in the overlap region with: (a) square edge adhesive layer and (b) Continuous adhesive layer.

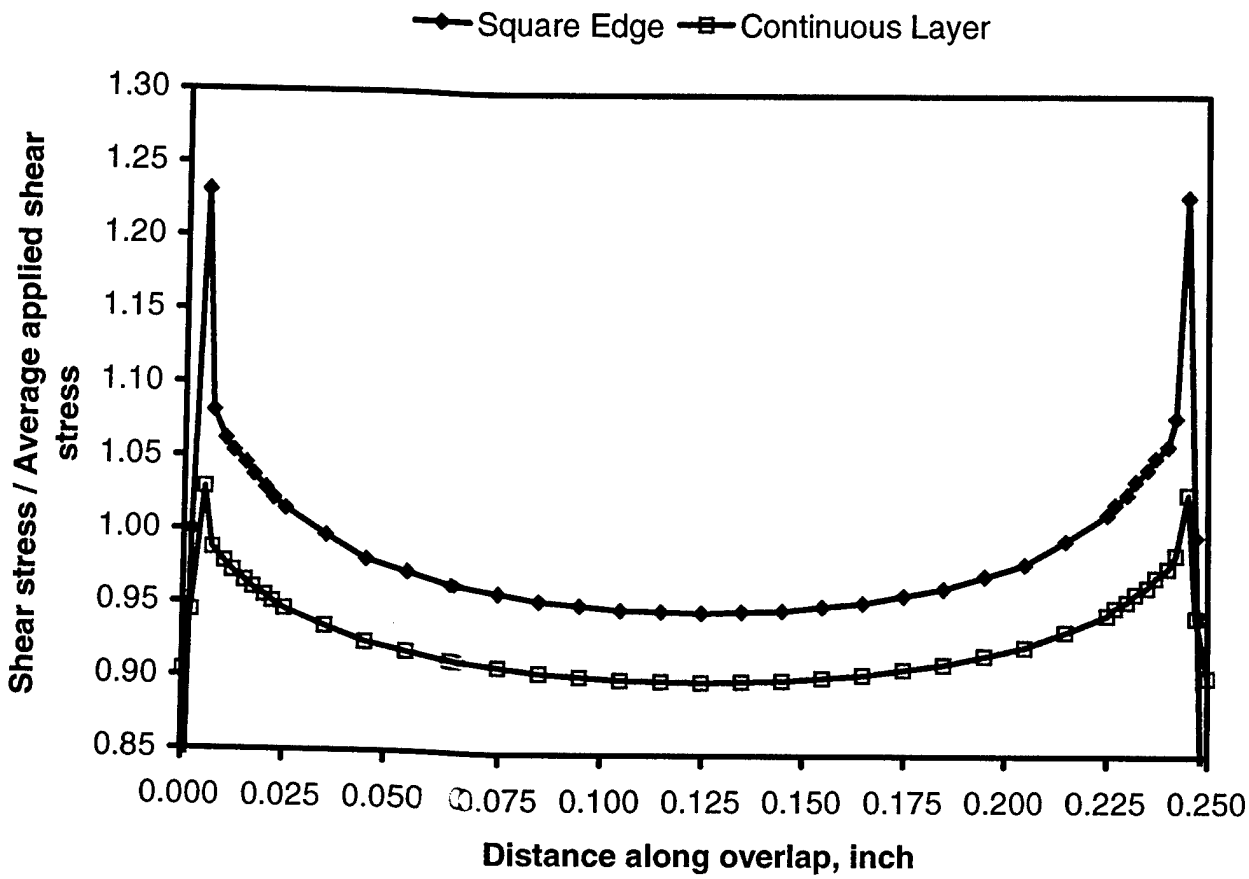

Figure 5.6. **Stress distribution profile in the bond overlap region for a square edge adhesive layer and continuous adhesive layer in DNS specimens.**

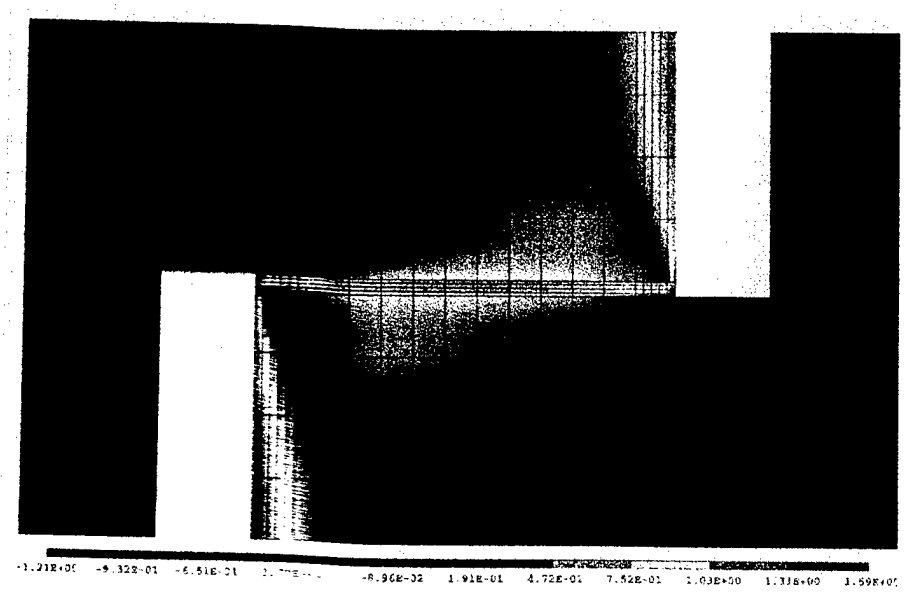

Figure 5.7. **Two-dimensional contour plot of maximum principal stress distribution in the overlap region of a DNS specimen.**

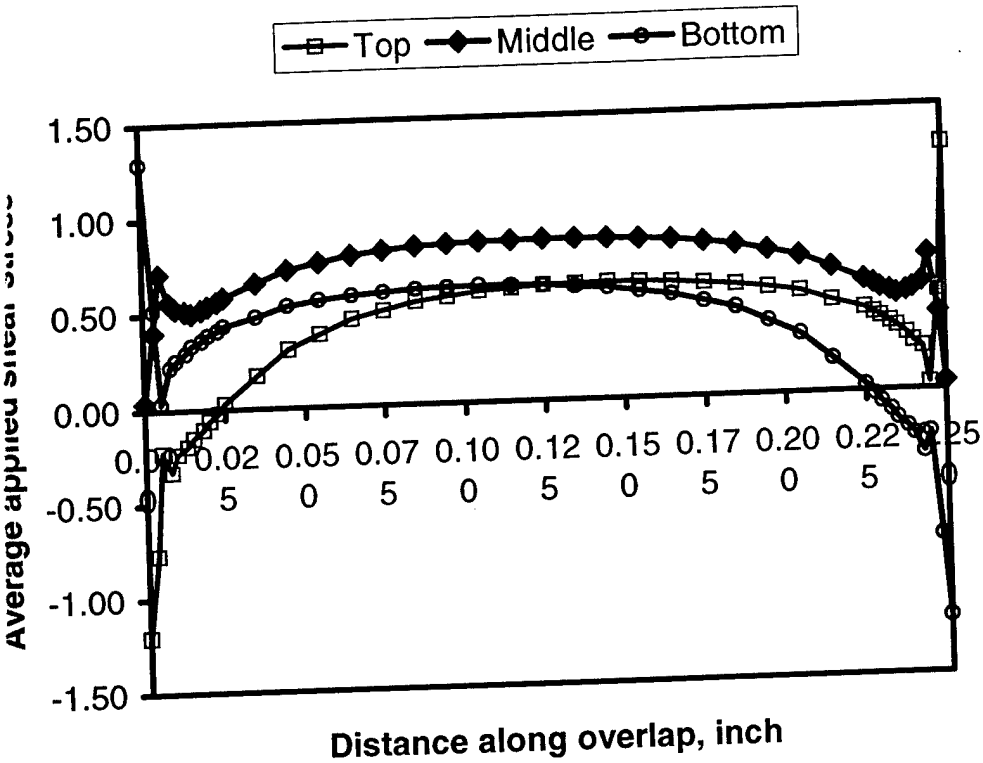

The maximum principal stress distribution is plotted as a function of bond overlap for the top, middle and bottom adhesive layers.

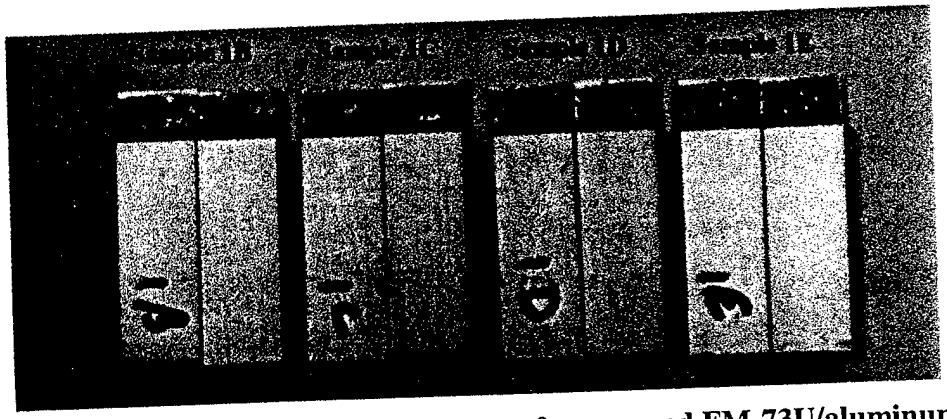

). The photographs of failure surfaces of unexposed FM-73U/aluminum DNS specimens

Summary

Molecular aspects of chemical and physical changes in adhesively bonded joints caused by absorbed moisture were investigated. The focus was on the pre-damage stage that precedes the formation of voids and microcracks. Dielectric relaxation spectroscopy was used as a non-destructive tool to characterize the molecular level changes in the adhesive when exposed to hygrothermal environments. Three adhesive types, a commercial epoxy-amine formulation (FM73U), a model epoxy formulation consisting of diglycidyl ether of Bisphenol A (DGEBA) and methylene dianiline (MDA), and a bismaleimide formulation consisting of 4,4' bismaleimidodiphenyl methane (component A) and 0,0' diallyl bisphenol A (component B) were studied. Local dynamics were monitored by broad-band dielectric relaxation spectroscopy (DRS) and the changes in the chemical state of the matter were monitored by FTIR. For epoxy-amine formulations, the result suggests that one portion of the absorbed water does not form hydrogen bonds with the network and gives rise to a fast relaxation process (termed γ) with activation energy of 28 kJ/mol. The local β dynamics are slowed down by the interactions between water and various sites on the network that include the ether oxygen, the hydroxyl group and the tertiary amine nitrogen. For bismaleimide adhesive system, absorbed water interacts with the BMI network and gives rise to a fast relaxation process (termed γ^*), characterized by an increase in the dielectric relaxation strength, an Arrhenius temperature dependence of the average relaxation time and an activation energy of 50 kJ/mol. The γ^* dynamics are slower than the relaxation of bulk liquid water because of the interactions between the absorbed water and various sites on the network (the ether oxygen, the hydroxyl group, the carbonyl group and the tertiary amine nitrogen). Also, FTIR spectra reveal the presence of non hydrogen-bonded water and hydrogen-bonded water; the latter bonded to one and/or two sites on the BMI network.

One particularly significant finding is that the average relaxation time for the β process (in epoxy-amine formulations) and γ^* process (in bismaleimide formulation) above 20^0C is of the order of nanoseconds or less, and hence its detection hinges on the ability to perform high precision DRS at frequencies above 1 MHz. This is an important consideration in the ongoing efforts aimed at the implementation of DRS as non-destructive inspection (NDI) tool for adhesive joints.

The influence of moisture on the strength and durability of adhesively bonded joints has been studied. Adhesively bonded specimens in double notch shear (DNS) and wedge test configurations were exposed to various temperatures at 95% relative humidity for various times in an environmental chamber. The wedge test specimen was periodically removed from the test chamber and crack length was measured and recorded as a function of time. At the end of the environmental conditioning, the DNS specimen was subjected to axial compression load to determine the shear strength. The main finding is that the shear strength decreases with the increase in duration of the exposure time at constant temperature. The FM-73U/aluminum bonded joint fails increasingly in the metal/adhesive interface (interfacial failure) as the exposure temperature and duration is increased. The interfacial failure starts along the edge of the bonded DNS specimen and move towards the center of the bonded area as the exposure temperature and duration is increased. The durability of FM-73U/aluminum bonded joints decreases with the increase in temperature. The durability of FM-73U/aluminum joints in 95% relative humidity at various temperatures follows the order: 40°C > 50°C > 60°C > 80°C. The wedge test and shear strength data for model epoxy/aluminum bonded joints suggests that the model epoxy is a better moisture resistant adhesive than the commercial FM-73U epoxy.

A reasonably good correlation between measured shear strength data and measured dielectric response was observed for model epoxy/aluminum joints and FM-73U/aluminum joints.